

**Studies on structures and properties of
cellulose-based functional films prepared using
aqueous alkali/urea systems**

(水系アルカリ-尿素系を用いて調製した機能性セル
ロース系フィルムの構造と特性)

YANG Quanling

楊 全嶺

**Studies on structures and properties of cellulose-
based functional films prepared using aqueous
alkali/urea systems**

YANG Quanling

**Department of Biomaterial Sciences
Graduate School of Agricultural and Life Sciences
The University of Tokyo**

Contents

Chapter 1

General Introduction

1.1 Background of cellulose	1
1.1.1 Brief history	
1.1.2 Structure	
1.2 Solvents of cellulose	5
1.2.1 N-methylmorpholine-N-oxide hydrate (NMMO)	
1.2.2 Ionic liquids (ILs)	
1.3 Aqueous alkali/urea solvent system	8
1.3.1 Dissolution of cellulose in aqueous alkali/urea system	
1.3.2 Fibers from aqueous cellulose/alkali/urea system	
1.3.3 Films from aqueous cellulose/alkali/urea system	
1.3.4 Spheres from aqueous cellulose/alkali/urea system	
1.3.5 Hydrogels from aqueous cellulose/alkali/urea system	
1.3.6 Aerogels from aqueous cellulose/alkali/urea system	
1.4 Objective of this study	14
1.5 References	15

Chapter 2

High Gas Barrier Cellulose Films Fabricated from Aqueous Alkali/Urea Solutions

2.1 Introduction	21
2.2 Experimental Section	22
2.2.1 Materials	
2.2.2 Preparation of films	
2.2.3 Characterizations	
2.3 Results and Discussion	24
2.3.1 Characteristics of AUC films	

2.3.2 Oxygen permeabilities of AUC films	
2.3.3 Oxygen permeability of AUC films under humid conditions	
2.4 Conclusions	35
2.5 References	36

Chapter 3

Improvement of Mechanical and Oxygen Barrier Properties of Cellulose Films by Controlling Drying Conditions of Regenerated Cellulose Hydrogels

3.1 Introduction	39
3.2 Experimental Section	41
3.2.1 Materials	
3.2.2 Preparation of regenerated cellulose hydrogel films	
3.2.3 Drying conditions of regenerated cellulose hydrogel films	
3.2.4 Characterizations	
3.3 Results and Discussion	43
3.3.1 Drying conditions of regenerated cellulose hydrogel films	
3.3.2 Properties of cellulose films	
3.3.3 Effects of drying conditions on mechanical and optical properties of regenerated cellulose films	
3.3.4 Effect of drying conditions on oxygen permeability of regenerated cellulose films	
3.4 Conclusions	60
3.5 References	60

Chapter 4

Cellulose Based Nanocomposites Reinforced with Nanoclay

4.1 Introduction	63
4.2 Experimental Section	64
4.2.1 Materials	

4.2.2 Film preparation	
4.2.3 Characterizations	
4.3 Results and Discussion	67
4.3.1 Structures of cellulose–clay nanocomposites	
4.3.2 Optical and mechanical properties of cellulose–clay nanocomposites	
4.3.3 Thermal properties of cellulose–clay nanocomposites	
4.3.4 Gas barrier properties of cellulose–clay nanocomposites	
4.3.5 Hydrophilicity of cellulose–clay nanocomposites	
4.4 Conclusions	85
4.5 References	86

Chapter 5

Hydrophobization of Cellulose Films by Surface Modification with Alkyl Ketene Dimer (AKD)

5.1 Introduction	89
5.2 Experimental Section	90
5.2.1 Materials	
5.2.2 Preparation of AKD-treated AUC films	
5.2.3 Analyses	
5.3 Results and Discussion	92
5.3.1 Treatment of AUC film with AKD	
5.3.2 Optical and mechanical properties of AKD-treated AUC films	
5.3.3 Hydrophobicity of AKD-treated AUC films	
5.3.4 Gas barrier properties of AKD-treated AUC films	
5.3.5 Chemical structures of AKD components on the AKD-treated AUC film surface	
5.4 Conclusions	102
5.5 References	103

Chapter 6

Chemical Structures of Alkylketene Dimer (AKD) at the AKD/Cellulose Interfaces

6.1 Introduction	105
6.2 Experimental Section	107
6.2.1 Materials	
6.2.2 Preparation of cellulose-AKD films	
6.2.3 Extractions of AKD from the cellulose-AKD films	
6.2.4 Analyses	
6.3 Results and Discussion	109
6.3.1 Extractions of AKD from CA film	
6.3.2 Extractions of AKD from CAH films	
6.3.3 Extractions of AKD from TA films	
6.4 Conclusions	122
6.5 References	123

Chapter 7

Summary

7.1 High gas barrier cellulose films	127
7.2 High-performance cellulose biocomposite materials	127
7.2.1 Cellulose based nanocomposites reinforced with nanoclay	
7.2.2 Hydrophobization of cellulose films by surface modification with AKD	

Research Achievement	129
-----------------------------------	-----

Acknowledgement	135
------------------------------	-----

Chapter 1

General Introduction

1.1 Background of cellulose

1.1.1 Brief history

Cellulose, the most ubiquitous and abundant polymers on the planet, has been used in the form of wood, cotton, and other plant fibers as an energy source, building materials, and clothing for thousands of years.¹ However, until 1838 it was first discovered by the French scientist Anselme Payen.²⁻⁴ He got a resistant fibrous substance that remained after treatment of various plant (wood, cotton and others) tissues with acids and ammonia, following by subsequent extractions with water, alcohol, and ether. His analysis revealed the chemical formula of the substance to be $C_6H_{10}O_5$. In 1839 he first used the name “cellulose” for this substance in a report of the French academy on his work.⁵



Figure 1.1. Anselme Payen who first discovered cellulose.¹²

After that, the source, structure, chemical and physical properties of cellulose have been exhaustively studied by the researches all over the world. The first industrial scale cellulose product, i.e. celluloid, was created from nitrocellulose and camphor by the Hyatt Manufacturing Company in 1870, which is the first thermoplastic polymer material.⁶ The polymeric structure of cellulose was elucidated by Hermann Staudinger in 1920⁷ and the research on cellulose had a huge influence on the development of polymer chemistry.^{8,9} Actually the structural features of macromolecules were mainly revealed with cellulose and this achievement led to the Nobel Prize for Hermann Staudinger in 1953, presumably the first Nobel Prize for a polymer chemist.¹⁰ In 1996 cellulose was synthesized for the first time in a purely chemical manner (no enzymatic catalyst).¹¹ Although synthetic polymers were rapidly developed in the 20th Century and widely used until now, the 1970s energy crisis make cellulose attract renewed interest for materials and energy applications owing to its renewability.⁸ Moreover, most of the synthetic polymers are not biodegradable or carbon neutral, thus causing environmental pollution. Therefore, development and utilization of renewable, biodegradable, and biocompatible cellulose materials have become significant requirements for a sustainable society of the 21th Century.

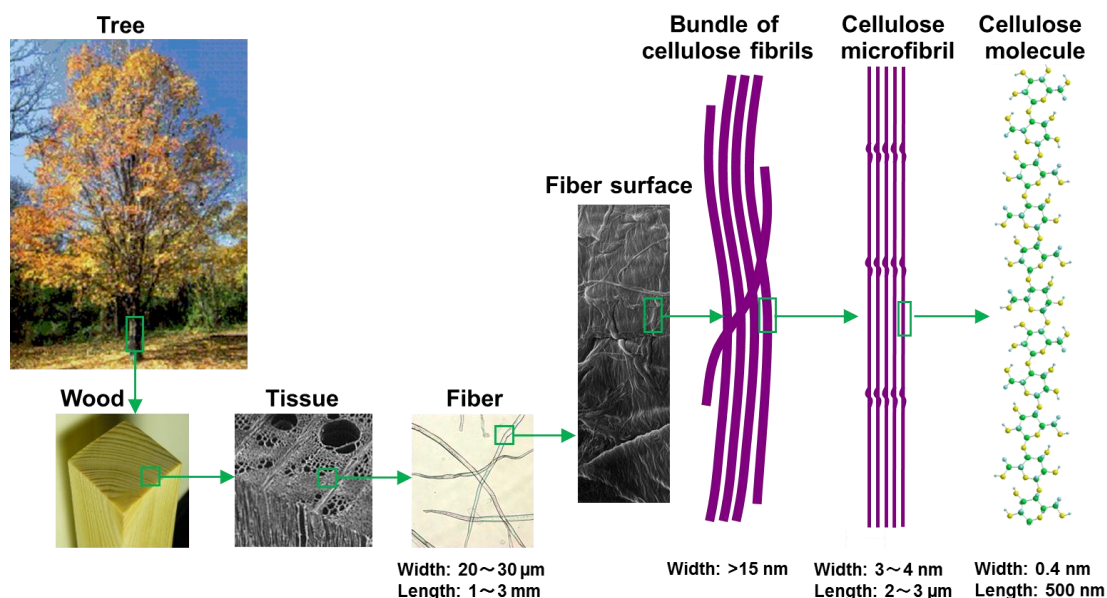


Figure 1.2. Hierarchical structure of wood cellulose.¹⁵

1.1.2 Structure

Cellulose is mainly produced by plants (wood, cotton, hemp, and others) in nature and also by certain bacteria, algae, tunicates, and fungi.^{13,14} Figure 1.2 shows the hierarchical structure of wood cellulose¹⁵ and Figure 1.3 shows the molecular structure of cellulose.

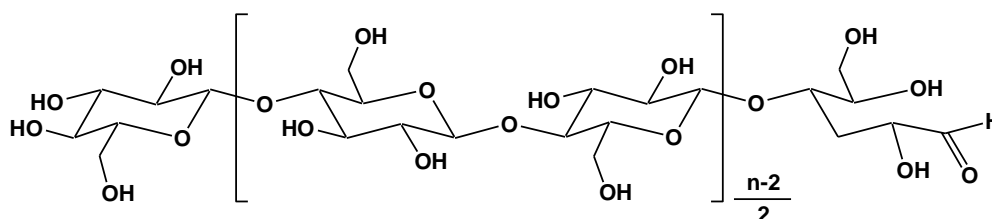


Figure 1.3. Molecular structure of cellulose ($n=DP$, degree of polymerization).

Cellulose is a polysaccharide generated from repeating β-D-glucopyranose molecules that are covalently linked through glycoside bonds between the equatorial OH group of C4 and the C1 carbon atom (β-1, 4-glucan).^{1,16} Therefore, cellulose is an extended and linear-chain polymer with a large number of hydroxyl groups present in the thermodynamically preferred 4C_1 conformation.¹⁷ To accommodate the preferred bond angles of the acetal oxygen bridges, every second anhydroglucose (AGU) ring is rotated 180° in the plane.¹ In this manner, two adjacent structural units define the disaccharide cellobiose. The chain length of cellulose expressed in the number of constituent AGUs (degree of polymerization, DP) varies with the origin and treatment of the raw material.¹ One end of the cellulose chain is terminated with a D-glucose unit with an original C4-OH group (the non-reducing end); the other end is terminated with an original C1-OH group, which is in equilibrium with the aldehyde structure (the reducing end).¹ The molecular structure imparts cellulose with its characteristic properties: hydrophilicity, chirality, degradability, and broad chemical variability initiated by the high donor reactivity of the OH groups.¹ It is also the basis for extensive hydrogen bond networks, which make cellulose as highly crystalline microfibrils with width of 3–4 nm consisting of uniaxially aligned cellulose molecules in biological structures (Figure 1.2).¹⁵

The properties of cellulose are therefore determined by a defined hierarchical order in supramolecular structure¹, which result in one approach to prepare cellulose materials by dissolution of cellulose molecules followed by its regeneration and the other by extraction of individual cellulose nanofibrils from native cellulose followed by preparation of the nanofibril materials.

Furthermore, it should be noted that cellulose molecule is amphiphilic.¹⁸ Figure 1.4 is a schematic representation of cellulose molecules with their hydrophilic and hydrophobic parts.^{18,19} The equatorial direction of the glucopyranose ring is hydrophilic because all three hydroxyl groups on the ring are located on the equatorial positions of the ring. In contrast, the axial direction of the ring is hydrophobic because hydrogen atoms of C–H bonds are located on the axial positions of the ring. Thus, cellulose molecules are intrinsically amphiphilic structure. Moreover, such structure may play an important role in the research and utilization of cellulosic materials.

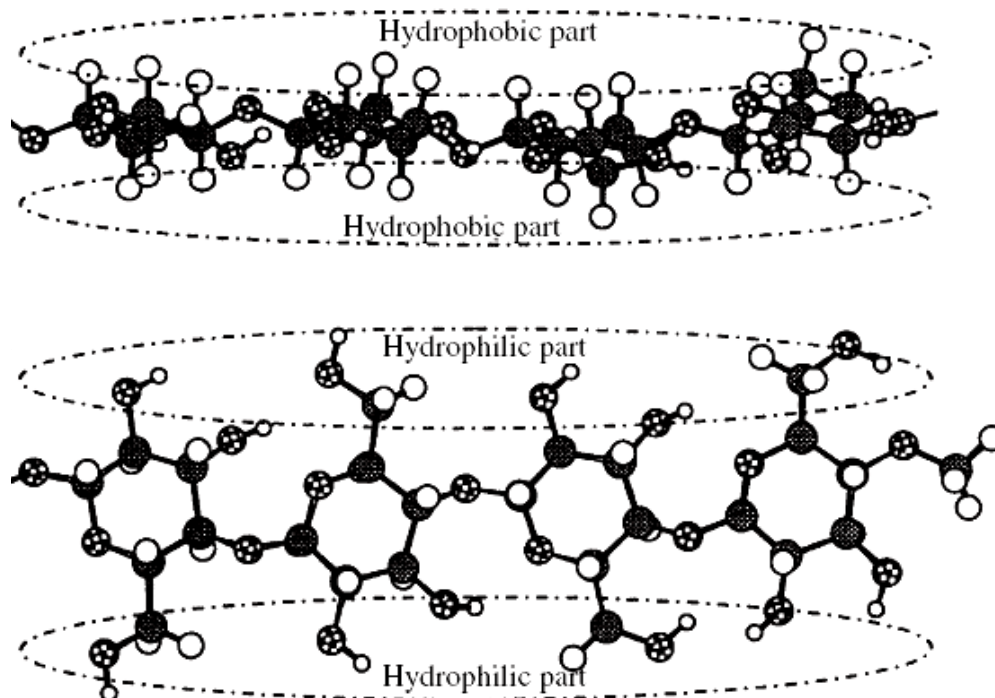


Figure 1.4. Hydrophobic and hydrophilic parts of cellulose molecule.^{18,19} Reproduction from ref. 19 with permission from Nature Publishing Group (© Nature Publishing Group 2006).

1.2 Solvents of cellulose

Cellulose is considered to be an almost inexhaustible source of raw material for the increasing demand for biodegradable and biocompatible products.^{20,21} However, cellulose is hard to dissolve in aqueous solutions and many organic solvents, which has been mainly explained in terms of the presence of strong inter- and intra-molecular hydrogen bonds of cellulose molecules. Most recently, Lindman et al. asserted that hydrogen bonding mechanism alone cannot explain the low solubility of cellulose in aqueous solvents, and the solubility or insolubility characteristics of cellulose are significantly dependent upon its amphiphilic and hydrophobic molecular interactions, which is named Lindman hypothesis.^{22,23} After debating the Lindman hypothesis by many cellulose chemists, both the hydrogen bonds and hydrophobic interactions of cellulose molecules are thought to be important for the dissolution of cellulose.²³ The efficient dissolution of cellulose by a “green” method and the relevant dissolution mechanism is still long-standing goal in the cellulose field until now.^{22–24}

The non-derivatizing solvents of cellulose mainly include aqueous inorganic complexes (cuoxam, cadoxen, and cuen),^{25–27} 8~10 wt % NaOH aqueous solution,^{28–31} NH₃/NH₄SCN aqueous solution,^{32,33} Ca(SCN)₂ and NaSCN aqueous solution,^{34,35} ZnCl₂ aqueous solution,^{36,37} N,N-dimethylacetamide (DMAc)/LiCl,^{38,39} dimethyl sulfoxide (DMSO)/LiCl,^{40,41} 1,3-dimethyl-2-imidazolinone (DMI)/LiCl,^{42,43} N-methylmorpholine-N-oxide (NMMO),^{44,45} ionic liquids,^{24,46,47} and alkali/urea or thiourea (NaOH/urea, NaOH/thiourea and LiOH/urea) aqueous systems,^{48–54} whereas the derivatizing solvents mainly are N,N-dimethylformamide (DMF)/N₂O₄,^{55,56} DMSO/paraformaldehyde⁵⁷ and NaOH/CS₂ (viscose route)⁵⁸. The traditional viscose route still dominates production methods. However, it inevitably generates hazardous byproducts (H₂S and CS₂) during manufacture and in post-treatment processes, resulting in serious pollution.^{1,59} Among the new cellulose solvents, NMMO, ionic liquids, and alkali/urea solutions are the most promising alternative cellulose solvent systems.

1.2.1 N-methylmorpholine-N-oxide hydrate (NMMO)

In 1969 Johnson described a cellulose solvent system using cyclic amine oxides,

particularly N-methylmorpholine-N-oxide (NMMO), and speculated about their potential application as dialysis membranes, food casings (sausage skins), fibers, films, paper coatings, and nonwoven binders.^{60,61} NMMO can be produced by oxidation of N-methylmorpholine with hydrogen peroxide, and is emerged as the best amine-oxide.⁶² Pure NMMO has a melting point of 170 °C. Hydration with one water molecule per NMMO molecule leads to the NMMO monohydrate with 13.3 wt % water content and it has a melting point of about 74 °C and improved dissolution strength for cellulose owing to its strong N-O dipole.⁴⁴ McCorsley and Varga developed a method to produce solutions of up to 23% cellulose by treating cellulose with NMMO/water mixtures and subsequently removing the water with vacuum until the dissolution was achieved.⁶³ Neither a cellulose derivatization nor a complexation takes place with NMMO.⁶⁴ NMMO could form hydrogen bonds between the oxygen of the strong N-O dipoles in NMMO and hydroxyl groups of cellulose, which disrupt the cellulose hydrogen bond system, resulting the dissolution of cellulose.^{65,66} The NMMO/water system has been applied in large scale after overcoming the difficulties in high investment costs and recovery of the expensive solvent.⁵⁹ Now there are some commercial textile fibers from this system, such as Lyocell (Lenzing), Tencel (Courtaulds), Alceru (TITK Rudolstadt), and Newcell (Akzo Nobel). However, two problems are still present in the NMMO process, namely the instability of the solvent and the tendency of the Lyocell fiber towards fibrillation.⁵⁹ The instability of NMMO may cause a safety risk due to its possible spontaneous decomposition⁶⁷ and side reactions may cause consumption of the expensive solvent and can lead to undesired staining of the cellulose regenerated.⁶⁸ Additives such as propargyl gallate⁶⁹ as antioxidant, phosphates,⁷⁰ bases,⁷¹ sterically hindered phenols⁷² or mild reductants⁷³ were suggested to stabilize the solvent. Furthermore, the unique, highly crystalline structure of Lyocell, and weaker lateral links between the crystallites make the fibers undergo localized separation of fibrous elements at the surface, namely fibrillation, mainly under conditions of wet abrasion, which restricts the applications of Lyocell.⁷⁴ Suitable approaches to diminish fibrillation include treatments with NaOH,⁷⁵ use of cross-linking agents or reactive dyes such as divinyl sulphone, 4,6-(p-beta-sulphatoethylsulphonyl)-anilino-1,3,5-triazin-2(1H)-one and the commercial Cibatex AE4425, enzymes and a combination of these methods.⁷⁶

1.2.2 Ionic liquids (ILs)

The first work on dissolution of cellulose in ionic liquids (ILs) was reported by Charles Graenacher in 1934 by applying N-alkylpyridinium salts to dissolve cellulose and as media for homogeneous chemical reactions.⁷⁷ However, the value of dissolution of cellulose with ionic liquids has not been evaluated until 2002, when Rogers' group published a study on the use of comparable salts (1-butyl-3-methylimidazolium chloride (BMIMCl)) to dissolve cellulose⁴⁶. They carried out comprehensive studies on cellulose dissolution in ionic liquids and its regeneration, and successfully prepared cellulose fibers, films and cellulose beads.⁷⁸ Therefore, Rogers won the 2005 US Presidential Green Chemistry Challenge Awards owing to the great contribution in the cellulose field. Furthermore, Zhang and his coworkers have also conducted extensive research in this field and they found 1-alkyl-3-methylimidazolium chloride (AMIMCl) is also a good ionic liquid to dissolve cellulose.⁷⁹ Ionic liquids are a group of new organic salts that exist as liquids at a relatively low temperature (below 100 °C), which have many attractive properties, such as chemical and thermal stability, non-flammability and immeasurably low vapor pressure.²⁴ The very low vapor pressure of them reduces the risk of exposure that is a clear advantage over the use of the classical volatile solvents.⁸⁰ Thus, they are called “green” solvents and have been widely used.⁸¹ Cellulose solubility and the solution properties can be controlled by selection of the ionic liquid constitutes.²⁴ Microwave heating can significantly accelerate its dissolution. Solutions containing up to 25 wt % cellulose can be prepared in BMIMCl under microwave heating.²⁴ The high chloride concentration and activity in BMIMCl, which is assumed highly effective in breaking the extensive hydrogen-bonding network present in cellulose, plays an important role in its dissolution. The presence of water in BMIMCl greatly decreases the solubility of cellulose through competitively hydrogen-bonding.⁴⁶ Cellulose in its BMIMCl solution can be easily precipitated by addition of water, ethanol or acetone.²⁴ By changing regeneration processes, the regenerated cellulose can be in a range of structural forms, such as powder, tube, bead, fiber and film.²⁴ The regenerated cellulose has almost the same degree of polymerization and polydispersity as the initial one, but its morphology is significantly changed and its microfibrils are fused into a relatively homogeneous macrostructure.²⁴

1.3 Aqueous alkali/urea solvent system

1.3.1 Dissolution of cellulose in aqueous alkali/urea system

In recent years, aqueous alkali/urea systems including NaOH/urea and LiOH/urea aqueous solutions pre-cooled to $-12\text{ }^{\circ}\text{C}$ to dissolve cellulose have been developed by Zhang's group.⁴⁸⁻⁵³ Cellulose with weight-average molecular weight (M_w) smaller than 1.2×10^5 could be dissolved in the NaOH/urea aqueous solution within 2 min on a typical laboratory scale and within 5 min even in a dissolution tank of 1000 L capacity (Jiangsu Long-Ma Green Fibers Co. Ltd.).⁸² In fact, several seconds may be required because of the appearance of the Weissenberg phenomenon within a 30-sec time period. It represents the most rapid dissolution of native cellulose, not to mention the speed of the dissolution process.⁸² Usually, the dissolution of normal polymers includes a slow diffusion based on the interchangeability of solvent and polymer, and needs a long time (the heating may accelerate the process).⁸² Moreover, this process is still relatively low-cost and non-polluting because the by-products (mainly urea and Na_2SO_4) can be easily separated and recycled to be reutilized.^{83,84} Compared with the solvents mentioned above, the components of this solvent (NaOH, urea and water) are more common and cheaper.

Zhang et al. demonstrated that NaOH “hydrates” can be easily attracted to cellulose chains through the formation of new hydrogen-bonded networks at low temperatures, while the urea hydrates cannot associate directly with cellulose, but can self-assemble at the surface of the NaOH hydrogen-bonded cellulose to form a worm-like inclusion complex (IC), leading to good dispersion of cellulose. The cellulose dissolution at low temperature arises as a result of a fast dynamic self-assembly process among solvent small molecules (NaOH, urea and water) and the cellulose macromolecules.^{85,86} The solubility of cellulose in LiOH/urea aqueous solution is stronger than that of cellulose in NaOH/urea aqueous solution, in terms of dissolution of celluloses with higher molecular weights and preparation of cellulose solutions with higher cellulose concentrations. The dissolution mechanism and solution properties of cellulose in LiOH/urea system are similar to that in NaOH/urea aqueous system. In LiOH/urea system, a channel IC hosted by urea encages the cellulose macromolecule bonded with LiOH hydrated. The solvent containing Li^+ having relatively small ionic radius and high

charge density more easily penetrates into cellulose than Na^+ ions to be imbibed on the cellulose chain, leading to the relatively stable IC and higher dissolubility of cellulose.^{51,82}

Furthermore, the solubility of cellulose in NaOH/urea solution was improved significantly by the introduction of a small amount of ZnO (0.5 wt %), which existed as $\text{Zn}(\text{OH})_4^{2-}$ in the alkali system.⁸⁶ $\text{Zn}(\text{OH})_4^{2-}$ can probably form stronger (or more stable) hydrogen bonds with cellulose than hydrated NaOH, leading to improvement of the dissolution power of cellulose. Moreover, celluloses with higher molecular weight such as 1.7×10^5 became soluble in the ZnO/NaOH/urea systems, while those are not completely soluble in the NaOH/urea systems without ZnO.^{86,87}

1.3.2 Fibers from aqueous cellulose/alkali/urea system

From the cellulose dope in NaOH/urea system, high-quality cellulose multi-filament fibers were successfully prepared via a pilot machine, and the cellulose fibers had a circular cross-sectional shape (similar to Lyocell) and a smooth surface as well as good mechanical properties.⁴⁹ The novel filaments possessed relatively high tensile strength (~ 330 MPa), with the mechanical properties being close to the commercial viscose rayon.^{49,88} Moreover, the mechanical properties of the novel cellulose filaments can be improved significantly after further optimization of the spinning process with the design and the conditions for the multi-stage draw. It is worth noting that the sulfate content in the novel multifilament fibers is essentially zero, whereas viscose rayon contains about 8 mg/100 g multifilaments.⁸² Thus, the new cellulose fibers can be used to make nonwoven fabrics and greaseproof paper, which are used to wrap snack foods, cookies, candy bars, and tea bags. Furthermore, magnetic nanocomposite fibers by introducing in situ synthesized iron oxide (Fe_2O_3) nanoparticles into the porous structure in the wet cellulose fibers were also prepared.⁸⁹ The magnetic fibers containing Fe_2O_3 with a mean diameter of 18 nm exhibited high mechanical strength, strong capability to absorb UV ray and superparamagnetic properties. Moreover, fiber-like Fe_2O_3 macroporous nanomaterials were obtained by calcinations of Fe_2O_3 /cellulose nanocomposite fibers to remove out cellulose matrix.⁹⁰ The 1D inorganic nanomaterials with retention of the macropore structure and superior electrochemical activities have potential applications in the functional material fields. Fiber-like TiO_2 nanomaterials could also be prepared by in situ

synthesis of TiO₂ nanoparticles in the wet NaOH/urea regenerated cellulose fibers, followed by calcination at 400–800 °C.⁹¹ The mean diameter of the fiberlike TiO₂ nanomaterials consisting of TiO₂ nanoparticles with a mean size from 21 to 37 nm was 7–8 μm.⁹¹ The TiO₂ nanomaterials exhibited different crystallinity phases from anatase to rutile, depending on the calcinating temperature. The photocatalytic activity for the degradation of methyl orange of the anatase fibers calcined at 400 °C was the highest, compared with that at 600 and 800 °C.⁹¹ It provided a simple and “green” pathway for the preparation of inorganic nanomaterials with different crystal structures by using porous regenerated cellulose fiber as the matrix.

1.3.3 Films from aqueous cellulose/alkali/urea system

Novel transparent, flexible regenerated cellulose films were prepared from aqueous NaOH/urea or LiOH/urea solution.^{92–94,83} After kept in soil at 30 °C for 20 days, the cellulose film almost completely decomposed, indicating its good biodegradation caused by the microorganisms.⁸³ Moreover, these cellulose films are safe and stable, therefore, they are promising as the packaging materials.⁸² Furthermore, fluorescent and long after-glow photoluminescent cellulose films were prepared by treating the regenerated cellulose films with fluorescent dyes and blending with photoluminescent (PL) pigments, respectively.⁸³ The photoluminescent cellulose films could absorb light for several minutes and then emits a visible light for more than 10 h in the dark. All-cellulose composite films were prepared from native cellulose nanowhiskers and cellulose matrix regenerated from aqueous NaOH/urea solvent system on the basis of their temperature-dependent solubility.⁹⁵ The cellulose whiskers retained their needlelike morphology with mean length and diameter of 300 nm and 21 nm as well as native crystallinity when added to the latter solution at ambient temperature. The tensile strength of the nanocomposite films could reach 157 MPa through a simple drawing process, with the calculated Hermans’ orientation parameter of 0.30. All-cellulose composite films reinforced with ramie fibers were also prepared using the aqueous NaOH/urea solvent system.⁹⁶ These composite films exhibited high tensile strength, optical transmittance, and thermal stability. They have potential applications as packaging materials because of the “green” production process. Cellulose/corn protein composite films were prepared from NaOH/urea aqueous solutions.⁹⁷ These films exhibited high mechanical

properties (tensile strength of 91 MPa) and high thermal stability (decomposition temperature of 283 °C), when compared with the pure corn protein materials (tensile strength of 10 MPa, decomposition temperature of 179 °C). The results indicated that strong interactions such as multiple hydrogen bonds were formed and existed between cellulose and corn protein molecules in the composite films. In addition, the results of cell culture experiments revealed that the cellulose/corn protein composite films had high performance in cell adhesion and proliferation. Therefore, the cellulose/corn protein films had potential application to such cell scaffold materials.

1.3.4 Spheres from aqueous cellulose/alkali/urea system

Regenerated cellulose microspheres (RCS) with different diameter were fabricated from cellulose solution in NaOH/urea aqueous solvent by sol–gel transition method.⁹⁸ Moreover, novel magnetic cellulose microspheres (MRCS) were also created by in situ synthesis of Fe₃O₄ nanoparticles into the cellulose pore as a reaction micro-chamber.⁹⁸ The Fe₃O₄ nanoparticles with diameter about 20 nm were synthesized from FeCl₃/FeCl₂ aqueous solution by in situ co-precipitation in the cellulose pores. The MRCS microspheres exhibit sensitively magnet induced transference, extremely small hysteresis loop, as well as good adsorption and release capabilities for bovine serum albumin (BSA). The Fe₃O₄ nanoparticles were dispersed uniformly and immobilized in the cellulose matrix, as a result of a strong electrostatic interaction between Fe₃O₄ and the cellulose. The Fe₃O₄ nanoparticles in the cellulose microspheres played important roles in both the creation of the magnetic-induced transference and the improvement of the targeting protein delivery and release.⁹⁸ By blending cellulose with the γ -Fe₂O₃ nanoparticles and activated carbon (AC) in the NaOH/urea aqueous solvent, millimeter-scale magnetic cellulose beads, coded as MCB-AC, were fabricated via an optimal dropping technology.⁹⁹ The cellulose composite beads containing Fe₂O₃ nanoparticles displayed sensitive magnetic response. The MCB-AC sorbent has good adsorption capacity to the dye particles through physical interaction, and the used sorbents can be removed out and recovered easily through a magnetic field.

1.3.5 Hydrogels from aqueous cellulose/alkali/urea system

Transparent cellulose hydrogels were prepared from cellulose/NaOH/urea aqueous solutions by using epichlorohydrin (ECH) as crosslinker.¹⁰⁰ Cellulose hydrogels prepared by heating displayed better light transmittance, higher equilibrium swelling ratios, higher water uptakes and relatively weaker mechanical strength. However, cellulose hydrogels prepared by freezing method had faster swelling rate and higher mechanical strength. To improve the mechanical properties of the cellulose hydrogels, cellulose/polyvinyl alcohol hydrogels were prepared by freezing/throwing method which had dense structure and exhibited high strength and storage modulus.¹⁰¹ Macroporous hydrogels fabricated from cellulose and sodium alginate (SA) in NaOH/urea aqueous system by chemical crosslinking had high swelling ratio.¹⁰² In the hydrogels, SA played an important role on increasing pore size and swelling ratio, whereas cellulose contributed to support the pore wall. Furthermore, novel superabsorbent hydrogels were fabricated by using cellulose as support and carboxymethylcellulose sodium as high hydrophilic polymer, which had superabsorbent capability and high swelling ratio (more than 1000).¹⁰³ The hydrogels were sensitive to inorganic aqueous solution, physical saline water and synthetic urine, showing smart swelling and shrinking behaviors, as well as controlled release of BSA. Strong fluorescent hydrogels were prepared from cellulose and the CdSe/ZnS quantum dots (QDs) in NaOH/urea aqueous system via a mild chemical cross-linking process.¹⁰⁴ The relatively hydrophobic CdSe/ZnS core-shell nanoparticles were dispersed well and embedded firmly in the cellulose matrices through electrostatic attraction and hydrophobic interactions. The cellulose-QDs hydrogels emitted strong fluorescence with different colors of green, greenish-yellow, yellow and red, depending on the size of the CdSe/ZnS nanoparticles, and exhibited relatively high PL quantum yields as well as good transparency and mechanical strength.

1.3.6 Aerogels from aqueous cellulose/alkali/urea system

Highly porous and strong cellulose aerogels were prepared by gelation of cellulose from aqueous alkali/urea solution, followed by drying with supercritical CO₂.⁵² By using supercritical CO₂ drying, the network structure in the hydrogel was well preserved in the aerogel and the aerogels had pore sizes ranging from 10 nm to 40 nm. The cellulose aerogels had large surface areas (400–500 m²g⁻¹). Furthermore, these cellulose aerogels could be used

as supporting medium for metal nanoparticles.⁵³ Silver, gold, and platinum nanoparticles were synthesized in the gel by hydrothermal reduction by cellulose or by added reductant. Both methods gave nanoparticles embedded with high dispersion in cellulose gels. Supercritical CO₂ drying of the metal-carrying gel gave corresponding aerogels with high transmittance, porosity, surface area, moderate thermal stability, and good mechanical strength. The cellulose gels were also used as template for the in situ preparation of cellulose–silica composite aerogels by a sol–gel process from tetraethyl orthosilicate (TEOS), followed by drying with supercritical CO₂.⁵⁰ The resulting composite aerogels retained the mechanical strength and flexibility, large surface area, semi-transparency, and low thermal conductivity of the cellulose aerogels.

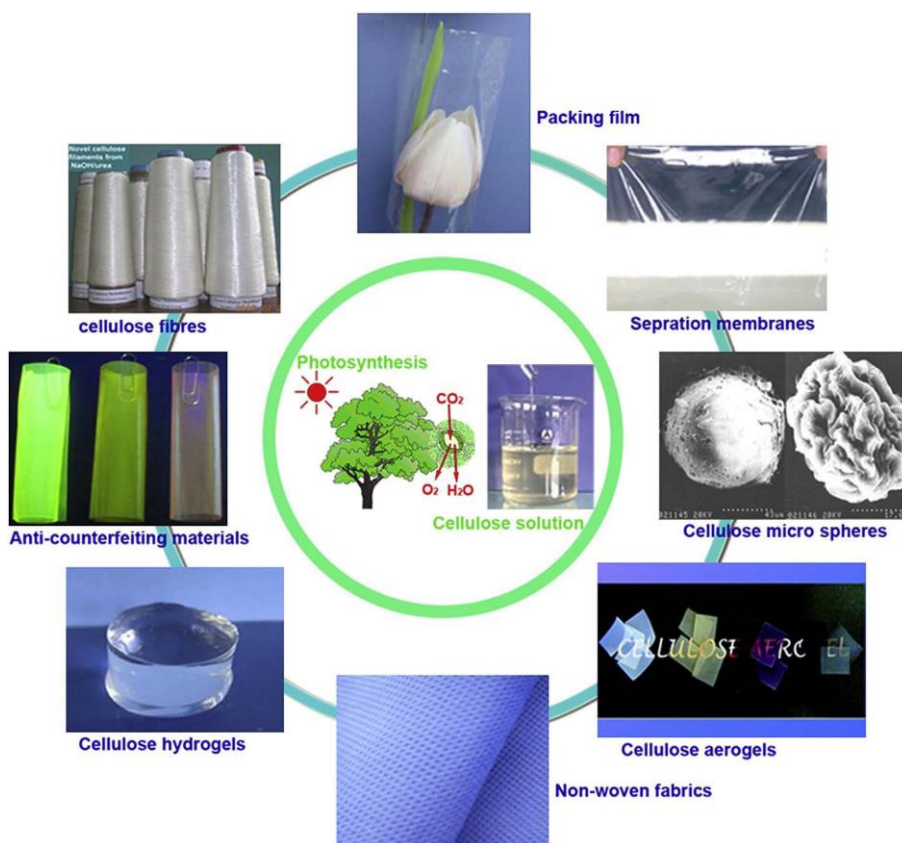


Figure 1.5. Schematic illustration of novel cellulose materials from cellulose/alkali/urea solution.⁸² Reproduction from ref. 82 with permission from Elsevier (© Elsevier 2013).

Figure 1.5 shows schematic illustration of novel cellulose materials from cellulose/alkali/urea solution.⁸² They are promising in the fields of textile, packaging, separation technology, biomedicine, etc.

1.4 Objective of this study

Cellulose is the most abundant natural polymer on earth and the alkali/urea solvents have been developed to dissolve cellulose and produce regenerated cellulose materials. Compared to other newly developed cellulose solvents like ionic liquids and NMMO, this new technique shows great economic advantages. Moreover, it is an environmentally friendly processing without toxic gas emission. It is meaningful to expand potential applications of alkali/urea systems and to deepen related fundamental studies. Recently, high-performance gas barrier materials with high optical transparency, flexibility, mechanical strength, thermal stability, and biodegradability have become a prominent research area of high-tech materials such as flexible organic light-emitting diode (OLED) displays, encapsulation of electronic devices, and high performance packaging materials for food, medicine, etc. Most gas barrier polymer materials are petroleum-derived synthetic polymers that are non-biodegradable and give environmental problems. Therefore, the objective of this work is to do fundamental and applied studies to develop new high-performance cellulose functional materials (cellulose and cellulose-based nano-composites) with good gas barrier properties, hydrophobicity, thermal stability, mechanical strength, and optical transparency from alkali/urea solutions. It is a new route of an advance “green” cellulose technology focusing on its application to produce cellulose functional materials as novel bio-based, fully-degradable, environmentally-friendly, high-performance packaging and optoelectronic display materials. The research and application of the new high-performance cellulose functional materials are very important for a sustainable society. The commercialization of these cellulose products will benefit our future life.

1.5 References

- (1) Klemm, D.; Heublein, B.; Fink, H.-P.; Bohn, A. *Angew. Chem. Int. Ed.* **2005**, *44*, 3358–3393.
- (2) Payen, A.; Hebd, C. R. *Seances Acad. Sci.* **1838**, *7*, 1052.
- (3) Payen, A.; Hebd, C. R. *Seances Acad. Sci.* **1838**, *7*, 1125.
- (4) Hess, K. *Zellst. Pap.* **1938**, *18*, 302–305.
- (5) Brogniart, A.; Pelonze, A. B.; Dumas, R. *Comptes Rendus* **1839**, *8*, 51–53.
- (6) Balsler, K.; Hoppe, L.; Eichler, T.; Wendel, M.; Astheimer, A.-J. *Ullmann's Encyclopedia of Industrial Chemistry*, Vol. A5 (Eds.: Gerhartz, W.; Yamamoto, Y. S.; Campbell, F. T.; Pfefferkorn, R.; Rounsaville, J. F.), VCH, Weinheim, **1986**, pp. 419–459.
- (7) Staudinger, H. *Ber. Dtsch. Chem. Ges.* **1920**, *53*, 1073–1085.
- (8) Nevell, T. P.; Zeronian, S. H. *Ellis Horwood*, Chichester, **1985**, pp. 552.
- (9) Hon, D. N.-S. *Cellulose*, **1994**, *1*, 1–25.
- (10) Ringsdorf, H. *Angew. Chem.* **2004**, *116*, 1082.
- (11) Nakatsubo, F.; Kamitakahara, H.; Hori, M. *J. Am. Chem. Soc.* **1996**, *118*, 1677–1681.
- (12) <http://cell.sites.acs.org/anselmepayenaward.htm>.
- (13) Brett, C. T. *Int. Rev. Cytol.* **2000**, *199*, 161–199.
- (14) Siró, I.; Plackett, D. *Cellulose* **2010**, *17*, 459–494.
- (15) Isogai, A.; Saito, T.; Fukuzumi, H. *Nanoscale*, **2011**, *3*, 71–85.
- (16) Klemm, D.; Philipp, B.; Heinze, T.; Heinze U.; Wagenknecht, W. *Comprehensive Cellulose Chemistry*, Vol, 1, Wiley-VCH Verlag GmbH, **1999**.
- (17) Nehls, L.; Wagenknecht, W.; Philipp, B.; Stscherbina, D. *Prog. Polym. Sci.* **1994**, *19*, 29–78.
- (18) Isogai, A. *Seruroosu no Zairyoukagaku (Material Science of Cellulose)*, The University of Tokyo Ed., **2001**, pp. 2.
- (19) Yamane, C.; Aoyagi, T.; Ago, M.; Sato, K.; Okajima, K.; Takahashi, T. *Polym. J.* **2006**, *38*, 819–826.
- (20) Schurz, J. *Prog. Polym. Sci.* **1999**, *24*, 481–483.

- (21) Eichhorn, S. J.; Young, R. J.; Davies, G. R. *Biomacromolecules* **2005**, *6*, 507–513.
- (22) Medronho, B.; Ramano, Q.; Graca Miguel, M. A.; Stigsson, L.; Lindman, B. *Cellulose* **2012**, *19*, 581–587.
- (23) Glasser, W. G.; Atalla, R. H.; Blackwell, J.; Brown, R. M.; Burchard, W.; French, A. D.; Klemm, D.; Nishiyama, Y. *Cellulose* **2012**, *19*, 589–598.
- (24) Zhu, S.; Wu, Y.; Chen, Q.; Yu, Z.; Wang, C.; Jin, S.; Ding, Y.; Wu, G. *Green Chem.* **2006**, *8*, 325–327.
- (25) Fuchs, R.; Habermann, N.; Klüfers, P. *Angew. Chem. Int. Ed. Engl.* **1993**, *32*, 852–854.
- (26) Burchard, W.; Habermann, N.; Klüfers, P.; Seger, B.; Wilhelm, U. *Angew. Chem. Int. Ed. Engl.* **1994**, *33*, 884–887.
- (27) Burchardt, W.; Habermann, N.; Klüfers, P.; Seger, B.; Wilhelm, U. *Angew. Chem.* **1994**, *106*, 936–939.
- (28) Kamide, K.; Okajima, K.; Matsui, T.; Kowsaka, K. *Polymer J.* **1984**, *16*, 857–866.
- (29) Yamashiki, T.; Kamide, K.; Okajima, K.; Kowsaka, K.; Matsui, T.; Fukase, T. *Polymer J.* 1988, *20*, 447–457.
- (30) Isogai, A. *Cellulose* **1997**, *4*, 99–107.
- (31) Isogai, A.; Atalla, R. H. *Cellulose* **1998**, *5*, 309–319.
- (32) Cuculo, J. A.; Smith, C.; Sangwatanaroj, U.; Stejskal, E.; Sankar, S. *J. Polym. Sci., Part A: Polym. Chem.* **1994**, *32*, 229–239.
- (33) Cuculo, J. A.; Smith, C.; Sangwatanaroj, U.; Stejskal, E.; Sankar, S. *J. Polym. Sci., Part A: Polym. Chem.* **1994**, *32*, 241–247.
- (34) Hattori, M.; Koga, T.; Shimaya, Y.; Saito, M. *Polym. J.* **1998**, *30*, 43–48.
- (35) Hattori, M.; Shimaya, Y.; Saito, M. *Polym. J.* **1998**, *30*, 49–55.
- (36) Chen, L. F. *US Patent* 5290349, **1994**.
- (37) Xu, Q.; Chen, L. F. *J. Appl. Polym. Sci.* **1999**, *71*, 1441–1446.
- (38) McCormick, C. L.; Callais, P. A.; Hutchinson, B. H. *Macromolecules* **1985**, *18*, 2394–2401.
- (39) Dawsey, T. R.; McCormick, C. L. *J. Macromol. Sci., Rev. Macromol. Chem. Phys.* **1990**, *C30*, 405–440.
- (40) Wang, Z.; Liu, S.; Matsumoto, Y.; Kuga, S. *Cellulose* **2012**, *19*, 2, 393–399.

- (41) Wang, Z.; Yokoyama, T.; Chang, H.; Matsumoto, Y. *J. Agric. Food Chem.* **2009**, *57*, 6167–6170.
- (42) Chanzy, H.; Peguy, A. *J. Polym. Sci. Polym. Phys. Ed.* **1980**, *18*, 1137–1144.
- (43) Namikoshi, H. *Japan Kokai Patent* 59-124933, **1984**.
- (44) Fink, H.-P.; Weigel, P.; Purz, H. J.; Ganster, J. *Prog. Polym. Sci.* **2001**, *26*, 1473–1524.
- (45) Schurz, J.; Lenz, J. *Macromol. Symp.* **1994**, *83*, 273–289.
- (46) Swatloski, R. P.; Spear, S. K.; Holbrey, J. D.; Rogers, R. D. *J. Am. Chem. Soc.* **2002**, *124*, 4974–4975.
- (47) Kosan, B.; Michels, C.; Meister, F. *Cellulose* **2008**, *15*, 59–66.
- (48) Cai, J.; Zhang, L. *Macromol. Biosci.* **2005**, *5*, 539–548.
- (49) Cai, J.; Zhang, L.; Zhou, J.; Qi, H.; Chen, H.; Kondo, T.; Chen, X.; Chu, B. *Adv. Mater.* **2007**, *19*, 821–825.
- (50) Cai, J.; Liu, S.; Feng, J.; Kimura, S.; Wada, M.; Kuga, S.; Zhang, L. *Angew. Chem. Int. Ed.* **2012**, *51*, 2076–2079.
- (51) Cai, J.; Zhang, L.; Chang, C.; Cheng, G.; Chen, X.; Chu, B. *ChemPhysChem* **2007**, *8*, 1572–1579.
- (52) Cai, J.; Kimura, S.; Wada, M.; Kuga, S.; Zhang, L. *ChemSusChem* **2008**, *1*, 149–154.
- (53) Cai, J.; Kimura, S.; Wada, M.; Kuga, S. *Biomacromolecules* **2009**, *10*, 87–94.
- (54) Ruan, D.; Zhang, L.; Lue, A.; Zhou, J.; Chen, H.; Chen, X.; Chu, B.; Kondo, T. *Macromol. Rapid Commun.* **2006**, *27*, 1495–1500.
- (55) MacDonald, D. M. *Solvent spun rayon, modified cellulose fibers and derivatives*, Turbak, A. F. Ed., American Chemical Society, Washington, DC, **1977**, pp. 25–39.
- (56) Hummer, R. B.; Turbak, A. F. *Solvent spun rayon, modified cellulose fibers and derivatives*, Turbak, A. F. Ed., American Chemical Society, Washington, DC, 1977, pp. 44–51.
- (57) Hudson, S.; Cuculo, J. *J. Polym. Sci. Polym. Chem. Ed.* **1980**, *18*, 3469–3481.
- (58) Hyden, W. L. *Ind. Eng. Chem.* **1929**, *21*, 405–410.
- (59) Liebert, T. *Cellulose Solvents: For Analysis, Shaping and Chemical Modification*, ACS Symposium Series, Vol. 1033, American Chemical Society: Washington, DC, **2010**.
- (60) Johnson, D. L. *US Patent* 3,447,939, **1969**.

- (61) Johnson, D. L. *US Patent* 3,508,941, **1970**.
- (62) Zimmermann R. L. *US patent* 5,216,154, assigned to Texaco Chemical Company.
- (63) McCorsley, C. C.; Varga, J. K. *US Patent* 4,142,913, **1979**.
- (64) Gagnaire, D.; Mancier, D.; Vincendon, M. *J. Polym. Sci. Polym. Chem. Ed.* **1980**, *18*, 13–25.
- (65) Chanzy, H.; Nawrot, S.; Peguy, A.; Smith, P. *J. Polym. Sci., Polym. Phys. Ed.* **1982**, *20*, 1909–1924.
- (66) Berger, W.; Keck, M.; Philipp, B. *Cell Chem Technol* **1988**, *22*, 387–397.
- (67) Konkin, A.; Wendler, F.; Meister, F.; Roth, H.-K.; Aganov, A. O. *Ambacher Spectroch. Acta Part A: Mol. Biomol. Spectr.* **2008**, *69*, 1053.
- (68) Rosenau, T.; Potthast, A.; Sixta, H.; Kosma, P. *Prog. Polym. Sci.* **2001**, *26*, 1763.
- (69) Brandner, A.; Zengel, H. G. *German Patent* DE 3,034,685, **1980**.
- (70) Laity, P. R. *PCT Int. Appl.* 8,304,415, **1993**.
- (71) Reusche, F. H.; Schoen, P.; Wiesener, W.; Taeger, E.; Schleicher, H.; Lukanoff, B. *German Patent* 218104, **1985**.
- (72) Michels, C.; Mertel, H. *German Patent* 229708, **1985**.
- (73) Lukanoff, B.; Schleicher, H. *German Patent* 158656, **1983**.
- (74) Karypidis, M.; Wilding, M. A.; Carr, C. M.; Lewis, D. M. *AATCC Rev.* **2001**, *1*, 40.
- (75) Goswami, P.; Blackburn, R.; El-Dessouky, H. M.; Taylor, J.; White, P. *Eur. Polym. J.* **2009**, *45*, 455.
- (76) Zhang, W.; Okubayashi, S.; Badura, W. *J. Appl. Polym. Sci.* **2006**, *100*, 1176.
- (77) Graenacher, C. *US Patent* 1,943,176, **1934**.
- (78) Gutowski, K.; Broker, G.; Willauer, H.; Huddleston, J.; Swatloski, R.; Holbrey, J.; Rogers, R. *J. Am. Chem. Soc.* **2003**, *125*, 6632–6633.
- (79) Zhang, H.; Wu, J.; Zhang, J.; He, J. S. *Macromolecules* **2005**, *38*, 8272–8277.
- (80) Zakrzewska, M. E.; Bogel-Lukasik, E.; Bogel-Lukasik, R. *Energy Fuels* **2010**, *24*, 737–745.
- (81) Seddon, K. R. *J. Chem. Technol. Biotechnol.* **1997**, *68*, 351–356.
- (82) Luo X.; Zhang, L. *Food Res. Int.* **2013**, *52*, 387–400.
- (83) Qi, H.; Chang, C.; Zhang, L. *Green Chem.* **2009**, *11*, 177–184.

- (84) Li, R.; Chang, C.; Zhou, J.; Zhang, L.; Gu, W.; Li, C.; Liu, S.; Kuga, S. *Ind. Eng. Chem. Res.* **2010**, *49*, 11380–11384.
- (85) Cai, J.; Zhang, L.; Liu, S.; Liu, Y.; Xu, X.; Chen, X.; Chu, B.; Guo, X.; Xu, J.; Cheng, H.; Han, C. C.; Kuga, S. *Macromolecules* **2008**, *41*, 9345–9351.
- (86) Yang, Q.; Qi, H.; Lue, A.; Hu, K.; Cheng, G.; Zhang, L. *Carbohydr. Polym.* **2011**, *83*, 1185–1191.
- (87) Yang, Q.; Qin, X.; Zhang, L. *Cellulose* **2011**, *18*, 681–688.
- (88) Qi, H.; Cai, J.; Zhang, L.; Nishiyama, Y.; Rattaz, A. *Cellulose* **2008**, *15*, 81–89.
- (89) Liu, S.; Zhang, L.; Zhou, J.; Wu, R. *J. Phys. Chem. C* **2008**, *112*, 4538–4544.
- (90) Liu, S.; Zhang, L.; Zhou, J.; Xiang, J.; Sun, J.; Guan, J. *Chem. Mater.* **2008**, *20*, 3623–3628.
- (91) Zeng, J.; Li, R.; Liu, S.; Zhang, L. *ACS Appl. Mater. Interfaces* **2011**, *3*, 2074–2079.
- (92) Mao, Y.; Zhou, J.; Cai, J.; Zhang, L. *J. Membr. Sci.* **2006**, *279*, 246–255.
- (93) Cai, J.; Wang, L.; Zhang, L. *Cellulose* **2007**, *14*, 205–215.
- (94) Liu, S.; Zhang, L. *Cellulose* **2009**, *16*, 189–198.
- (95) Qi, H.; Cai, J.; Zhang, L.; Kuga, S. *Biomacromolecules* **2009**, *10*, 1597–1602.
- (96) Yang, Q.; Lue, A.; Zhang, L. *Compos. Sci. Technol.* **2010**, *70*, 2319–2324.
- (97) Yang, Q.; Lue, A.; Qi, H.; Sun, Y.; Zhang, X.; Zhang, L. *Macromol. Biosci.* **2009**, *9*, 849–856.
- (98) Luo, X.; Liu, S.; Zhou, J.; Zhang, L. *J. Mater. Chem.* **2009**, *19*, 3538–3545.
- (99) Luo, X.; Zhang, L. *J. Hazard. Mater.* **2009**, *171*, 340–347.
- (100) Chang, C.; Zhang, L.; Zhou, J.; Zhang, L.; Kennedy, J. F. *Carbohydr. Polym.* **2010**, *82*, 122–127.
- (101) Chang, C.; Lue, A.; Zhang, L. *Macromol. Chem. Phys.* **2008**, *209*, 1266–1273.
- (102) Chang, C.; Duan, B.; Cai, J.; Zhang, L. *Eur. Polym. J.* **2010**, *46*, 92–100.
- (103) Chang, C.; Duan, B.; Zhang, L. *Polymer* **2009**, *50*, 5467–5473.
- (104) Chang, C.; Peng, J.; Zhang, L.; Pang, D. W. *J. Mater. Chem.* **2009**, *19*, 7771–7776.

Chapter 2

High Gas Barrier Cellulose Films Fabricated from Aqueous Alkali/Urea Solutions

2.1 Introduction

High-performance films with high flexibility, optical transparency, thermal stability, mechanical strength, biodegradability, and gas barrier properties are in great demand for a wide range of applications.¹⁻⁵ The gas barrier properties are particularly important because ingress of even very small amounts of oxygen causes most products to deteriorate.⁶⁻⁹ Petroleum-derived synthetic polymers such as poly(vinylidene chloride), ethylene vinyl alcohol copolymer, nylon, and polymers with vapor-deposited coatings have been extensively used as gas barrier films for food, medicine, and electronic packaging.^{2,10} Most plastic packaging films are discarded as burnable waste or used as landfill after use. This causes environmental problems because such synthetic polymers are not biodegradable or carbon neutral.¹¹ Therefore, there is a growing demand to develop new bio-based, high-performance packaging materials.¹² Various cellulose¹³⁻¹⁷ and hemicellulose¹⁸⁻²¹ films have been studied as bio-based oxygen barrier materials. Some of the films have quite low oxygen transmission rates, which are explained in terms of abundant hydrogen bonds formed in the films and hence small free volumes.²²

Commercial films of regenerated cellulose (i.e., cellophane) are transparent, durable, bendable, and impervious to air, grease, bacteria, and dirt.¹³ However, cellophane is prepared through the viscose route that inevitably generates hazardous byproducts (CS₂ and H₂S) during manufacture and in post-treatment processes, resulting in serious pollution. Thus, N-methylmorpholine-N-oxide hydrate (NMMO),^{23,24} ionic liquids,²⁵⁻²⁷ and aqueous NaOH solutions²⁸ have been developed as alternative cellulose solvent systems to prepare new regenerated cellulose films and fibers, and the related fundamental and application studies have been extensively carried out.²⁹

In recent years, safe and low-cost alkali/urea solvents (AU) have been developed for producing regenerated cellulose materials without producing any hazardous byproducts.^{30,31} They can readily dissolve even highly crystalline cellulose without significant degradation. New cellulose multifilament fibers,³² films,^{33–38} and porous aerogels³⁹ have been prepared from the cellulose dopes. These cellulose materials possess a wide range of mechanical properties, excellent thermal stabilities, and high biodegradabilities due to the nature of cellulose.

In the present chapter⁴⁰, I found that transparent and bendable cellulose films prepared from aqueous alkali/urea/cellulose solutions (AUC) exhibit high oxygen barrier properties. The oxygen barrier properties of these AUC films are significantly superior to those of commercial cellophane or synthetic polymer films used as oxygen barriers such as poly(vinylidene chloride) and poly(vinyl alcohol). Series of these AUC films were prepared by varying the regeneration bath components, regeneration temperature, cellulose raw material, and cellulose concentration of the solutions. They were then characterized primarily in terms of oxygen permeability and density.

2.2 Experimental Section

2.2.1 Materials

Filter paper pulp (FP, highly purified cotton linters, Advantec Co., Ltd., Japan), Whatman CF11 microcrystalline cellulose powder (Whatman International Ltd., UK), another cotton linters pulp (CP, Hubei Chemical Fiber Co. Ltd., China), and softwood bleached kraft pulp (SBKP, Nippon Paper Industries Co., Ltd.) were used as cellulose samples. Viscosity-average molecular weights of FP, CF11, CP, and SBKP were determined to be 8.6×10^4 , 3.6×10^4 , 10.0×10^4 , and 19.4×10^4 g mol⁻¹, respectively.^{39,41} Commercial cellophane containing glycerol as a plasticizer was kindly provided by Rengo Co., Ltd., Japan. All reagents and solvents were laboratory grade and were purchased from Wako Pure Chemical Industries, Ltd.; they were used as received.

2.2.2 Preparation of films

The solvent mixture, NaOH/urea/H₂O with a weight ratio of 7:12:81 or LiOH/urea/H₂O with a weight ratio of 4.6:15:80.4 was precooled at -12 °C. The desired amount of cellulose was dispersed in the precooled solvent and the mixture was vigorously stirred for 2 min. It formed a transparent and viscous solution. The cellulose solution thus obtained was centrifuged to degas and remove the remaining undissolved fractions, spread on a glass plate as a 0.5 mm thick layer, and then immersed in a coagulation bath for regeneration. The regeneration bath solutions and conditions varied as follows: 5 wt % H₂SO₄ at 0–60 °C for 5 min, 5 wt % H₂SO₄ containing 5 wt % Na₂SO₄ at 20 °C for 5 min, EtOH at 20 °C for 30 min, *t*-BuOH at 20 °C for 30 min, and acetone at 0–20 °C for 30 min. These regeneration baths were selected to prepare regenerated cellulose films with different densities. The sheet-like hydrogel of regenerated cellulose was thoroughly washed with deionized water by soaking, fixed on a poly(methyl methacrylate) plate with adhesive tapes to prevent shrinkage, and air dried at ambient temperature.³³ The air-dried AUC films were further dried in a desiccator containing phosphorus pentoxide at room temperature and 0% relative humidity (RH) for at least for 3 days.

2.2.3 Characterizations

The film thickness was measured by a micrometer, and each value was expressed as an average of five measurements for different position. Thicknesses of the AUC films ranged from 30 to 60 μm, depending on the cellulose concentration in the solutions and regeneration conditions used. Statistical errors in thickness of each film were within ±3%. The density (ρ) of the dried cellulose film was determined from the area, thickness, and dry weight. The oxygen and water vapor permeability rates of the cellulose films were respectively determined at 23 °C and 37.8 °C using a Mocon Ox-Tran Model 2/21MH and a Mocon Permatran-W Model 1/50G (Modern Controls Inc., US) under standard conditions (ASTM 3985). Each measurement was continued until the O₂ or water vapor permeability rate reached a stable value. X-ray diffraction patterns of the films were acquired in reflection mode using a Rigaku RINT 2000 with monochromator-filtered Cu K α radiation ($\lambda = 0.15418$ nm) at 40 kV and 40 mA. The crystallinities of the cellulose samples were estimated from the areas of diffraction

peaks obtained using the Lorentz peak separation method.⁴² The optical transmittances of the films were measured from 200 to 900 nm using a Shimadzu UV-1700 UV-Vis spectrophotometer. Tensile tests were performed using a Shimadzu EZ-TEST instrument equipped with a 500 N load cell. Rectangular strips 2×30 mm in size were cut from the cellulose films and tested with a span length of 10 mm at a rate of 1.0 mm min⁻¹. Cellulose films were conditioned at 23 °C and 50% RH for 2 days and the moisture contents under these conditions were calculated from the film weights before and after heating at 105 °C for 3 h.

2.3 Results and Discussion

2.3.1 Characteristics of AUC films

The first step involved preparing regenerated cellulose films from aqueous AU solutions under various conditions and characterizing the obtained films (Table 2.1). Because the FP cellulose gave regenerated cellulose hydrogels and films with better mechanical and optical properties than others, we primarily used FP as the cellulose raw material in this study. Table 2.1 also lists the oxygen permeabilities of the AUC films at 0% RH. The oxygen permeabilities of the AUC films varied depending on the dissolution and regeneration conditions. The lowest oxygen permeability of 0.003 ml $\mu\text{m m}^{-2} \text{day}^{-1} \text{kPa}^{-1}$ was achieved for the film prepared from a 6 wt % cellulose solution in LiOH/urea/H₂O by regeneration with acetone at 0 °C; this oxygen permeability is one order of magnitude lower than that of cellophane. No plastic films have been reported to have comparable oxygen permeability to this AUC film. For example, high-density poly(ethylene), poly(ethylene terephthalate), nylon-6, poly(vinylidene chloride), and poly(vinyl alcohol) have oxygen permeabilities of respectively 500, 8, 6, 0.4, and 0.04 ml $\mu\text{m m}^{-2} \text{day}^{-1} \text{kPa}^{-1}$ at 0% RH.⁴³ Moreover, the AUC films have high optical transparencies, reasonable bendability, and high mechanical strengths (Figures 2.1 and 2.2). The cellulose film prepared from a 5 wt % FP cellulose solution in NaOH/urea/H₂O by regeneration with 5 wt % H₂SO₄ at 0 °C had a tensile strength of 150 MPa, a Young's modulus of 6 GPa, and an elongation at break of 12 %.

Table 2.1. Preparation conditions of AUC films and characteristics of them.^a Reproduction from ref. 40 with permission from American Chemical Society (© American Chemical Society 2011).

Solvent	Cellulose source	C (wt %)	Regeneration bath	<i>T</i> (°C)	Density (g cm ⁻³)	Oxygen permeability (ml μm m ⁻² day ⁻¹ kPa ⁻¹)
NaOH/urea	FP	5	5% H ₂ SO ₄	0	1.54	0.0058
NaOH/urea	FP	5	5% H ₂ SO ₄	20	1.40	0.0185
NaOH/urea	FP	5	5% H ₂ SO ₄	60	1.35	0.0304
NaOH/urea	FP	5	5% H ₂ SO ₄ and 5% Na ₂ SO ₄	20	1.45	0.0140
LiOH/urea	FP	3	5% H ₂ SO ₄ and 5% Na ₂ SO ₄	20	1.39	0.0296
LiOH/urea	FP	4	5% H ₂ SO ₄ and 5% Na ₂ SO ₄	20	1.43	0.0153
LiOH/urea	FP	5	5% H ₂ SO ₄ and 5% Na ₂ SO ₄	20	1.44	0.0137
LiOH/urea	FP	6	5% H ₂ SO ₄ and 5% Na ₂ SO ₄	20	1.45	0.0124
LiOH/urea	FP	6	EtOH	20	1.49	0.0109
LiOH/urea	FP	6	<i>t</i> -BuOH	20	1.51	0.0084
LiOH/urea	FP	6	Acetone	20	1.55	0.0045
LiOH/urea	FP	6	Acetone	0	1.55	0.0033
LiOH/urea	CF11	6	5% H ₂ SO ₄ and 5% Na ₂ SO ₄	20	1.38	0.0196
LiOH/urea	CP	4	5% H ₂ SO ₄ and 5% Na ₂ SO ₄	20	1.44	0.0149
LiOH/urea	SBKP	4	5% H ₂ SO ₄ and 5% Na ₂ SO ₄	20	1.45	0.0145
Cellophane	–	–	–	–	1.35	0.0481

^a FP: filter paper pulp, CF11: cellulose powder, CP: cotton linters pulp, SBKP: softwood bleached kraft pulp. *C* is cellulose concentration in the AU solution. *T* is the temperature of the regeneration bath. Oxygen permeabilities of the films were measured at 0% RH.

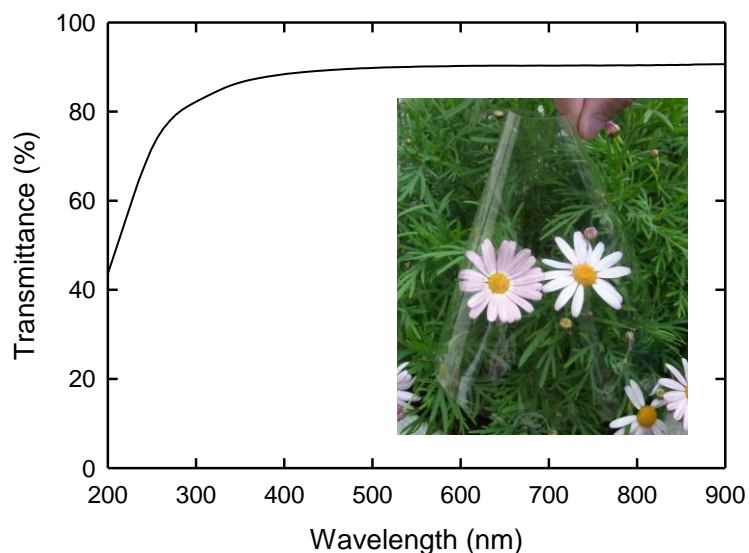


Figure 2.1. UV-Vis transmittance and appearance of an approximately 50 μm thick cellulose film prepared from 5 wt % FP cellulose solution in NaOH/urea/ H_2O by regeneration with 5 wt % H_2SO_4 at 0 $^\circ\text{C}$. Reproduction from ref. 40 with permission from American Chemical Society (© American Chemical Society 2011).

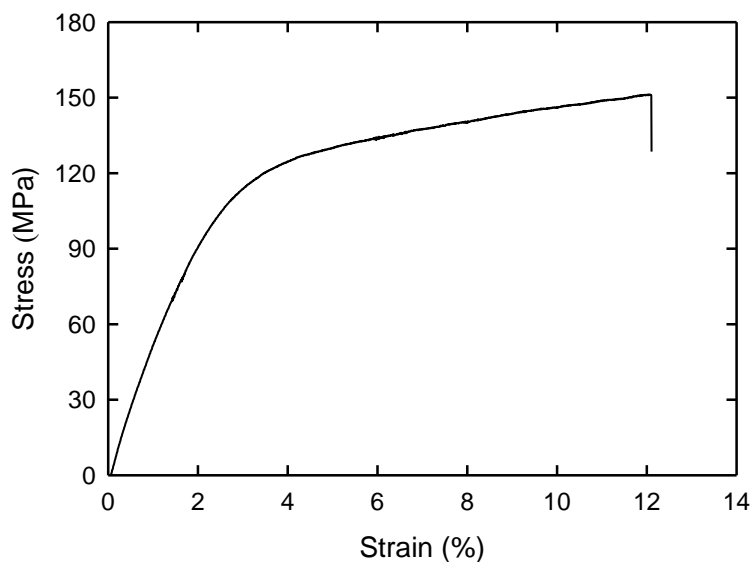


Figure 2.2. Stress-strain curve of cellulose film prepared from 5 wt % FP cellulose solution in NaOH/urea/ H_2O by regeneration with 5 wt % H_2SO_4 at 0 $^\circ\text{C}$. Reproduction from ref. 40 with permission from American Chemical Society (© American Chemical Society 2011).

2.3.2 Oxygen permeabilities of AUC films

Figure 2.3 shows the effect of regeneration bath temperature of 5 wt % H_2SO_4 on oxygen permeabilities and densities of cellulose films prepared from 5 wt % FP solution in $\text{NaOH}/\text{urea}/\text{H}_2\text{O}$. The oxygen permeability decreased drastically from 0.03 to $0.006 \text{ ml } \mu\text{m m}^{-2} \text{ day}^{-1} \text{ kPa}^{-1}$ when the regeneration bath temperature was reduced from 60 to $0 \text{ }^\circ\text{C}$. This reduction in the oxygen permeability is explained by the increased density of the AUC films: the densities increased from 1.35 to 1.54 g cm^{-3} when the regeneration bath temperature was reduced from 60 to $0 \text{ }^\circ\text{C}$, which is inversely correlated to that of the oxygen permeability. The regeneration of cellulose at high temperatures is likely to form a more robust network of cellulose chains or a stiffer physical hydrogel,⁴⁴ leading to the low density of the AUC film obtained by drying the regenerated hydrogel.

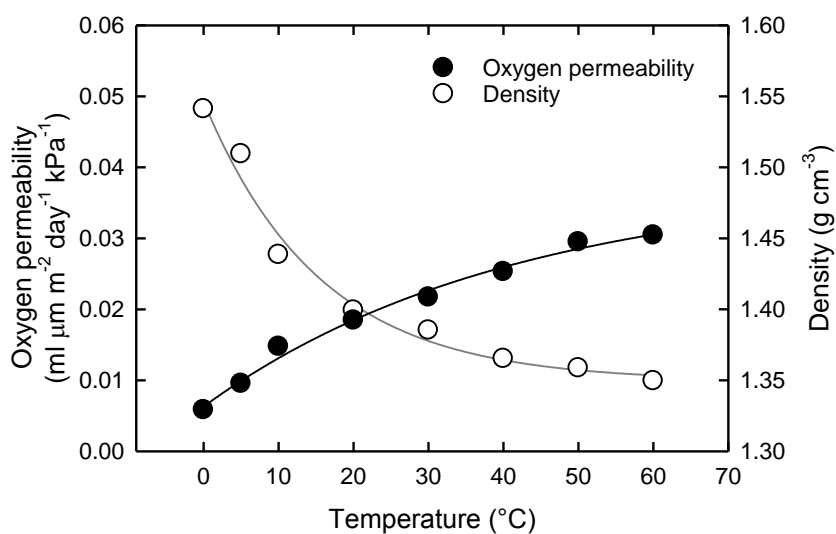


Figure 2.3. Effect of temperature of regeneration bath of 5 wt % H_2SO_4 on oxygen permeabilities and densities of cellulose films prepared from 5 wt % FP cellulose solution in $\text{NaOH}/\text{urea}/\text{H}_2\text{O}$. Reproduction from ref. 40 with permission from American Chemical Society (© American Chemical Society 2011).

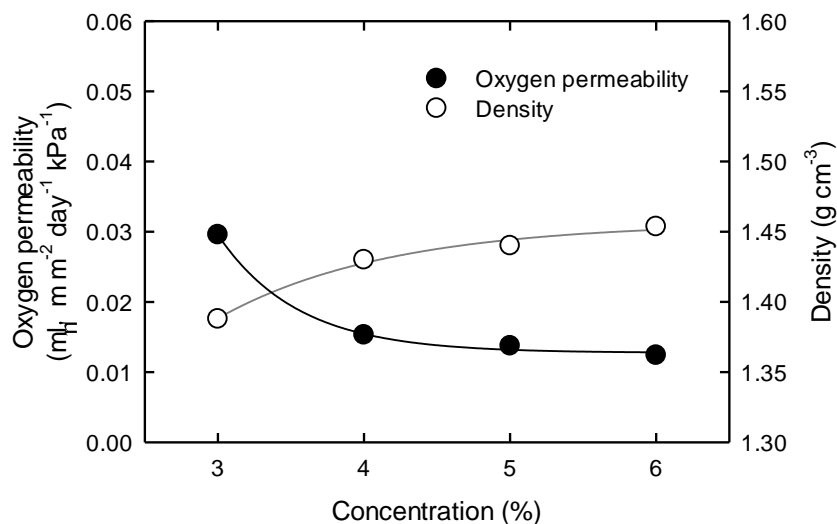


Figure 2.4. Effects of FP cellulose concentration of LiOH/urea/H₂O solutions on oxygen permeabilities and densities of cellulose films prepared from solutions by regeneration with 5 wt % H₂SO₄/5 wt % Na₂SO₄ at 20 °C. Reproduction from ref. 40 with permission from American Chemical Society (© American Chemical Society 2011).

Figure 2.4 depicts the effect of FP cellulose concentration in LiOH/urea/H₂O solutions on oxygen permeabilities and densities of cellulose films prepared from the solutions by regeneration with 5 wt % H₂SO₄/5 wt % Na₂SO₄. In this case, the regeneration temperature was fixed at 20 °C. The oxygen permeability of the AUC films decreased from 0.03 to 0.012 ml μm m⁻² day⁻¹ kPa⁻¹ when the cellulose concentration was increased from 3 to 6 wt %. Correspondingly, the density of the AUC films increased from 1.39 to 1.45 g cm⁻³. This is the same trend as that shown in Figure 2.3; the oxygen permeability of the AUC films decreases with increasing film density. The results of Figures 2.3 and 2.4 demonstrate that regeneration of cellulose at lower temperatures from higher concentration solutions produce AUC films with lower oxygen permeabilities. Note that it was difficult to form flat, smooth films from solutions with cellulose concentrations below 2 wt %. Moreover, the FP cellulose could not be dissolved completely, when the cellulose concentrations were higher than 6 wt %; this low

upper-limit of cellulose concentrations would be one of the shortcomings of AU solutions in practical applications.

As shown in Table 2.1, the oxygen permeability of the AUC films could be further reduced by appropriate selection of the regeneration bath. When ethanol (EtOH), *t*-butanol (*t*-BuOH), or acetone was used as the regeneration bath, the oxygen permeability of the films further decreased to 0.003–0.01 ml $\mu\text{m m}^{-2} \text{day}^{-1} \text{kPa}^{-1}$. These films also had higher densities than the other films. The difference in the densities of the cellulose films prepared from the same AU solutions but under different regeneration conditions is probably due to different diffusion rates of the regeneration solvent into the cellulose solution;^{45–48} a lower diffusion rate or a longer regeneration time produces more homogeneous hydrogels, resulting in AUC films with higher densities. To be more precise, when aqueous H_2SO_4 or $\text{H}_2\text{SO}_4/\text{Na}_2\text{SO}_4$ solutions were used as the regeneration bath, neutralization of the cellulose/alkali/urea solution induces more rapid regeneration of cellulose. The lower regeneration bath temperature probably reduces the exchange rate from the cellulose solvent components to the regeneration bath components in cellulose hydrogels, which may have brought about the higher density of the AUC films. In addition, solvent exchange from the AU solution to an organic solvent such as *t*-BuOH or acetone may have resulted in longer cellulose regeneration than neutralization with an aqueous H_2SO_4 or $\text{H}_2\text{SO}_4/\text{Na}_2\text{SO}_4$ solution.

No obvious differences in the oxygen permeabilities were observed for cellulose films fabricated using other solvent systems (i.e., NaOH/urea and LiOH/urea solutions). The effect of different cellulose raw materials on oxygen permeability of the obtained AUC films was also not clear, although mechanical and optical properties of AUC hydrogels and films were different between cellulose raw materials. Thus, the film density is the primary factor influencing oxygen barrier properties.

Figure 2.5 shows the relationship between the densities of the AUC films and their oxygen permeabilities at 0% RH. The oxygen permeability of the AUC films is inversely proportional to the density, irrespective of the preparation conditions of the cellulose solutions or their regeneration conditions. The AUC films with higher densities have smaller spaces for oxygen molecules to penetrate, resulting in lower oxygen permeabilities. The oxygen permeability of cellophane is also plotted in Figure 2.5; it clearly deviates from the linear

relationship of the AUC films. This indicates that cellophane has different structures from those of the AUC films even at the same density and that oxygen molecules can penetrate cellophane more easily.

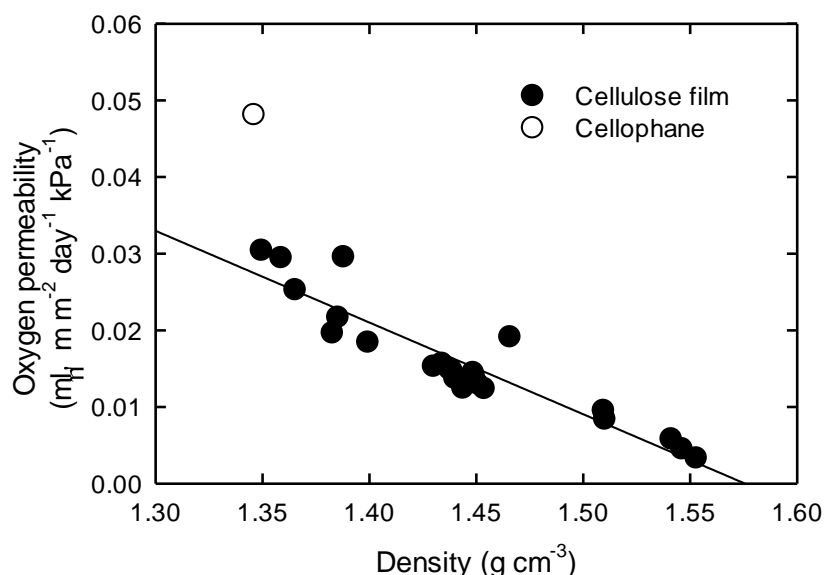


Figure 2.5. Relationship between densities and oxygen permeabilities of cellulose films prepared from cellulose/alkali/urea/H₂O solutions under various conditions. The value for cellophane is also plotted for comparison. Reproduction from ref. 40 with permission from American Chemical Society (© American Chemical Society 2011).

X-ray diffraction analysis (Figure 2.6) revealed that the AUC films and cellophane had the same crystal structure of cellulose II but different crystallinity indices. All AUC films had similar crystallinity indices of 0.50–0.52 regardless of the regeneration conditions, while they had clearly different densities from 1.35 to 1.55 g cm⁻³ (Table 2.1). Thus, porous structures or free volumes of disordered regions are probably different between the AUC films, resulting in the different film densities and consequently different oxygen barrier properties in Figure 2.5. On the other hand, the crystallinity index of cellophane was as low as 0.37 even at the film

density of 1.35 g cm^{-3} . The high crystallinities of the AUC films might have been responsible for their high oxygen barrier properties.¹⁰ In addition, the presence of plasticizer and higher hemicellulose content for the commercial cellophane may have resulted in its low oxygen barrier properties.

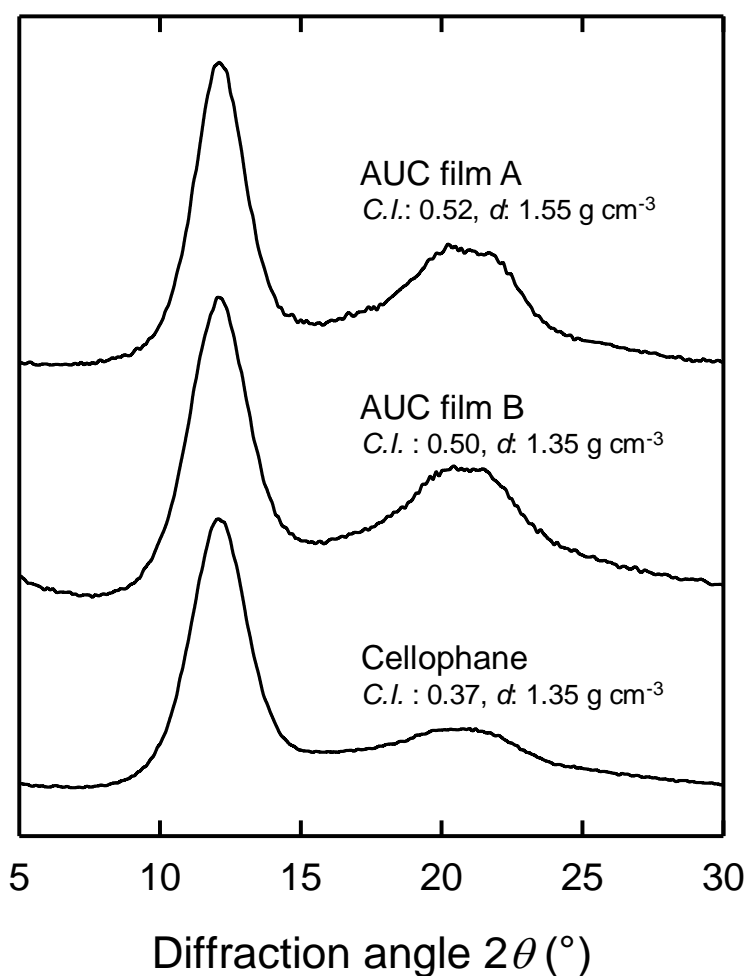


Figure 2.6. XRD patterns of AUC films prepared from 6 wt % FP cellulose solution by regeneration with acetone at 20°C (AUC film A), from 5 wt % FP cellulose solution by regeneration with 5 wt % H_2SO_4 at 60°C (AUC film B), and that of cellophane. C.I.: crystallinity index; d : density. Reproduction from ref. 40 with permission from American Chemical Society (© American Chemical Society 2011).

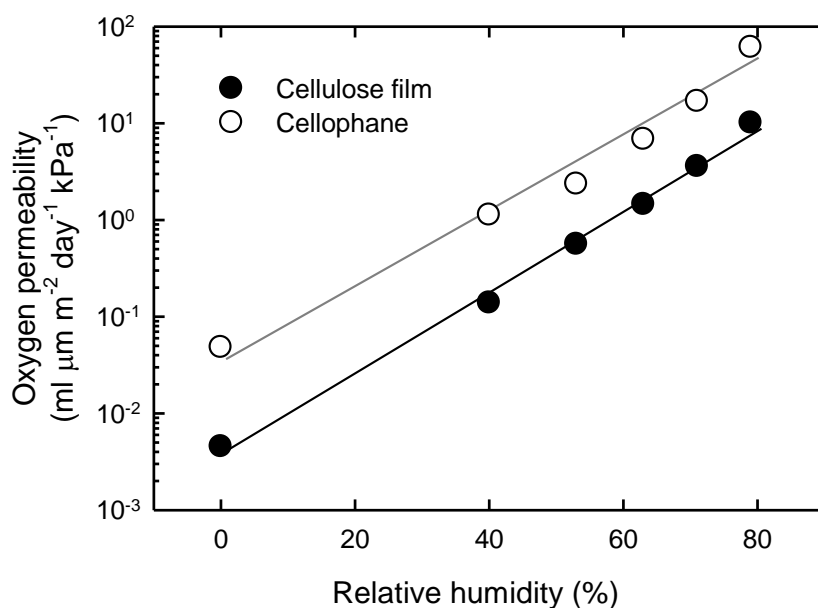


Figure 2.7. Effects of relative humidity on oxygen permeabilities of AUC film and cellophane. The AUC film was prepared from 6 wt % FP cellulose solution in LiOH/urea/H₂O by regeneration with acetone at 20 °C. Reproduction from ref. 40 with permission from American Chemical Society (© American Chemical Society 2011).

2.3.3 Oxygen permeability of AUC films under humid conditions

Figure 2.7 shows the oxygen permeabilities measured at various RH for cellophane and a cellulose film prepared from a 6 wt % FP cellulose solution in LiOH/urea/H₂O by regeneration with acetone at 20 °C. The oxygen permeability of the AUC film was always approximately one order of magnitude lower than that of cellophane over the entire RH range. The oxygen permeabilities of the AUC film remained almost parallel with those of cellophane with increasing RH. Cellulosic materials generally absorb moisture because cellulose molecules have many hydroxyl groups. This hydrophilicity of cellulose results in greater amounts of moisture sorption under higher RH conditions, and thus promotes dissolution of more oxygen molecules in moisture sorption on cellulose films, leading to a significant increase in the oxygen permeability. Furthermore, the increase in free volume accompanied

with the increased swelling of the films may also have led to the increase in the oxygen permeability with increased RH. A similar increase in oxygen permeability has been observed for poly(vinyl alcohol) and ethylene vinyl alcohol copolymer, which are used as oxygen barrier films in practical applications.⁴⁹ The AUC films were also found to have substantially lower water vapor permeabilities than cellophane over the entire RH range; the water vapor permeabilities of the AUC films remained almost parallel with those of cellophane with increasing RH (Figure 2.8).

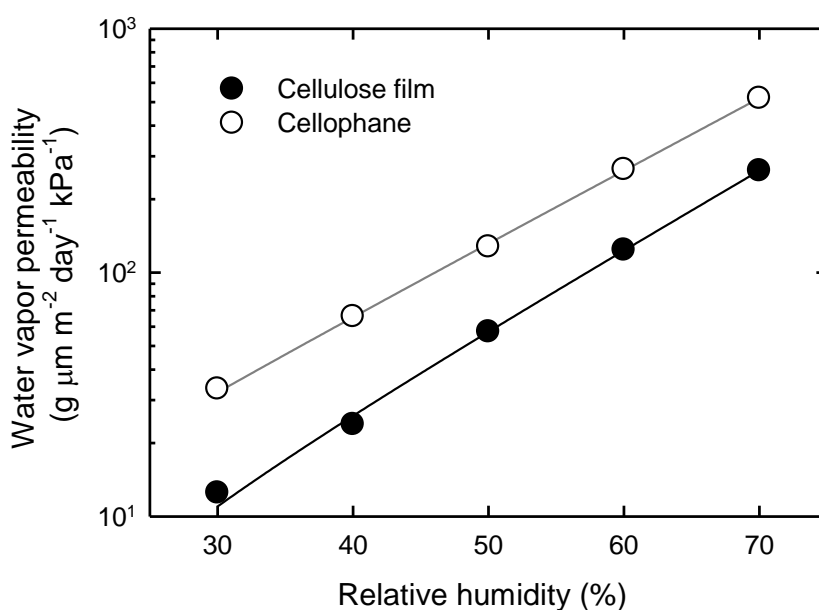


Figure 2.8. Effects of relative humidity on water vapor permeabilities of AUC and cellophane. The AUC film was prepared from 6 wt % FP cellulose solution in LiOH/urea/H₂O by regeneration with acetone at 20 °C. Reproduction from ref. 40 with permission from American Chemical Society (© American Chemical Society 2011).

The moisture contents of the AUC films are inversely proportional to their densities, irrespective of the preparation conditions of the cellulose solutions in alkali/urea/H₂O or the

regeneration conditions; the higher the density is, the lower the moisture content the AUC films have at the same RH. (Figure 2.9). The moisture content of cellophane is also plotted in Figure 2.9. This value was clearly higher than those of the AUC films at the same film density probably because cellophane had lower crystallinity index (Figure 2.6) and contained a plasticizer. It is advantageous that the cellulose films prepared from cellulose solutions in alkali/urea/H₂O systems have lower oxygen and water vapor permeabilities than cellophane over the entire RH range.

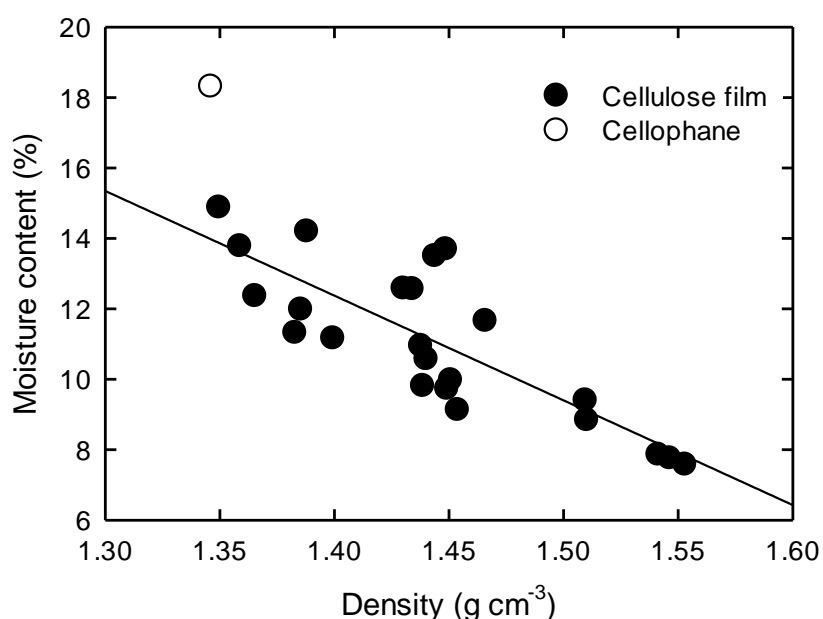


Figure 2.9. Relationship between densities of AUC films in the dry state and their moisture contents at 23 °C and 50% RH. Reproduction from ref. 40 with permission from American Chemical Society (© American Chemical Society 2011).

The AUC films have higher oxygen barrier properties in the wide RH range than those of other regenerated cellulose films reported so far.^{13,14} Similar high oxygen barrier properties have been reported also for some nanocellulose films,^{5,16,17} although detailed mechanisms

have not been clarified.¹⁶ On the other hand, the AUC films, other regenerated cellulose films and also nanocellulose films have remarkably higher water vapor permeabilities than those of poly(ethylene) and poly(propylene) films, which is one of the typical disadvantages for cellulose-based films.^{14,15,50} Hence, improvement of water-vapor barrier properties of the AUC films is significant for future practical applications. Some studies have been carried out to obtain high barrier films for both water vapor and oxygen gas by compositing with hydrophobic polymers^{14,51} or inorganic fillers,⁵² metalizing on the film surfaces,¹⁴ and chemical modifications.⁵³ These techniques may be applicable also to the AUC films to improve water vapor barrier properties.

2.4 Conclusions

Transparent and bendable cellulose films regenerated from cellulose solutions in aqueous AU systems exhibit high oxygen barrier properties. The regenerated AUC films have substantially lower oxygen permeabilities than practical oxygen barrier films such as poly(vinylidene chloride) and poly(vinyl alcohol). The oxygen permeabilities of the AUC films at 0% RH vary from 0.003 to 0.03 ml $\mu\text{m m}^{-2} \text{day}^{-1} \text{kPa}^{-1}$ depending on their preparation conditions. The oxygen permeabilities of the AUC films are inversely proportional to their densities, and the AUC films prepared from solutions with high cellulose concentrations by regeneration with a solvent at low temperatures have low oxygen permeabilities and high densities. The lowest oxygen permeability of 0.003 ml $\mu\text{m m}^{-2} \text{day}^{-1} \text{kPa}^{-1}$ was achieved for the film prepared from a 6 wt % cellulose solution by regeneration with acetone at 0 °C. The transparent, bendable, high oxygen barrier cellulose films developed in this study are promising as high-performance packaging materials since they are biodegradable and environmentally compatible. However, improvement of water-vapor barrier properties of the AUC films is required in future work. Furthermore, recovery systems of Na or Li ions and urea molecules in the regeneration effluents, their reuse systems, and processes to increase cellulose concentrations to 7–10 wt % should be established for practical applications of the alkali/urea cellulose solvent systems.

2.5 References

- (1) Ebina, T.; Mizukami, F. *Adv. Mater.* **2007**, *19*, 2450–2453.
- (2) Lange, J.; Wyser, Y. *Packag. Technol. Sci.* **2003**, *16*, 149–158.
- (3) Compton, O.; Kim, S.; Pierre, C.; Torkelson, J.; Nguyen, S. *Adv. Mater.* **2010**, *22*, 4759–4763.
- (4) Selke, S.; Cutler, J.; Hernandez, R. In *Plastics Packaging: Properties, Processing, Applications, and Regulations*, Hansen Garner Publications, Inc., Cincinnati, OH 2004; pp. 2–6.
- (5) Fukuzumi, H.; Saito, T.; Iwata, T.; Kumamoto, Y.; Isogai, A. *Biomacromolecules* **2009**, *10*, 162–165.
- (6) Jakobsen, M.; Risbo, J. *Packag. Technol. Sci.* **2008**, *21*, 207–216.
- (7) Möller, M.; Lunkenbein, T.; Kalo, H.; Schieder, M.; Kunz, D.; Breu, J. *Adv. Mater.* **2010**, *22*, 5245–5249.
- (8) Garcfa-Ayuso, G.; Salvarezza, R.; Martinez-Duart, J.; Sánchez, O.; Vázquez, L. *Adv. Mater.* **1997**, *9*, 654–658.
- (9) Ashley, R. in *Polymer Permeability*, Comyn, J. Ed.; Chapman and Hall, London, 1985; pp. 269–308.
- (10) Wang, H.; Keum, J. K.; Hiltner, A.; Baer, E.; Freeman, B.; Rozanski, A.; Galeski, A. *Science* **2009**, *323*, 757–760.
- (11) Yu, L.; Dean, K.; Li, L. *Prog. Polym. Sci.* **2006**, *31*, 576–602.
- (12) Gross, R. A.; Kalra, B. *Science* **2002**, *297*, 803–806.
- (13) Hyden, W. L. *Ind. Eng. Chem.* **1929**, *21*, 405–410.
- (14) Revell, K. M. US Patent 5021298, 1991.
- (15) Jin, Z.; Wang, S.; Wang, J.; Xu, M. *Polymer Plast. Tech. Eng.* **2010**, *49*, 1371–1377.
- (16) Siró, I.; Plackett, D. *Cellulose* **2010**, *17*, 459–494.
- (17) Syverud, K.; Stenius, P. *Cellulose* **2008**, *16*, 75–85.
- (18) Zhu Ryberg, Y. Z.; Edlund, U.; Albertsson, A. C. *Biomacromolecules* **2011**, *12*, 1355–1362.
- (19) Edlund, U.; Zhu Ryberg, Y. Z.; Albertsson, A. C. *Biomacromolecules* **2010**, *11*, 2532–

2538.

- (20) Hartman, J.; Albertsson, A. C.; Sjöberg, J. *Biomacromolecules* **2006**, *7*, 1983–1989.
- (21) Hartman, J.; Albertsson, A. C.; Lindblad, M. S.; Sjöberg, J. *J. Appl. Polym. Sci.* **2006**, *100*, 2985–2991.
- (22) Miller, K. S.; Krochta, J. M. *Trends Food Sci. Technol.* **1997**, *8*, 228–237.
- (23) Fink, H.-P.; Weigel, P.; Purz, H. J.; Ganster, J. *Prog. Polym. Sci.* **2001**, *26*, 1473–1524.
- (24) Schurz, J.; Lenz, J. *Macromol. Symp.* **1994**, *83*, 273–289.
- (25) Swatloski, R. P.; Spear, S. K.; Holbrey, J. D.; Rogers, R. D. *J. Am. Chem. Soc.* **2002**, *124*, 4974–4975.
- (26) Zhu, S.; Wu, Y.; Chen, Q.; Yu, Z.; Wang, C.; Jin, S.; Ding, Y.; Wu, G. *Green Chem.* **2006**, *8*, 325–327.
- (27) Kosan, B.; Michels, C.; Meister, F. *Cellulose* **2008**, *15*, 59–66.
- (28) Isogai, A.; Atalla, R. H. *Cellulose* **1998**, *5*, 309–319.
- (29) Kontturi, E.; Tammelin, T.; Österberg, M. *Chem. Soc. Rev.* **2006**, *35*, 1287–1304.
- (30) Yang, Q.; Qi, H.; Lue, A.; Hu, K.; Cheng, G.; Zhang, L. *Carbohydr. Polym.* **2011**, *83*, 1185–1191.
- (31) Cai, J.; Zhang, L.; Chang, C.; Cheng, G.; Chen, X.; Chu, B. *ChemPhysChem* **2007**, *8*, 1572–1579.
- (32) Cai, J.; Zhang, L.; Zhou, J.; Qi, H.; Chen, H.; Kondo, T.; Chen, X.; Chu, B. *Adv. Mater.* **2007**, *19*, 821–825.
- (33) Qi, H.; Chang, C.; Zhang, L. *Green Chemistry* **2009**, *11*, 177–184.
- (34) Yang, Q.; Qin, X.; Zhang, L. *Cellulose* **2011**, *18*, 681–688.
- (35) Yang, Q.; Lue, A.; Zhang, L. *Compos. Sci. Technol.* **2010**, *70*, 2319–2324.
- (36) Yang, Q.; Lue, A.; Qi, H.; Sun, Y.; Zhang, X.; Zhang, L. *Macromol. Biosci.* **2009**, *9*, 849–856.
- (37) Yan, L.; Chen, J.; Bangal, P. R. *Macromol. Biosci.* **2007**, *7*, 1139–1148.
- (38) Morgado, D. L.; Frollini, E.; Castellan, A.; Rosa, D. S.; Coma, V. *Cellulose* **2011**, *18*, 699–712.
- (39) Cai, J.; Kimura, S.; Wada, M.; Kuga, S.; Zhang, L. *ChemSusChem* **2008**, *1*, 149–154.
- (40) Yang, Q.; Fukuzumi, H.; Saito, T.; Isogai, A.; Zhang, L. *Biomacromolecules* **2011**, *12*,

2766–2771.

- (41) Cai, J.; Liu, Y.; Zhang, L. *J. Polym. Sci., Part B: Polym. Phys.* **2006**, *44*, 3093–3101.
- (42) Rabek, J. In *Experimental methods in polymer chemistry*, John Wiley & Sons: Chichester, 1980; pp. 507.
- (43) Toray Research Center. In *Kinousei Housouzairyō Kaihatsu no Saishin Doko*, Toray Research Center, Tokyo, Japan, 2000.
- (44) Cai, J.; Zhang, L. *Biomacromolecules* **2006**, *7*, 183–189.
- (45) Liu, S.; Zhang, L. *Cellulose* **2009**, *16*, 189–198.
- (46) Mao, Y.; Zhou, J.; Cai, J.; Zhang, L. *J. Membr. Sci.* **2006**, *279*, 246–255.
- (47) Kamide, K.; Iijima, H.; Matsuda, S. *Polym. J.* **1993**, *25*, 1113–1131.
- (48) Van de Witte, P.; Dijkstra, P.; Van de Berg, J.; Feijen, J. *J. Membr. Sci.* **1996**, *117*, 1–31.
- (49) Muramatsu, M.; Okura, M.; Kuboyama, K.; Ougizawa, T.; Yamamoto, T.; Nishihara, Y.; Saito, Y.; Ito, K.; Hirata, K.; Kobayashi, Y. *Radiat. Phys. Chem.* **2003**, *68*, 561–564.
- (50) Hauser, P. M.; McLaren, A. D. *Ind. Eng. Chem.* **1948**, *40*, 112–117.
- (51) Zhang, L.; Zhou, Q. *Ind. Eng. Chem. Res.* **1997**, *36*, 2651–2656.
- (52) Amberg-Schwab, S.; Hoffmann, M.; Bader, H.; Gessler, M. *J. Sol. Gel. Sci. Tech.* **1998**, *13*, 141–146.
- (53) Bras, J.; Vaca-Garcia, C.; Borredon, M. E.; Glasser, W. *Cellulose* **2007**, *14*, 367–374.

Chapter 3

Improvement of Mechanical and Oxygen Barrier Properties of Cellulose Films by Controlling Drying Conditions of Regenerated Cellulose Hydrogels

3.1 Introduction

There has been a growing demand to develop new bio-based materials with features of renewability, sustainability, biocompatibility, and biodegradability.¹⁻⁸ Regenerated cellulose and nanofibrillated cellulose films have potential applications as bio-based materials with high thermal stability and gas barrier properties because of the highly crystalline and hierarchical network structures of cellulose that arise from abundant and ordered intra- and inter-molecular hydrogen bonds.⁹⁻²¹

In the previous chapter, transparent and flexible regenerated cellulose films prepared from aqueous alkali/urea solutions under suitable regeneration conditions were found to exhibit high oxygen barrier properties that were superior to both conventional cellophane and to those of practical oxygen barrier films such as poly(vinylidene chloride) and poly(vinyl alcohol).¹⁵ Because alkali/urea cellulose solvents are categorized as green systems,^{15,22-28} they have potential applications in producing regenerated cellulose films and fibers at the industrial level. Furthermore, properties of regenerated cellulose films prepared from alkali/urea solutions can be widely controlled by controlling the dissolution and regeneration conditions.¹⁵ The lowest oxygen permeability of $0.003 \text{ ml } \mu\text{m}^{-2} \text{ day}^{-1} \text{ kPa}^{-1}$ was obtained for a cellulose film prepared from a 6 wt % cellulose solution by regeneration with acetone at 0 °C.¹⁵ However, because regeneration of cellulose with acetone at 0 °C cannot be used in practical applications, alternative processes to improve mechanical and oxygen barrier properties of cellulose films are required.

Native cellulose fibers such as cotton lint, cotton linters and wood pulps have critical

limitations in terms of their variety of formability, whereas systems for dissolution and regeneration of natural celluloses allow us to produce cellulose fibers with various cross-sectional shapes and almost infinite lengths, and cellulose films with uniform thicknesses and large areas. However, regenerated cellulose fibers usually have lower strength than native cellulose fibers because they have lower cellulose II crystallinities than the cellulose I crystallinities of native celluloses.²⁹ The mechanical properties of regenerated cellulose fibers depend on the process parameters,³⁰ and a tensile strength of 1,300 MPa and an elastic modulus of 45 GPa were achieved at the laboratory scale by increasing the degree of orientation of cellulose chains along the fiber axis.³¹ Cellophanes can be prepared with a tensile strength and an elastic modulus of 125 MPa and 5.4 GPa, respectively, by controlling the degree of orientation of cellulose chains in the films. Regenerated cellulose films prepared from N-methylmorpholine-N-oxide (NMMO) solutions can have a tensile strength and an elastic modulus of 300 MPa and 8 GPa, respectively,³² cellulose films made from solutions in lithium chloride/N,N-dimethylacetamide can give a tensile strength and an elastic modulus of 396 MPa and 26.4 GPa, respectively²⁹ and aqueous LiOH/urea cellulose solutions can produce cellulose films with a tensile strength and an elastic modulus of 213 MPa and 11 GPa, respectively.³³ However, these excellent mechanical properties have been achieved only when measuring in the direction of the highly orientated cellulose chains, while the mechanical properties of the films are significantly poorer when measured in other film directions.

Recently, several drying methods for preparation of regenerated cellulose films³⁴ and nanocellulose films,^{12,17} including oven, vacuum, hot-press, and air drying have been studied and the resulting mechanical properties of the films were shown to have vary accordingly. Moreover, nanocellulose films prepared by vacuum drying under compression (press-vacuum drying) resulted in higher tensile strengths and Young's moduli, which were explained by higher in-plane orientations of the nanofibers and also higher film densities caused by drying under constrained conditions of the cellulose nanofibers.¹⁷ However, the effects of various drying conditions on the detailed properties of regenerated cellulose films have not been reported before now.

In the present chapter³⁵, I report the effects of various drying conditions for regenerated cellulose hydrogel films prepared from aqueous cellulose/alkali/urea solutions on mechanical,

thermal and oxygen barrier properties. It was found that these properties were remarkably improved solely by controlling the drying conditions, primarily through control of the crystallinity of cellulose II within the films.

3.2 Experimental Section

3.2.1 Materials

A filter paper pulp (highly purified cotton linters, Advantec Co., Ltd., Japan) was used as the cellulose sample with a viscosity-average molecular weight of $8.6 \times 10^4 \text{ g mol}^{-1}$.¹⁵ All reagents and solvents were of laboratory grade (Wako Pure Chemicals, Tokyo, Japan), and used as received.

3.2.2 Preparation of regenerated cellulose hydrogel films

A solvent mixture, LiOH/urea/H₂O with a weight ratio of 4.6:15:80.4 was precooled at –12 °C. A desired amount of cellulose was dispersed in the precooled solvent and the mixture was stirred vigorously at 1200 rpm for 2 min to form a transparent and viscous solution of a 6 wt % cellulose concentration. The cellulose solution thus obtained (35 ml) was degassed by centrifugation at 10000g for 10 min, spread on a glass plate, and then immersed in an aqueous solution (~2.5 l) containing 5 wt % H₂SO₄ and 5 wt % Na₂SO₄ at 20 °C for regeneration. The film-like hydrogel of regenerated cellulose thus formed, which had ~1 mm thickness and ~500 cm² area, was repeatedly washed with an excess volume of water by soaking.

3.2.3 Drying conditions of regenerated cellulose hydrogel films

Each hydrogel film was placed on a metal plate and the periphery of the hydrogel film was stuck on the plate with several Scotch tape strips to avoid shrinkage of the film during drying. Then, the hydrogel films were dried under the following five conditions: Air drying (Drying-1): drying of the hydrogel film on the metal plate at 20 °C in air for 24 h, in which the upper side of the hydrogel film was exposed to air; vacuum drying (Drying-2): drying of the hydrogel film on the metal plate at various atmospheric pressures in a vacuum oven at

20 °C, in which the upper side of the hydrogel film was exposed to air at a reduced pressure; press-vacuum drying (Drying-3): the hydrogel film was sandwiched between two metal plates and loaded under various compressive pressures controlled with steel weights placed on the upper metal plate in a vacuum oven at 1 kPa and 20 °C for 11 h; pre-pressing and press-vacuum drying (Drying-4): the hydrogel film was sandwiched between two metal plates and loaded at a 1.5 MPa compressive pressure using a press in air at 20 °C for 1 h, followed by the above press-vacuum drying at a compressive pressure of 4 kPa in a vacuum oven at 1 kPa and 20 °C for 11 h; and pre-pressing and press-vacuum-heat drying (Drying-5): the hydrogel films pre-pressed under the above conditions were subsequently dried under press-vacuum conditions at a compressive pressure of 4 kPa in a vacuum oven at 1 kPa and 20–80 °C. All cellulose films were conditioned at 23 °C and 50% relative humidity (RH) for more than 2 days before testing. In the case of measurement of oxygen transmission rates, the cellulose films were further dried in a desiccator containing P₂O₅ at room temperature and 0% RH for at least 3 days.

3.2.4. Characterizations

The film thickness was measured with a micrometer and each value was expressed as an average of five measurements. Thicknesses of the cellulose films ranged from 27 to 50 μm, depending on the drying conditions adopted. Statistical errors in thickness of each film were within ±3%. The density of the dried cellulose film was determined from the area, thickness, and dry weight. Oxygen transmission rates of the cellulose films were determined at 23 °C and 0% RH using a Mocon Ox-Tran Model 2/21MH (Modern Controls Inc., USA) under standard conditions (ASTM 3985). Each measurement was continued until the O₂ transmission rate reached a stable value. The oxygen permeability was determined from the oxygen transmission rate and the film thickness, and the standard deviations for each film were within ±5%. Tensile tests were performed using a Shimadzu EZ-TEST instrument equipped with a 500 N load cell. Rectangular strips 2×30 mm in size were cut from the cellulose films and tested with a span length of 10 mm at a rate of 1.0 mm min⁻¹. The visible light transmittances of the films were measured from 400 to 800 nm using a Shimadzu UV-1700 UV-Vis spectrophotometer. X-ray diffraction (XRD) patterns of the films were acquired

in reflection mode using a Rigaku RINT 2000 with monochromator-filtered Cu K α radiation at 40 kV and 40 mA. The crystallinities of the cellulose films were estimated from the areas of diffraction peaks obtained using the Lorentz peak separation method.³⁶ Crystal widths of (1 -1 0) reflections due to cellulose II were calculated from the full widths at half heights of the diffraction peaks by Scherrer's equation.³⁷ The solid-state nuclear magnetic resonance (NMR) experiments were performed on a Bruker Avance spectrometer operating at a ¹³C frequency of 100 MHz using the combined technique of proton dipolar decoupling (DD), magic angle sample spinning (MAS), and cross-polarization (CP). The spectra were acquired at room temperature with a proton 90° pulse of 2.5 μ s at a spinning rate of 12 kHz. The cross-polarization transfer was achieved using ramped amplitude sequence for an optimized total time of 2 ms. The repetition time was 4 s, and the average number of 20000 scans was acquired for each spectrum. The crystallinities of the cellulose films were also calculated by dividing the area of the crystalline peak (integrating the peak from 86.2 to 90.2 ppm) by the total area assigned to the C4 peaks (integrating the region from 79.7 to 90.2 ppm).³⁸ Cellulose films were conditioned at 23 °C and 50% RH for 2 days and the moisture contents under these conditions were calculated from the film weights before and after heating at 105 °C for 3 h. Thermal expansivity of the films, which were preheated at 120 °C for 10 min, were determined at 0.03 N load in a nitrogen atmosphere from 28 to 100 °C at 5 °C min⁻¹ using a Shimadzu TMA-60 instrument. The films were frozen in liquid nitrogen and immediately snapped and then vacuum-dried. The fracture surfaces (cross-sections) of the films were coated with osmium using a Meiwafoysis Neo osmium coater and observed with a Hitachi S4800 field-emission scanning electron microscope at 2 kV.

3.3 Results and Discussion

3.3.1 Drying conditions of regenerated cellulose hydrogel films

The regenerated cellulose hydrogel films prepared from aqueous cellulose/alkali/urea solutions were dried under five different conditions described in the Experimental Section and the fundamental properties of the dried and conditioned films are summarized in Table 3.1.

The drying times listed in Table 3.1 were fixed based on the results obtained in preliminary experiments, in which the film weight was monitored in terms of drying time under each drying condition. No further loss of weight was observed in each case after the drying time given in Table 3.1. Vacuum drying (Drying-2) removes water from the hydrogel films in less time than air drying (Drying-1) by forced removal of water under reduced pressure. For the cases of “press-vacuum drying” (Drying-3) and “pre-pressing + press-vacuum drying” (Drying-4) shown in Table 3.1, longer times were required for the film to reach a constant weight, because water in the hydrogel film was removed only from the small area at the edge of the film, which was sandwiched between two metal plates, even during vacuum drying.

Table 3.1. Characteristics of cellulose films prepared from regenerated cellulose hydrogels under various drying conditions. Reproduction from ref. 35 with permission from Springer (© Springer 2012).

Drying conditions	Drying temp. [°C]	Drying time [h]	Film density [g cm ⁻³]	Crystal width ^a [nm]	Crystallinity from XRD [%]	Crystallinity from NMR [%]	Moisture content [%]	CTE ^b [ppm k ⁻¹]
Drying-1 ^c	20	24	1.45 ± 0.01	3.47	50	36	14.1	15.5
Drying-2 ^d	20	3	1.51 ± 0.03	3.56	53	37	12.5	14.0
Drying-3 ^e	20	11	1.55 ± 0.01	3.68	58	40	11.4	11.6
Drying-4 ^f	20	11	1.57 ± 0.02	3.78	62	43	9.8	10.3
Drying-5 ^g	80	6	1.44 ± 0.02	3.40	47	35	15.8	16.1

^a Crystal width of the (1 -1 0) reflection peak due to cellulose II

^b CTE: Coefficient of thermal expansion

^c Air drying

^d Vacuum drying at air pressure of 1 kPa

^e Press-vacuum drying at compressive pressure of 4 kPa

^f Pre-pressing and press-vacuum drying

^g Pre-pressing and press-vacuum-heat drying

3.3.2 Properties of cellulose films

Thicknesses of the films changed according to the drying conditions and the film densities correspondingly varied from 1.44 to 1.57 g cm⁻³. X-ray diffraction patterns of the films are presented in Figure 3.1, showing that all the films had the same cellulose II crystal structures but different crystallinities. The diffraction intensities clearly increased with the film density and thus the crystallinity of cellulose II as well as the film density is controllable by controlling the drying conditions. In particular, because the diffraction intensity of the (1 -1 0) peak significantly increased with film density, the drying conditions are likely to control the regularity between hydrophilic interactions between cellulose chains of cellulose II, maintaining a similar hydrophobic chain stacking regularity.³⁹

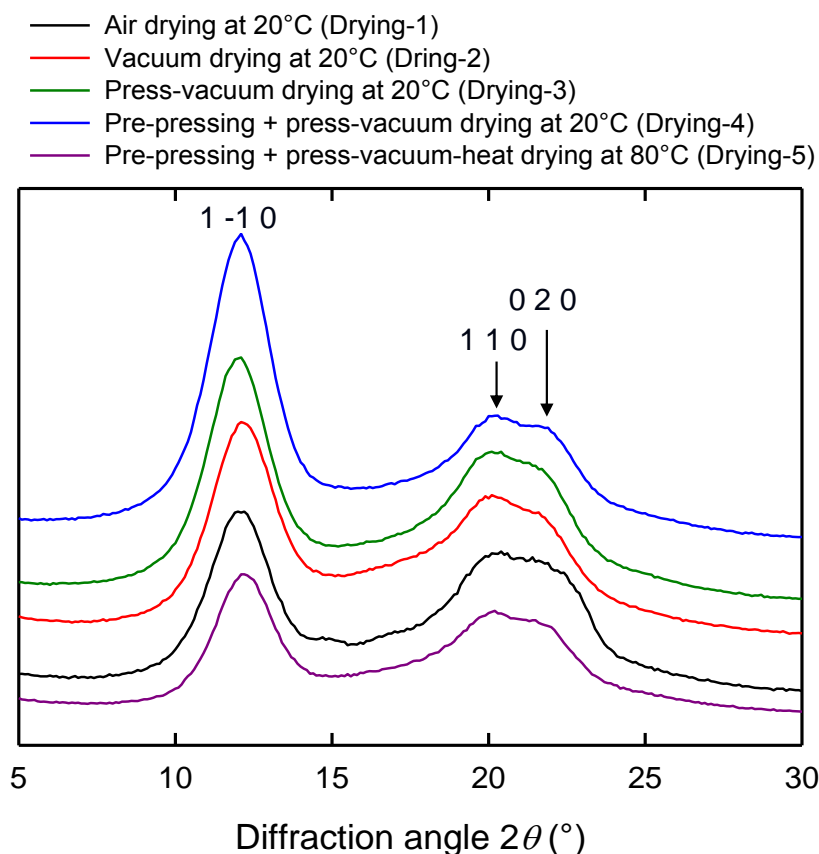


Figure 3.1. X-ray diffraction patterns of cellulose films prepared from regenerated cellulose hydrogel films under different drying conditions. See Table 3.1 and the Experimental Section for details of the drying conditions. Reproduction from ref. 35 with permission from Springer (© Springer 2012).

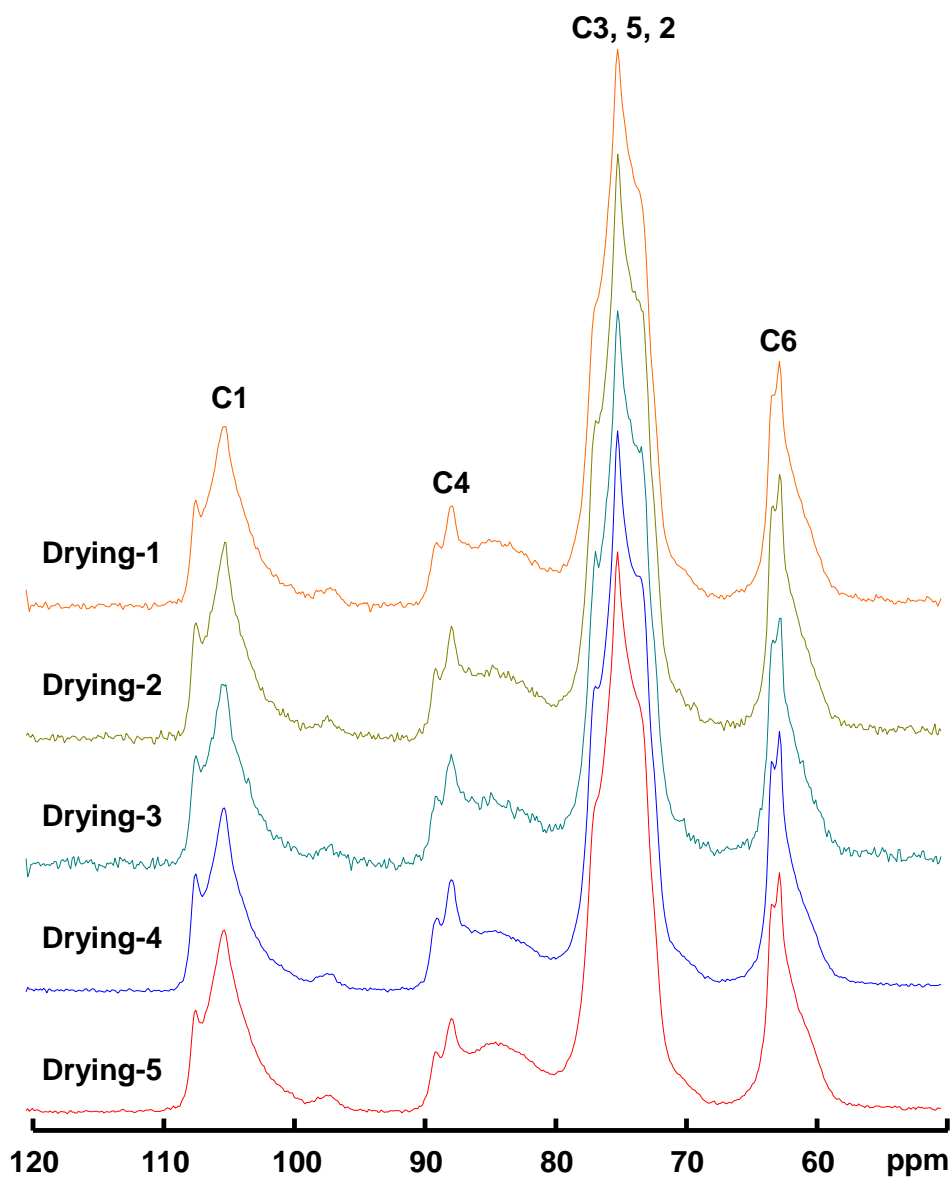


Figure 3.2. Solid-state CP/MAS ^{13}C NMR spectra of cellulose films prepared from regenerated cellulose hydrogel films under different drying conditions. See Table 3.1 and the Experimental Section for details of the drying conditions.

Solid-state CP/MAS ^{13}C NMR spectra of the films are shown in Figure 3.2. The peaks between 90.2 and 86.2 ppm are assigned to C4 carbons in ordered cellulose structures (crystalline regions), and the peaks between 86.2 and 79.7 ppm are assigned to C4 carbons of disordered cellulose (amorphous regions).³⁸ The results also show that all the films had the same cellulose II crystal structures but different crystallinities. Crystallinities calculated from XRD may be influenced by the planar orientations of films, whereas crystallinities calculated from NMR are not influenced by the planar orientations of films. However, crystallinities of the films calculated from NMR have the same trend to crystallinities calculated from XRD (Table 1). Both of them were controlled by drying conditions and showed clear increase with film densities. Therefore, only crystallinities calculated from XRD were discussed as crystallinities of the films in the following work.

Drying-4 resulted in the highest film density and the highest crystallinity of cellulose II (Table 3.1). Probably, highly regular intra- and inter-molecular hydrogen bonds of cellulose chains are formed during these two water-removal processes, in which water molecules within the hydrogel films are somewhat forcibly removed by the pre-pressing, pressing and vacuum drying treatments. On the other hand, rapid removal of water from the hydrogel films by Drying-5 at 80 °C led to a lower film density and lower crystallinity, indicating that high mobility of water molecules in the hydrogel films at high temperatures may have resulted in less regularity in terms of intra- and inter-molecular hydrogen bond formation in the cellulose films.

Moreover, as the cellulose II crystallinity of the cellulose films was increased, correspondingly both the moisture content at 23 °C and 50% relative humidity (RH) and the coefficient of thermal expansion (CTE) decreased (Table 3.1). A CTE value of 10 ppm K^{-1} was sufficiently low under dry conditions and close to that of glass (~ 9 ppm K^{-1})¹² or iron (~ 11.8 ppm K^{-1}).⁴⁰ Moreover, the CTE values of the cellulose films in Table 3.1 are much lower than those of most plastics (> 50 ppm K^{-1}),¹¹ because of the high crystallinity of the cellulose films. As shown in Figure 3.3, linear correlations were obtained between the film density and either the crystallinity, crystal width, moisture content or CTE of the films. In addition, good correlations between the density or crystallinity of the films and either tensile strength or Young's modulus were obtained, as shown in Figure 3.4. Thus, the forced removal

of water from the cellulose hydrogel films by vacuum drying effectively improves the mechanical properties of the films by increasing the crystallinity of cellulose II (see X-ray diffraction patterns of the samples prepared by Drying-1 and Drying-2 in Figure 3.1).

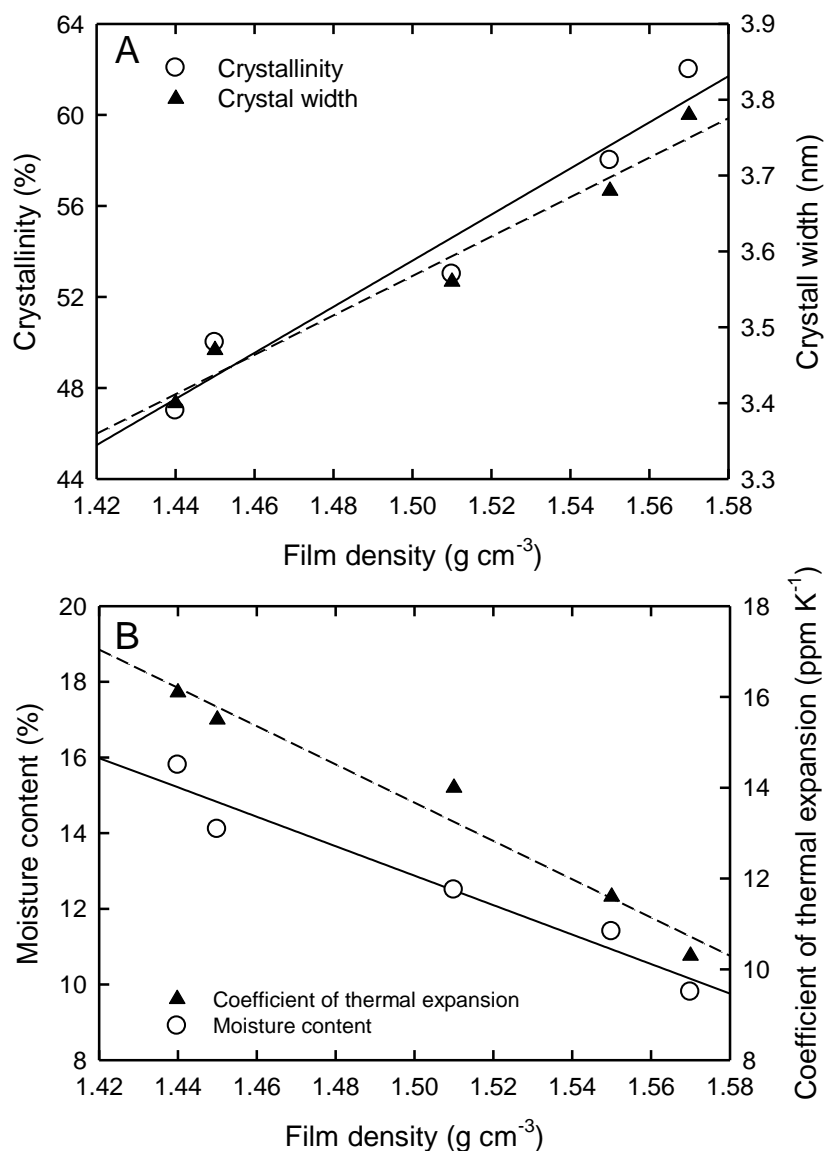


Figure 3.3. Relationships between cellulose film density and either crystallinity or crystal width (A), and between cellulose film density and either moisture content or coefficient of thermal expansion (B) of regenerated cellulose films. Reproduction from ref. 35 with permission from Springer (© Springer 2012).

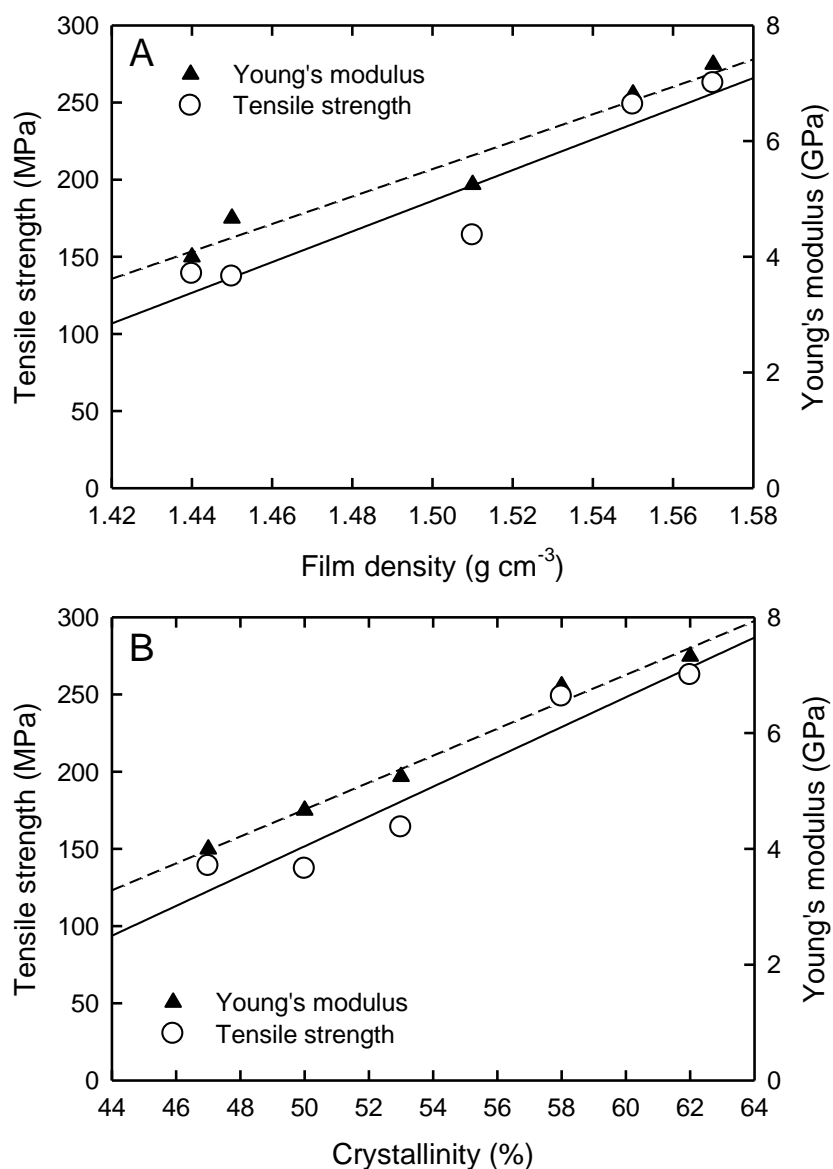


Figure 3.4. Relationships between film density and either tensile strength or Young's modulus (A), and between crystallinity and either tensile strength or Young's modulus (B) of regenerated cellulose films. Reproduction from ref. 35 with permission from Springer (© Springer 2012).

3.3.3 Effects of drying conditions on mechanical and optical properties of regenerated cellulose films

Figure 3.5 shows the effects of compression of cellulose hydrogel films during press-vacuum drying (Drying-3) at 20 °C and 1 kPa on tensile strength and Young's modulus of the cellulose films. These parameters increased from 164 to 249 MPa and from 5.2 to 6.8 GPa, respectively, when the compressive pressure was increased from 0 to 4 kPa. Thus, compression applied to the cellulose hydrogel films during vacuum drying is quite effective in increasing the tensile strength and Young's modulus of the cellulose films as well as the crystallinity of cellulose II (see X-ray diffraction patterns of the samples prepared by Drying-2 and Drying-3 in Figure 3.1). It was reported that mechanical properties of nanocellulose films are improved by vacuum drying of hydrogel films under constrained conditions¹⁷ which is consistent with the results of Drying-3 used in this study.

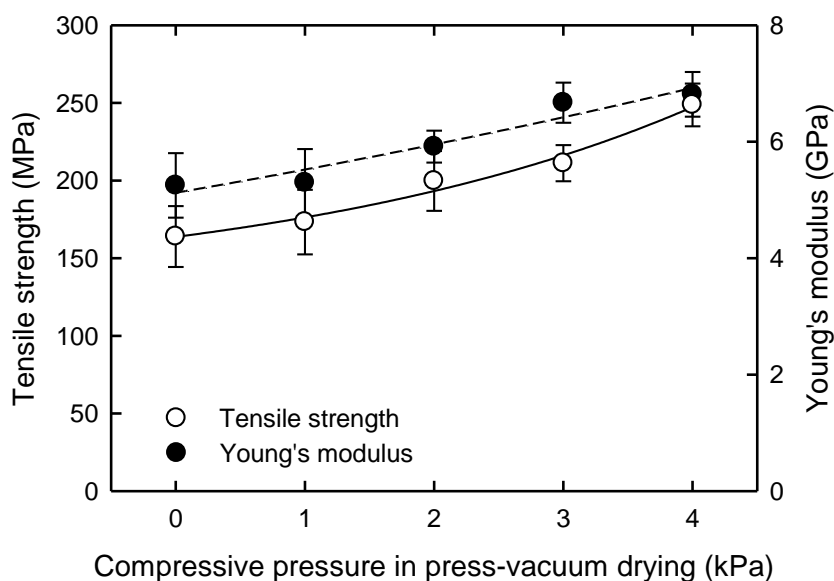


Figure 3.5. Effects of compression of the regenerated cellulose hydrogel films during vacuum drying at 1 kPa and 20 °C for 11 h (Drying-3) on tensile strength and Young's modulus of dried cellulose films. Reproduction from ref. 35 with permission from Springer (© Springer 2012).

The effects of pre-pressing the cellulose hydrogel films at 1.5 MPa at 20 °C for 1 h using a press machine on the tensile strength and Young's modulus of the cellulose films are presented in Figure 3.6. The tensile strength and Young's modulus of the films were further increased by the pre-pressing.

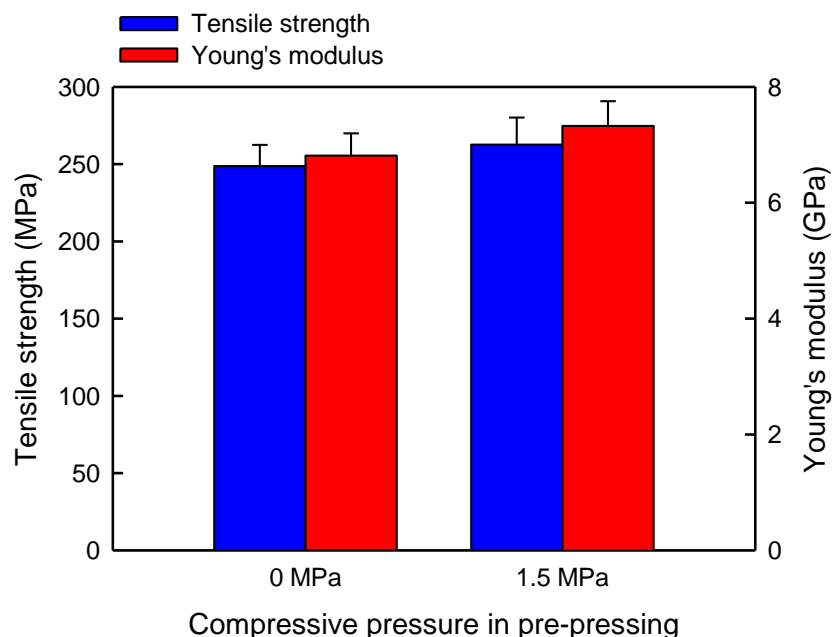


Figure. 3.6. Effects of pre-pressing of regenerated cellulose hydrogel films at 1.5 MPa for 1 h before press-vacuum drying (See Table 3.1) on tensile strength and Young's modulus of dried cellulose films. Reproduction from ref. 35 with permission from Springer (© Springer 2012).

Figure 3.7 shows the effects of temperature during Drying-5 of the cellulose hydrogel films on tensile strength and Young's modulus. All films were pre-pressed at 1.5 MPa for 1 h before Drying-5. Tensile strength and Young's modulus decreased from 263 to 139 MPa and from 7.3 to 4.0 GPa, respectively, as the temperature was increased from 20 to 80 °C, i.e. relative decreases of 47 and 45%, respectively, with increasing temperature. The drying time

can be reduced by Drying-5 at higher temperatures, because water is removed from the cellulose hydrogel films more effectively than at low temperatures. However, the rapid removal of water molecules from the cellulose hydrogel films by heating has a negative impact on the mechanical properties and reduces the increase in crystallinity (see the X-ray diffraction patterns of the samples prepared by Drying-4 and Drying-5 in Figure 3.1).

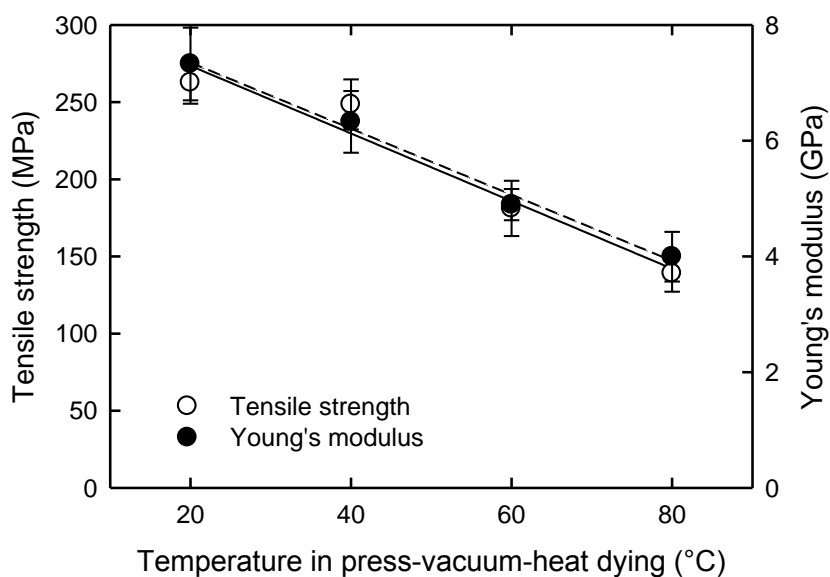


Figure 3.7. Effects of temperature during press-vacuum drying (Drying-5) of the pre-pressed cellulose hydrogel films on tensile strength and Young's modulus of dried cellulose films. Reproduction from ref. 35 with permission from Springer (© Springer 2012).

The stress-strain curves of the cellulose films prepared under different drying conditions in Table 3.1 are shown in Figure 3.8. Tensile strengths and Young's moduli of the films varied, depending on the drying conditions, but no obvious differences in elongations at break, i.e. 13–14 %, were observed amongst the cellulose films. It is probable that the tensile

strengths and Young's moduli are strongly influenced by crystallinity or density of the films, whereas elongation is primarily influenced by the properties of disordered regions in the cellulose films, which may be similar between the cellulose films dried under different conditions.

Figure 3.9 shows the visible light transmittances of the cellulose films with a normalized thickness of 40 μm prepared under different drying conditions. The light transmittances of all the films at 600 nm were quite similar and sufficiently high, ranging from 88 to 90%, which are suitable for transparent packaging films and flat display panels. Thus, the light transmittances are not significantly influenced by film density or the crystallinity of the films, which depend on the drying conditions of the cellulose hydrogel films.

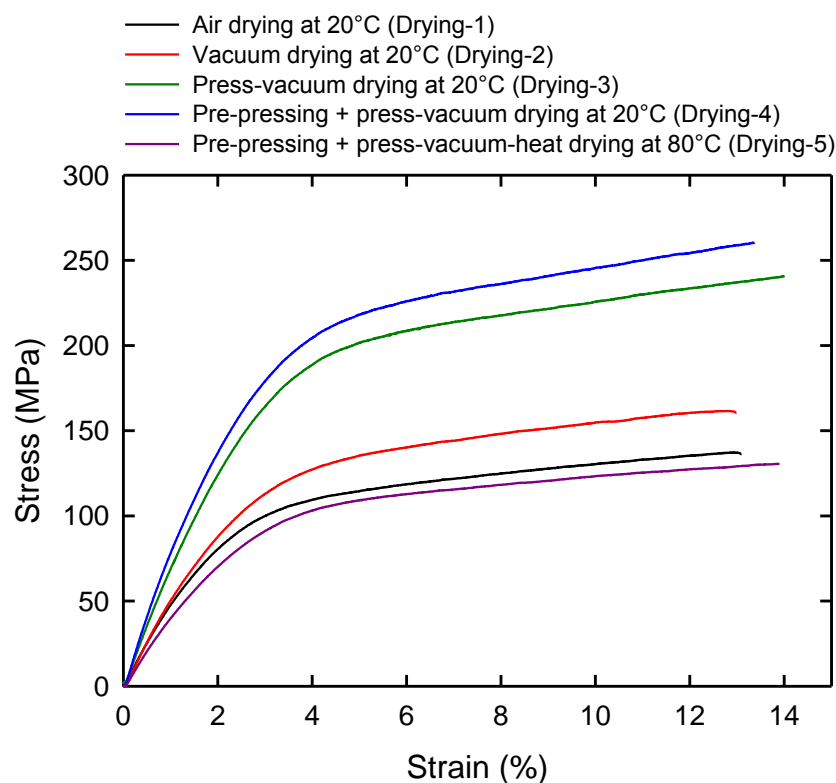


Figure 3.8. Stress-strain curves of cellulose films prepared from regenerated cellulose hydrogel films under various drying conditions. See Table 3.1 and the Experimental section for details of the drying conditions. Reproduction from ref. 35 with permission from Springer (© Springer 2012).

3.3.4 Effect of drying conditions on oxygen permeability of regenerated cellulose films

Figure 3.10 shows the effects of air pressure during vacuum drying (Drying-2) of the regenerated cellulose hydrogel films at 20 °C on the oxygen permeability of the obtained cellulose films, normalized by the film thicknesses. The oxygen permeability markedly decreased from 0.0124 to 0.0078 ml $\mu\text{m m}^{-2} \text{day}^{-1} \text{kPa}^{-1}$ (37% to the original value) as the air pressure of vacuum drying was reduced from atmospheric pressure to 1 kPa. 1 kPa was the lowest air pressure possible using the laboratory vacuum oven in this work. The increase in cellulose II crystallinity and the dense structures of the film by vacuum drying at low pressures may have resulted in the low oxygen permeability of the cellulose film.

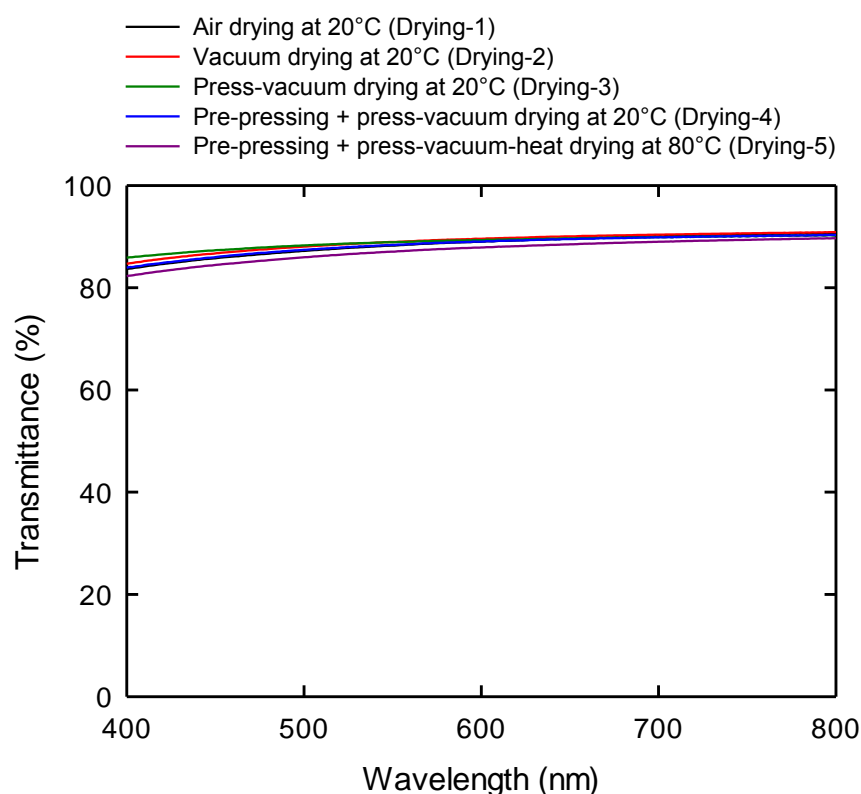


Figure 3.9. Visible light transmittances of cellulose films with 40 μm thickness, prepared from regenerated cellulose hydrogel films under various drying conditions. See Table 3.1 and the Experimental section for details of the drying conditions. Reproduction from ref. 35 with permission from Springer (© Springer 2012).

The effects of compression of the regenerated cellulose hydrogel films during press-vacuum drying at 1 kPa and 20 °C (Drying-3) on oxygen permeability are shown in Figure 3.11. The oxygen permeability was further reduced from 0.0078 to 0.0038 ml $\mu\text{m m}^{-2} \text{day}^{-1} \text{kPa}^{-1}$ (51% to the original value) as the compressive pressure was increased from 0 to 4 kPa in this case. This result exhibits that vacuum drying with compression pressure is quite effective in improving the oxygen barrier properties of the regenerated cellulose films.

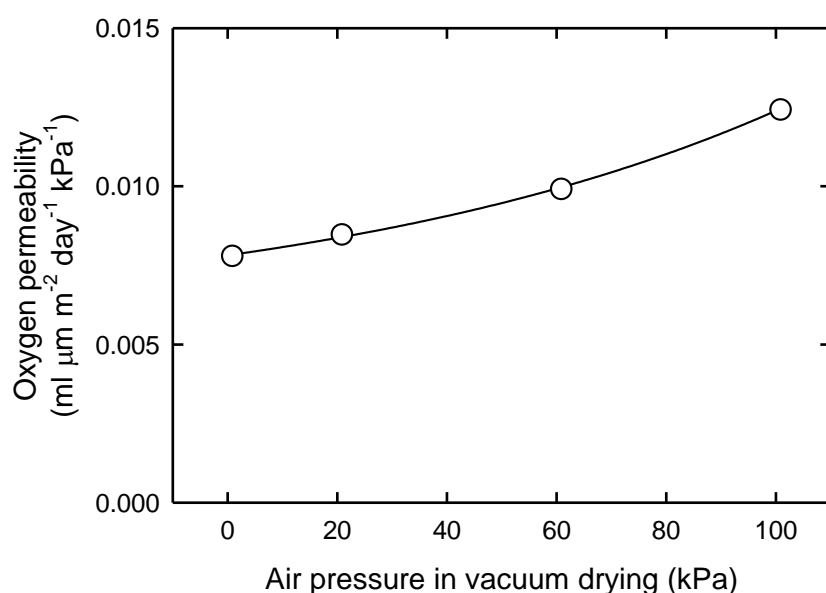


Figure 3.10. Effect of air pressure during vacuum drying (Drying-2) of regenerated cellulose hydrogel films at 20 °C on oxygen permeability of dried cellulose films. Reproduction from ref. 35 with permission from Springer (© Springer 2012).

In addition, we applied pre-pressing of the cellulose hydrogel films at 1.5 MPa for 1 h using a press before the films were subjected to press-vacuum drying at 1 kPa and 20 °C (Drying-4). The oxygen permeability of the films markedly decreased from 0.0038 (by Drying-3) to 0.0007 ml $\mu\text{m m}^{-2} \text{day}^{-1} \text{kPa}^{-1}$ (a reduction of 82% of the original value) by

press-vacuum drying combined with the pre-pressing treatment (Drying-4). This oxygen permeability value is close to those of nanofibrillated cellulose films,^{13,16} and extremely low in comparison with those of other bio-based or petroleum-based polymer films. For example, films made of microcrystalline wax, arabinoxylan, collagen, chitosan–glycerol (4:1 by weight), high-density poly(ethylene), poly(ethylene terephthalate), nylon-6, poly(vinylidene chloride), poly(vinyl alcohol) and ethylene vinyl alcohol have oxygen permeabilities of 1540, 2, 1.2, 0.01–0.04, 500, 8, 6, 0.4, 0.04 and 0.01–0.1 ml $\mu\text{m m}^{-2} \text{day}^{-1} \text{kPa}^{-1}$ at 0% RH, respectively.^{16,41} Moreover, it should be noted that the oxygen transmission rate of this cellulose film was lower than the lowest detection limit of the instrument (less than 0.0005 mL $\text{m}^{-2} \text{day}^{-1} \text{kPa}^{-1}$).

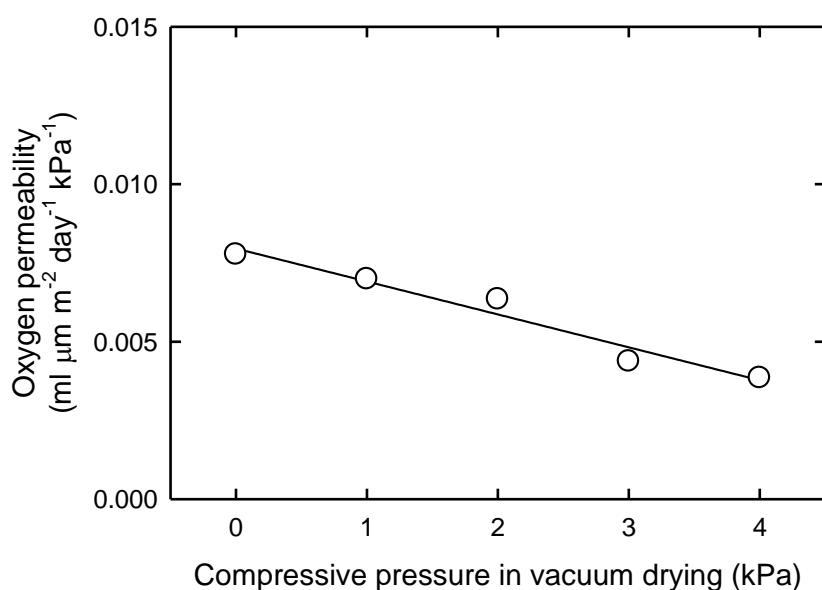


Figure 3.11. Effect of compression of regenerated cellulose hydrogel films during vacuum drying at 1 kPa and 20 °C for 11 h (Drying-3) on oxygen permeability of dried cellulose films. Reproduction from ref. 35 with permission from Springer (© Springer 2012).

Figure 3.12 shows the effect of drying temperature during Drying-5 on oxygen permeability of the cellulose films. The drying times were set to 11, 10, 8 and 6 h at heating temperatures of 20, 40, 60 and 80 °C, respectively, because the higher temperatures resulted in shorter drying times. The oxygen permeability of the films increased from 0.0007 to 0.0154 ml $\mu\text{m m}^{-2} \text{day}^{-1} \text{kPa}^{-1}$, as the drying temperature was increased from 20 to 80 °C. Thus, the rapid removal of water molecules from the cellulose hydrogel films by heating at high temperatures had a negative impact on oxygen permeability and the increase in crystallinity of the films (see the X-ray diffraction patterns of the samples prepared by Drying-4 and Drying-5 in Figure 3.1). Drying-5 at high temperatures causes lower film density, lower crystallinity and results in higher oxygen permeability of the films, indicating that high mobility of water molecules within the hydrogel films at high temperatures during the drying process may bring about less regularity in terms of intra- and inter-molecular hydrogen bond formation in the cellulose films.

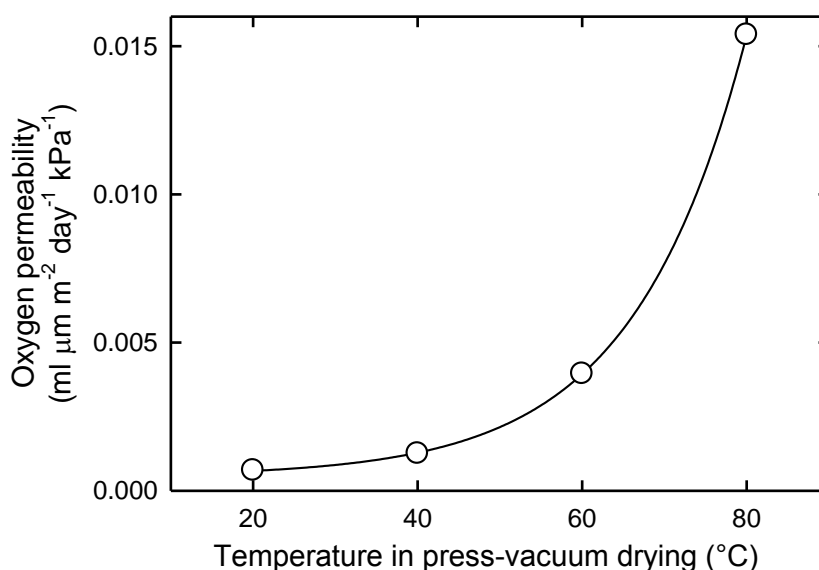


Figure 3.12. Effect of temperature during press-vacuum drying (Drying-5) of the pre-pressed cellulose hydrogel films on oxygen permeability of dried cellulose films. Reproduction from ref. 35 with permission from Springer (© Springer 2012).

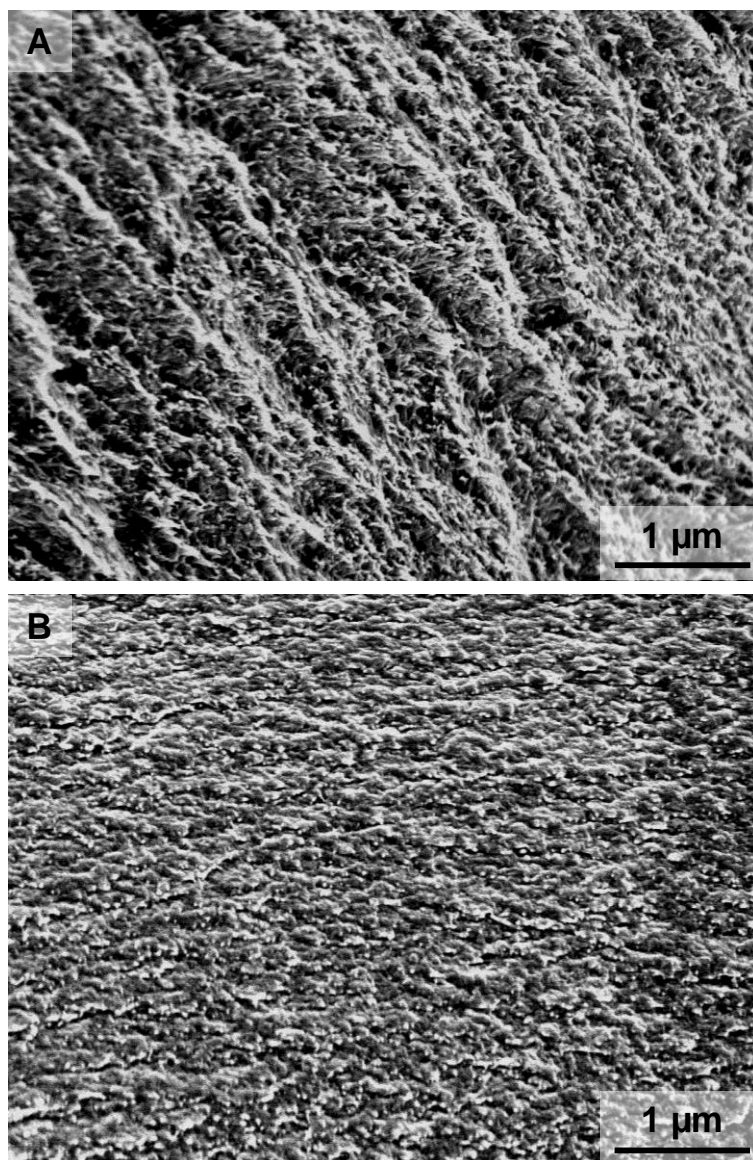


Figure 3.13. SEM images of cross-sections of cellulose films prepared by Drying-1 (A) and Drying-4 (B). Reproduction from ref. 35 with permission from Springer (© Springer 2012).

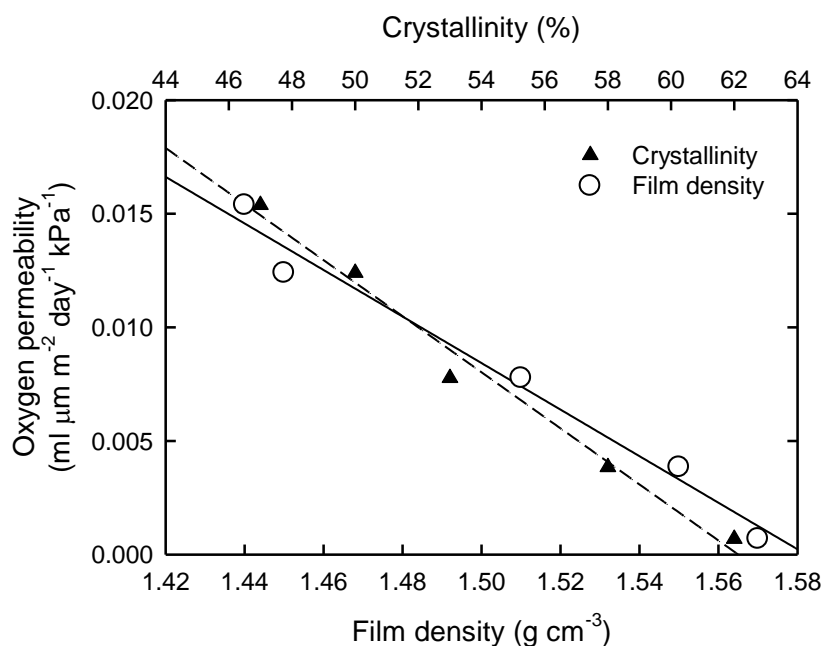


Figure 3.14. Relationships between either film density or crystallinity and oxygen permeability of regenerated cellulose films. Reproduction from ref. 35 with permission from Springer (© Springer 2012).

SEM images of cross sections of the cellulose films prepared by Drying-1 and Drying-4 of the cellulose hydrogel films are shown in Figure 3.13. The film prepared by Drying-4 clearly had denser structures compared with the film prepared by air drying. Thus, pre-pressing and subsequent press-vacuum drying is effective in the formation of cellulose films with a denser structure or a less porous structure, as well as a higher cellulose II crystallinity which leads to higher oxygen barrier properties, improved mechanical properties and lower coefficients of thermal expansion. The correlations between either the density or crystallinity of the cellulose films prepared under the different drying conditions and the oxygen permeability of the films at 0% RH are presented in Figure 3.14, which shows clearly linear relationships between these three factors.

3.4 Conclusions

The mechanical, thermal and oxygen barrier properties of cellulose films prepared by regeneration from aqueous cellulose/alkali/urea solutions can be significantly improved by controlling the drying conditions. Cellulose films prepared by Drying-4 had the highest film density (1.57 g cm^{-3}), crystallinity (62%), tensile strength (263 MPa) and Young's modulus (7.3 GPa), and the lowest moisture content (9.8%), coefficient of thermal expansion (10.3 ppm K^{-1}) and oxygen permeability ($0.0007 \text{ ml } \mu\text{m m}^{-2} \text{ day}^{-1} \text{ kPa}^{-1}$). Moreover, it should be noted that the oxygen transmission rates of them were lower than the lowest detection limit of the instrument (less than $0.0005 \text{ mL m}^{-2} \text{ day}^{-1} \text{ kPa}^{-1}$). These mechanical, thermal and oxygen barrier properties are clearly superior to those of regenerated cellulose films without orientation of cellulose chains, prepared using the conventional viscose, NMMO and other cellulose solvent systems. Thus, aqueous alkali/urea solvent systems for cellulose have potential applications in producing new and environmentally friendly cellulose films with high performances by controlling the drying conditions of regenerated cellulose hydrogel films. However, because long drying times were required in laboratory-scale experiments, more efficient drying processes and systems should be developed for practical production of regenerated cellulose films.

3.5 References

- (1) Ragauskas, A. J.; Williams, C. K.; Davison, B. H.; Britovsek, G.; Cairney, J.; Eckert, C. A.; Rederick, W. J.; Hallett, J. P.; Leak, D. J.; Liotta, C. L.; Mielenz, J. R.; Murphy, R.; Templer, R.; Tschaplinski, T. *Science* **2006**, *311*, 484–489.
- (2) Ohlrogge, J.; Allen, D.; Berguson, B.; DellaPenna, D.; Shachar-Hill, Y.; Stymne, S. *Science* **2009**, *324*, 1019–1020.
- (3) Read, S. M.; Bacic, T. *Science* **2002**, *295*, 59–60.
- (4) Klemm, D.; Heublein, B.; Fink, H.-P.; Bohn, A. *Angew. Chem. Int. Ed.* **2005**, *44*, 3358–3393.

- (5) Kontturi, E.; Tammelin, T.; Österberg, M. *Chem. Soc. Rev.* **2006**, *35*, 1287–1304.
- (6) Heinze, T.; Liebert, T. *Prog. Polym. Sci.* **2001**, *26*, 1689–1762.
- (7) Hirota, M.; Furihata, K.; Saito, T.; Kawada, T.; Isogai, A. *Angew. Chem. Int. Ed.* **2010**, *49*, 7670–7672.
- (8) Rüschen, Klaas, M.; Schöne, H. *ChemSusChem* **2009**, *2*, 127–128.
- (9) Hyden, W. L. *Ind. Eng. Chem.* **1929**, *21*, 405–410.
- (10) Syverud, K.; Stenius, P. *Cellulose* **2009**, *16*, 75–85.
- (11) Nogi, M.; Iwamoto, S.; Nakagaito, A.; Yano, H. *Adv. Mater.* **2009**, *21*, 1595–1598.
- (12) Fukuzumi, H.; Saito, T.; Iwata, T.; Kumamoto, Y.; Isogai, A. *Biomacromolecules* **2009**, *10*, 162–165.
- (13) Fukuzumi, H.; Saito, T.; Iwamoto, S.; Kumamoto, Y.; Ohdaira, T.; Suzuki, R.; Isogai, A. *Biomacromolecules* **2011**, *12*, 4057–4062.
- (14) Siró, I.; Plackett, D. *Cellulose* **2010**, *17*, 459–494.
- (15) Yang, Q.; Fukuzumi, H.; Saito, T.; Isogai, A.; Zhang, L. *Biomacromolecules* **2011**, *12*, 2766–2771.
- (16) Aulin, C.; Gällstedt, M.; Lindström, T. *Cellulose* **2010**, *17*, 559–574.
- (17) Sehaqui, H.; Liu, A.; Zhou, Q.; Berglund, L. A. *Biomacromolecules* **2010**, *11*, 2195–2198.
- (18) Zhu Ryberg, Y. Z.; Edlund, U.; Albertsson, A. C. *Biomacromolecules* **2011**, *12*, 1355–1362.
- (19) Edlund, U.; Zhu Ryberg, Y. Z.; Albertsson, A. C. *Biomacromolecules* **2010**, *11*, 2532–2538.
- (20) Hartman, J.; Albertsson, A. C.; Sjöberg, J. *Biomacromolecules* **2006**, *7*, 1983–1989.
- (21) Hartman, J.; Albertsson, A. C.; Lindblad, M. S.; Sjöberg, J. *J. Appl. Polym. Sci.* **2006**, *100*, 2985–2991.
- (22) Cai, J.; Zhang, L.; Zhou, J.; Qi, H.; Chen, H.; Kondo, T.; Chen, X.; Chu, B. *Adv. Mater.* **2007**, *19*, 821–825.
- (23) Cai, J.; Zhang, L.; Chang, C.; Cheng, G.; Chen, X.; Chu, B. *ChemPhysChem* **2007**, *8*, 1572–1579.
- (24) Qi, H.; Chang, C.; Zhang, L. *Green Chemistry* **2009**, *11*, 177–184.

- (25) Yang, Q.; Qi, H.; Lue, A.; Hu, K.; Cheng, G.; Zhang, L. *Carbohydr. Polym.* **2011**, *83*, 1185–1191.
- (26) Yang, Q.; Qin, X.; Zhang, L. *Cellulose* **2011**, *18*, 681–688.
- (27) Yang, Q.; Lue, A.; Zhang, L. *Compos. Sci. Technol.* **2010**, *70*, 2319–2324.
- (28) Yang, Q.; Lue, A.; Qi, H.; Sun, Y.; Zhang, X.; Zhang, L. *Macromol. Biosci.* **2009**, *9*, 849–856.
- (29) Gindl, W.; Martinschitz, K. J.; Boesecke, P.; Keckes, J. *Biomacromolecules* **2006**, *7*, 3146–3150.
- (30) Kong, K.; Eichhorn, S. J. *Polymer* **2005**, *46*, 6380–6390.
- (31) Northolt, M. G.; Boerstoel, H.; Maatman, H.; Huisman, R.; Veurink, J.; Elzerman, H. *Polymer* **2001**, *42*, 8249–8264.
- (32) Fink, H. P.; Weigel, P.; Purz, H. J.; Ganster, J. *Prog. Polym. Sci.* **2001**, *26*, 1473–1524.
- (33) Liu, S.; Zhang, L.; Sun, Y.; Lin, Y.; Zhang, X.; Nishiyama, Y. *Macromol. Biosci.* **2009**, *9*, 29–35.
- (34) Cai, J.; Wang, Q.; Zhang, L. *China Patent* **2010**, ZL20100235233.1.
- (35) Yang, Q.; Fujisawa, S.; Saito, T.; Isogai, A. *Cellulose* **2012**, *19*, 695–703.
- (36) Rabek, J. F. “*Experimental Methods in Polymer Chemistry*”, John Wiley & Sons, Chichester 1980, p. 507.
- (37) Alexander, L. E. “*X-ray Diffraction Methods in Polymer Science*”, Robert E. Kreiger Publishing Co., Humington, NY 1979, p. 423-424.
- (38) Park, S.; Baker, J. O.; Himmel, M. E.; Parilla, P. A.; Johnson, D. K. *Biotechnol. Biofuels* **2010**, *3*, 1–10.
- (39) Hori, R.; Wada, M. *Cellulose* **2006**, *13*, 281–290.
- (40) Nishino, T.; Matsuda, I.; Hirao, K. *Macromolecules* **2004**, *37*, 7683–7687.
- (41) Ebina, T.; Mizukami, F. *Adv. Mater.* **2007**, *19*, 2450–2453.

Chapter 4

Cellulose Based Nanocomposites Reinforced with Nanoclay

4.1 Introduction

Recently, understanding and exploiting the unique properties of polymer nanocomposites have received increasing attention.^{1–6} Inorganic films possess higher thermal and chemical resistance as well as a longer lifetime than their polymer counterparts, but they are brittle with poor film-forming ability.^{7,8} In polymer–inorganic nanocomposites, inorganic nanofillers are present in the polymer matrix at almost individual nano-element level and thus nanocomposites behave differently to conventional composites.^{9–11} Nanocomposites can exhibit a combination of the basic properties of the polymer and inorganic nanofiller, and in some cases offer specific advantages or synergistic properties at particular weight ratios of the two components, such as excellent gas barrier performance, good thermal and chemical resistance and adaptability to harsh environments, while maintaining similar film-forming ability to the original polymer.^{12–15}

Composites of polymers with nanolayered silicates or clays show improved gas barrier, modulus, tensile strength, and thermal stability properties than the polymer alone. The nanolayered platelets of clay form a “tortuous path” for gas molecules in polymer matrices, resembling biomimetic brick and mortar structures.^{4,16–19} The addition of nanoclays into polymers has been shown to enhance gas barrier properties relative to the original polymers, and the enhancement is related to the aspect ratio of the nanoclay.^{4,20} Individual clay nanoparticles that can act as gas-impermeable nanoflakes are approximately 1 nm thick, disk-shaped, and possess aspect ratios ranging from 20 to several thousand.^{21–24} Polymer–clay nanocomposite materials have been extensively studied since the 1970s.^{25–27} Sufficient dispersibility of individual nanoclay particles in the polymer matrix is the most significant factor influencing the properties of the composite. However, it is generally difficult to

maintain sufficient dispersion of nanoclay particles in composites with high clay loadings. Such clay aggregates cause increased opacity and random platelet alignment that ultimately reduce the gas barrier properties.^{28,29} Thus, incorporation of nanoclay particles into polymeric matrices with high degrees of exfoliation and orientation is currently the most important challenge to fabricate polymer–clay nanocomposites with enhanced properties.³⁰

Petroleum–based polymers are generally used as matrices in most polymer–clay nanocomposites, and thus are non–biodegradable and not environmentally friendly. New biopolymer materials that are renewable, biocompatible, and biodegradable are in great demand.^{31–32} Cellulose is the most abundant biopolymer on earth.^{33–35} In the previous chapters, regenerated cellulose films prepared from aqueous alkali/urea solutions were found to exhibit good mechanical properties, optical transparency, biocompatibility, biodegradability, and oxygen barrier properties under dry conditions.^{36–39} However, the oxygen permeability of the cellulose films significantly increased at high humidity.

In this chapter^{40,41}, cellulose–based nanocomposite films fabricated from LiOH/urea/cellulose (LUC) solutions were reinforced with clay particles to improve their mechanical strength, thermal stability and gas barrier properties under humid conditions. The relationships between the nanostructure of clay particles in the cellulose matrix and mechanical, optical, gas–barrier and hydrophilic properties are studied for cellulose–clay nanocomposites with various weight ratios. Moreover, differences in the properties of nanocomposites containing synthetic saponite (SPN) and natural montmorillonite (MTM) as nanoclays are also investigated. These cellulose–clay nanocomposites are expected to have superior properties as well as being new eco–friendly materials.

4.2 Experimental Section

4.2.1 Materials

A filter paper pulp (highly purified cotton linters, Advantec Co., Ltd., Japan) was used as the cellulose sample with an viscosity–average molecular weight of $8.6 \times 10^4 \text{ g mol}^{-1}$.³⁶ Commercially available synthetic smectite SPN with an aspect ratio of 50 (Smecton SA,

Kunimine Industries Co., Ltd., Japan) and natural MTM with an aspect ratio of 300–600 (Kunipia F, Kunimine Industries Co., Ltd., Japan) were used as nanoclay samples. The chemical formulae of SPN and MTM clays are $\text{Na}_{1/3}\text{Mg}_3(\text{Si}_{11/3}\text{Al}_{1/3})\text{O}_{10}(\text{OH})_2$, and $\text{Na}_{2/3}\text{Si}_8(\text{Al}_{10/3}\text{Mg}_{2/3})\text{O}_{20}(\text{OH})_4$, respectively. All reagents and solvents were of laboratory grade and used as received from Wako Pure Chemicals, Tokyo, Japan.

4.2.2 Film preparation

A solution of LiOH/urea/H₂O with a weight ratio of 4.6:15:80.4 was prepared. A desired amount of SPN or MTM was dispersed in the above solution, which was then stirred for 2 h at room temperature. The clay dispersion was further agitated at 7500 rpm for 2 min using a homogenizer (Excel Auto ED-4, Nissei, Japan) and then with an ultrasonic homogenizer with a 26 mm probe tip diameter at an output power of 300 W for 6 min (US-300T, Nissei, Japan) at room temperature. The clay dispersion thus obtained was then cooled to -12 °C in a refrigerator. A desired amount of cellulose was dispersed in the cooled clay dispersion, which was stirred immediately at 1200 rpm for 10 min to obtain a transparent solution with cellulose content of 4 wt %.³⁴ The blend solution was degassed by centrifugation at 5600g for 10 min, spread on a glass plate, and then immersed in acetone at room temperature for 30 min to allow regeneration.³⁴ The resulting sheet-like hydrogel was thoroughly washed by soaking in water, fixed on a poly(methyl methacrylate) plate with adhesive tape to prevent shrinkage, and air-dried at ambient temperature. The weight ratios of LUC and either SPN or MTM in the composite films investigated were 100:0, 95:5, 90:10, 85:15 and 80:20, which are denoted LUC, LUC-SPN5, LUC-SPN10, LUC-SPN15 and LUC-SPN20 or LUC, LUC-MTM5, LUC-MTM10, LUC-MTM15 and LUC-MTM20, respectively. To study the effects of drawing, the wet film (LUC-SPN15 or LUC-MTM15) were drawn and dried at a draw ratio of 1.15 for 8 h, using a tensile testing apparatus (Shimadzu EZ-TEST) at room temperature. The obtained drawn film is denoted here as LUC-SPN15D or LUC-MTM15D, respectively.

In addition, a desired amount SPN or MTM was dispersed in deionized water, and the dispersion was stirred and agitated as described above to prepare a 2 wt % dispersion of SPN or MTM. The obtained clay dispersions were dried in a ventilated oven at 40 °C for 3 days to obtain films of SPN and MTM.

4.2.3 Characterizations

X-ray diffraction (XRD) patterns of the films were acquired in reflection mode using a RINT 2000 diffractometer (Rigaku, Tokyo, Japan) with monochromator-filtered Cu $K\alpha$ radiation ($\lambda = 0.15418$ nm) at 40 kV and 40 mA. Two-dimensional X-ray diffraction patterns (2D XRD) were obtained at room temperature using nickel-filtered Cu $K\alpha$ radiation with a wavelength of 0.15418 nm, which was generated using a rotating anode X-ray generator (Rigaku RU-200BH) operating at 50 kV and 100 mA. The X-ray beam was applied to the film surface plane or film cross-section. The patterns were recorded on flat-plate imaging plates (Fuji Film BAS-IP SR 127) using an evacuated camera. Sodium fluoride ($d = 0.23166$ nm) was dusted on the surface of the samples to provide a calibration. From the azimuthal intensity distribution graphs for the (1 -1 0) reflection of cellulose II or the (0 0 1) reflection of SPN, two orientation factors—the degree of orientation (IT), and Herman's orientation parameter (f)—were calculated according to a previously reported method.⁴²

The films were frozen in liquid nitrogen, immediately snapped and then vacuum-dried. The surfaces and cross-sections (fracture surfaces) of the films were coated with osmium using a Meiwafoysis Neo osmium coater at 10 mA for 5 s, and observed with a Hitachi S4800 field-emission scanning electron microscope (SEM) at 2 kV. Energy-dispersive X-ray (EDX) analysis of SPN, MTM and their composite films was carried out using a Horiba EMAX Energy spectroscope attached to the SEM. In the case of SEM-EDX analysis, the acceleration voltage and accumulation time were set to 10 kV and 500 s, respectively.

The optical transmittance of the films was measured from 400 to 800 nm using a JASCO V-670 UV-Vis spectrophotometer. Tensile tests were performed using a Shimadzu EZ-TEST instrument equipped with a 500 N load cell. Rectangular strips 2×30 mm in size were cut from the films and tested with a span length of 10 mm at a rate of 1.0 mm min⁻¹. At least 10 measurements were carried out for each sample. The thermal expansion of the films following preheating at 120 °C for 10 min was determined under a load of 0.03 N and a nitrogen atmosphere from 28 to 100 °C at 5 °C min⁻¹ using a Shimadzu TMA-60 thermomechanical analyzer.

The rates of oxygen and water vapor transmission of the films were determined at 23 and 37.8 °C, respectively, using a Mocon Ox-Tran Model 2/21MH and Mocon Permatran-W

Model 1/50G (Modern Controls Inc., US) under standard conditions (ASTM 3985). Each measurement was continued until the rate of O₂ or water vapor transmission reached a stable value. The gas permeability was calculated from the gas transmission rate and film thickness, and the standard deviations for each film were within $\pm 5\%$. The films were conditioned at 23 °C and 50% relative humidity (RH) for 2 days and the moisture contents under these conditions were calculated from the film weights before and after heating at 105 °C for 3 h. The films were immersed in deionized water at room temperature for 6 days to reach swelling equilibrium and water uptakes ($W_{(\text{water uptake})}$) were calculated from the film weights before and after heating at 105 °C for 3 h according to the following equation:

$$W_{(\text{water uptake})} = (m_{(\text{wet})} - m_{(\text{dry})})/m_{(\text{cellulose})} \times 100\%,$$

where $m_{(\text{wet})}$ is the weight of the film after being immersed in water, $m_{(\text{dry})}$ is the weight of the film after heating, and $m_{(\text{cellulose})}$ is the dry weight of cellulose in the film. Contact angles of water droplets with a volume of 2 μL on the films were measured at 23 °C and 50% RH using a FAMAS DM500 instrument (Kyowa Interface Science Co. Ltd., Japan).

4.3 Results and Discussion

4.3.1 Structures of cellulose–clay nanocomposites

Figure 4.1 shows XRD patterns of the LUC, SPN, MTM, and LUC–SPN and LUC–MTM composites. The d -spacings of (001) planes of SPN and MTM were both calculated to be 1.2 nm from the diffraction peak at $2\theta = 6.6^\circ$ using the Bragg equation. LUC has no diffraction peak in the 2θ range from 2 to 10° . The d -spacing of SPN increased from 1.2 to 1.9 nm in the LUC–SPN composites and from 1.2 to 1.6 nm in the LUC–MTM composites as the cellulose content was increased from 0 to 95 wt %, revealing the formation of intercalated structures of SPN and MTM platelets in the cellulose matrix films. The (001) d -spacings of the LUC–MTM composites were smaller than those of the LUC–SPN ones, indicating higher intercalation efficiency of SPN platelets than MTM. The d -spacing of 1.6 nm for SPN in the LUC–SPN20 film or MTM in the LUC–MTM5 film was 0.4 nm greater than that of the neat SPN or MTM film (1.2 nm), which corresponds to the presence of a single layer (ca. 0.4 nm)

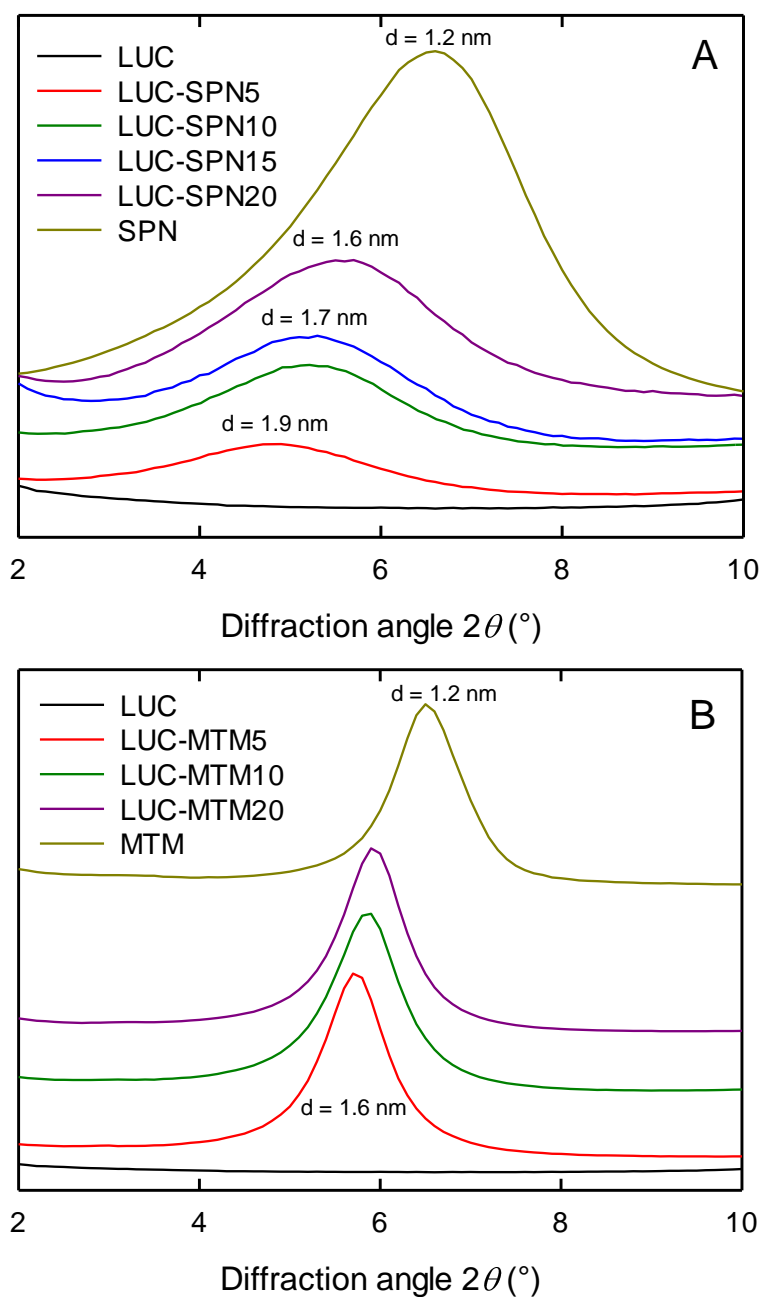


Figure 4.1. XRD patterns of LUC, SPN, MTM, and LUC–SPN and LUC–MTM composite films. Reproduction from ref. 40 with permission from Elsevier (© Elsevier 2012) and ref. 41 with permission from John Wiley and Sons (© John Wiley and Sons 2013).

of cellulose molecules between the SPN or MTM platelets.^{27,43} The d -spacing of SPN in the LUC-SPN5 film increased to 1.9 nm, which correspond to the presence of a double layer of cellulose molecules between the SPN platelets.

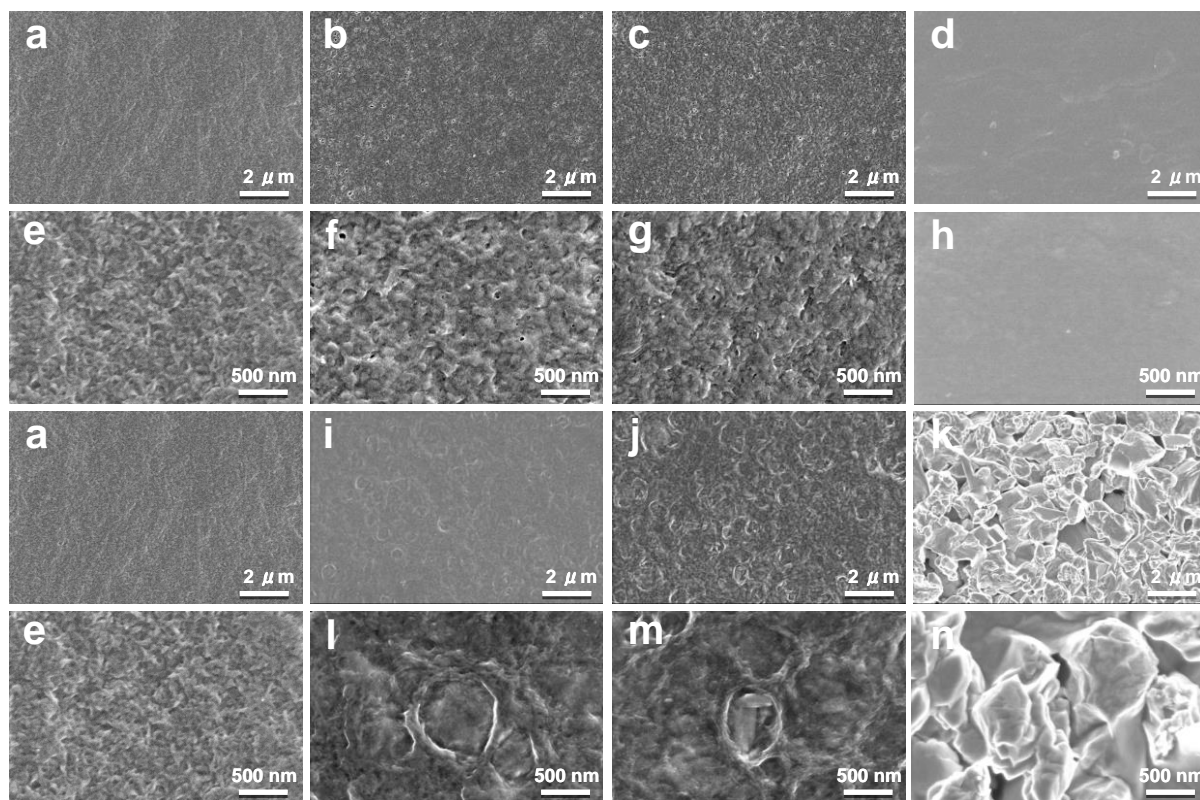


Figure 4.2. SEM images of the surface of (a, e) LUC, (b, f) LUC-SPN5, (c, g) LUC-SPN15, (d, h) SPN, (i, l) LUC-MTM5, (j, m) LUC-MTM15, and (k, n) MTM films. Reproduction from ref. 40 with permission from Elsevier (© Elsevier 2012) and ref. 41 with permission from John Wiley and Sons (© John Wiley and Sons 2013).

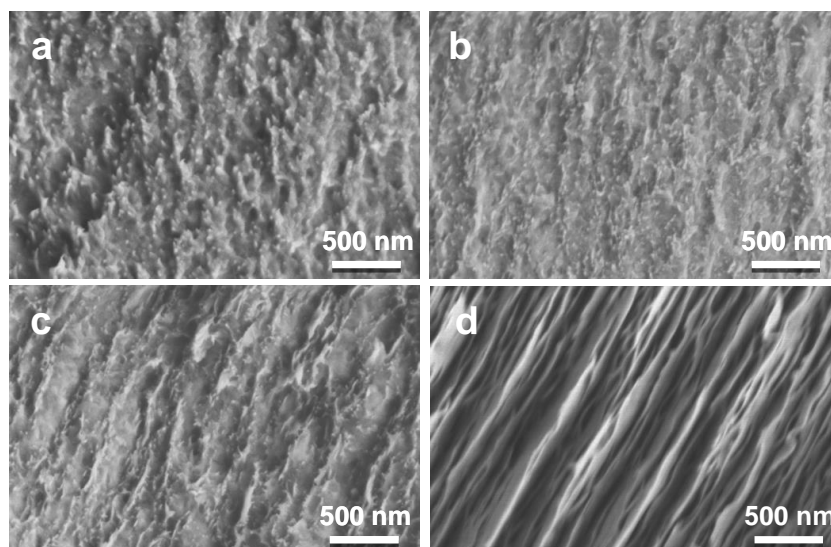


Figure 4.3. SEM images of cross-sections of (a) LUC, (b) LUC–SPN5, (c) LUC–SPN15 and (d) SPN films. Reproduction from ref. 41 with permission from John Wiley and Sons (© John Wiley and Sons 2013).

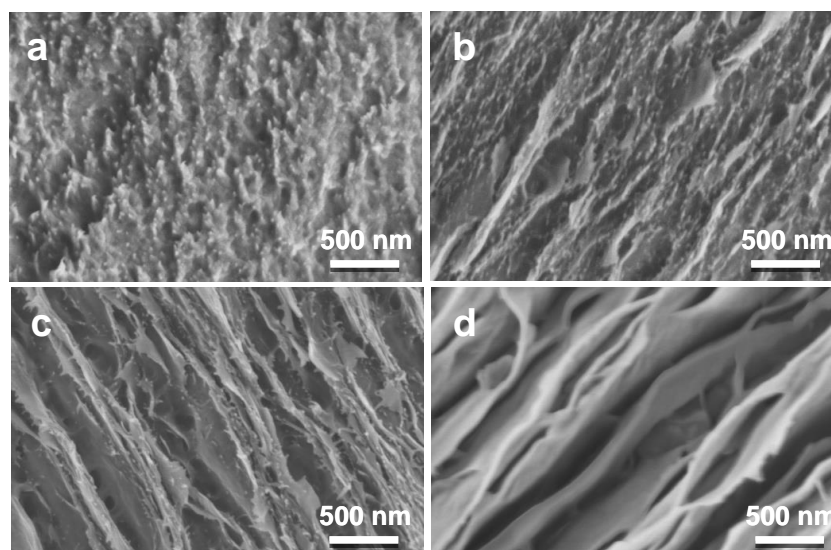


Figure 4.4. SEM images of cross-sections of (a) LUC, (b) LUC–MTM5, (c) LUC–MTM15 and (d) MTM films. Reproduction from ref. 40 with permission from Elsevier (© Elsevier 2012).

Figures 4.2 show SEM images of the surfaces of the films. The size of MTM platelets in the planar direction was ~ 500 nm, which was much larger than that of SPN platelets. Figures 4.3 and 4.4 show SEM images of the cross-sections of the films. The SPN and MTM films displayed regularly layered platelet structures. The SPN film had thinner and more uniform platelets with smaller interstices than the MTM film. Nanolayered structures regularly appeared in the composites with an increase in SPN or MTM content, and the layered structures were parallel to the film surface. Meanwhile, the SPN or MTM platelets became thinner and displayed smaller interstices as cellulose content in the composite increased. The XRD and SEM results indicate the formation of intercalated nanolayered platelet structures of SPN and MTM in the LUC matrix to form cellulose–clay nanocomposite films.^{1,2,16}

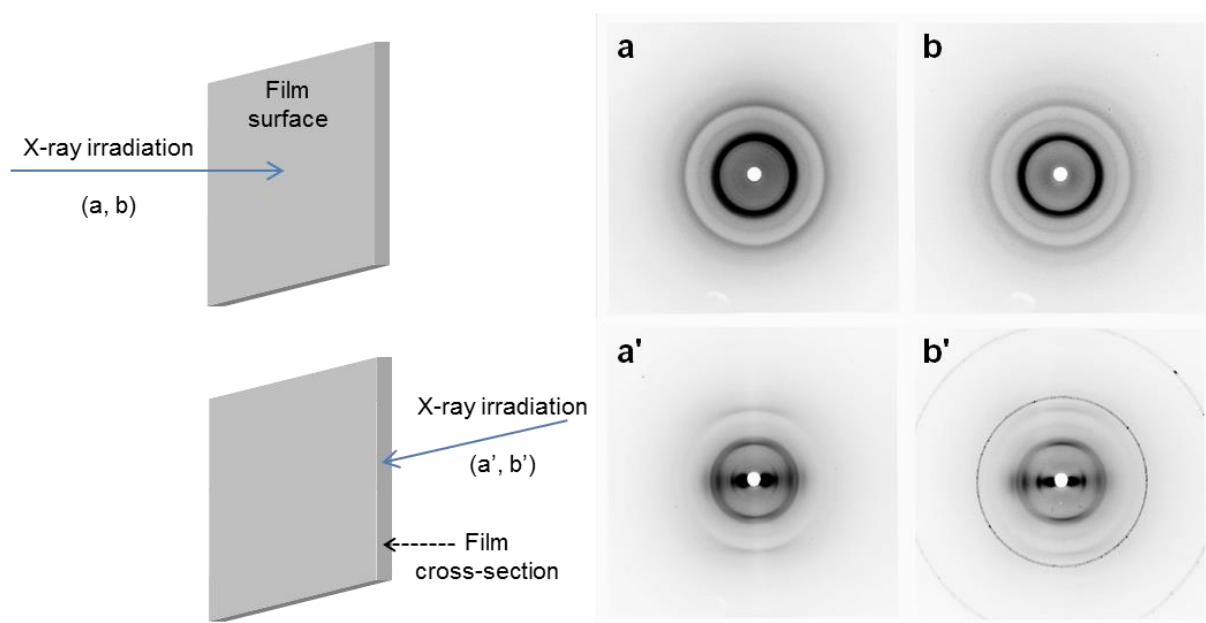


Figure 4.5. Two-dimensional XRD diagrams for LUC-SPN15 (a, a') and LUC-SPN15D (b, b') films. The X-ray beam was applied perpendicular (a, b) and parallel (a', b') to the film surface plane, respectively. Reproduction from ref. 41 with permission from John Wiley and Sons (© John Wiley and Sons 2013).

Table 4.1. Degree of orientation (I) and Herman’s orientation parameter (f) of LUC–SPN15 and LUC–SPN15D films. Reproduction from ref. 41 with permission from John Wiley and Sons (© John Wiley and Sons 2013).

Sample	Crystal plane	Degree of orientation, I (%)	Herman’s orientation parameter, f
LUC–SPN15	(1-10) of cellulose	82.2	0.84
LUC–SPN15D	(1-10) of cellulose	84.2	0.88
LUC–SPN15	(001) of SPN	82.6	0.86
LUC–SPN15D	(001) of SPN	87.0	0.89

The orientation behavior of the clay platelets and cellulose II crystallites in the LUC–SPN15 and LUC–SPN15D composite films was studied using 2D XRD (Figure 4.5). Ring diffractions indicate the random orientation of crystallites, whereas arc diffractions are characteristic of their preferred orientations. The cellulose II crystallites and the SPN platelets were randomly oriented in the film plane in both the LUC–SPN15 and LUC–SPN15D composite films. In contrast, clear diffraction arcs were observed for both SPN and cellulose II when X-ray irradiation was applied to the film cross-sections. Thus, the longitudinal directions of both the SPN platelets and the cellulose II crystallites were highly oriented parallel to the film surface. Degree of orientation (I) and Herman’s orientation parameter (f) values were calculated for the cellulose II crystallites and SPN platelets in the LUC–SPN15 and LUC–SPN15D films from the 2D XRD patterns, and are listed in Table 4.1. Both the SPN platelets and the cellulose II crystallites showed a high degree of orientation parallel to the film surface in the composite films, forming layered structures. Both SPN and cellulose II showed a higher degree of orientation in the drawn film LUC–SPN15D than in the undrawn film LUC–SPN15. These nano-layered clay platelet structures had a positive influence on the mechanical, gas barrier, and thermal properties, as discussed later.⁶

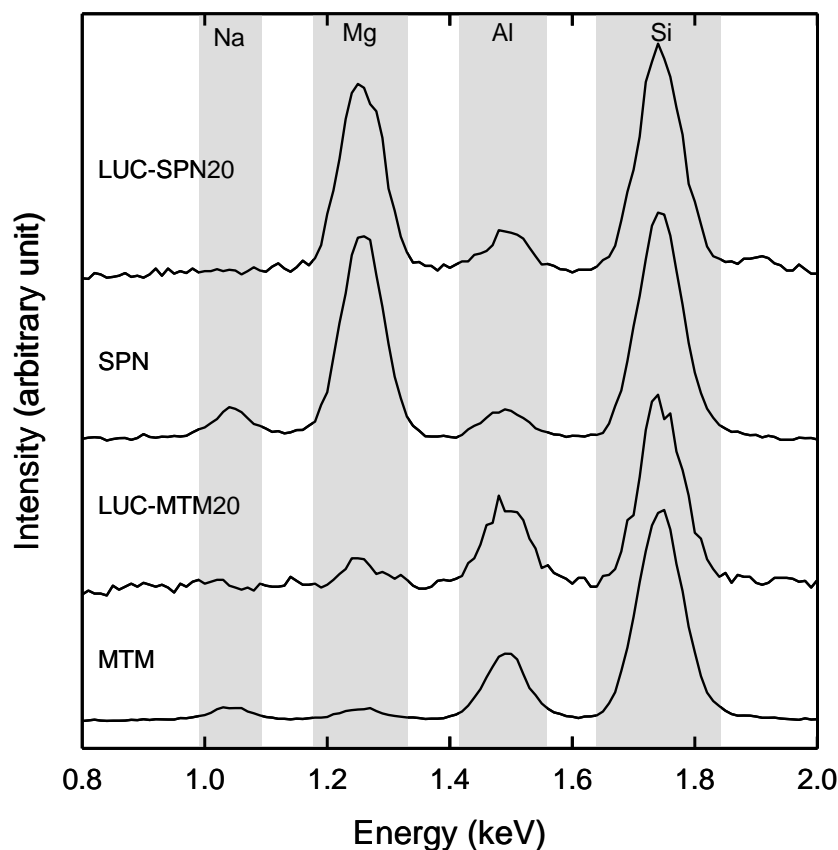


Figure 4.6. SEM–EDX patterns of SPN, MTM, LUC–SPN20 and LUC–MTM20 films. Reproduction from ref. 40 with permission from Elsevier (© Elsevier 2012) and ref. 41 with permission from John Wiley and Sons (© John Wiley and Sons 2013).

Because aqueous LiOH/urea solution was used for dissolution of cellulose and dispersion of SPN or MTM platelets, it is possible for Na ions in SPN or MTM to be exchanged for Li ions in the composites. Figure 4.6 shows SEM–EDX patterns of SPN, MTM, LUC–SPN20 and LUC–MTM20 composite films. As expected, most of the Na ions originally present in SPN or MTM were absent from the LUC–SPN20 and LUC–MTM20 films. Even though the presence of Li in the composite films could not be directly detected by SEM–EDX analysis because of analytical limitation, it is likely that almost all of the Na ions in the original SPN and MTM were substituted for Li ions in the composites. Moreover, such ion-exchange in

SPN and MTM platelets may enhance the formation of nanolayered structures in LUC–SPN and LUC–MTM composites.

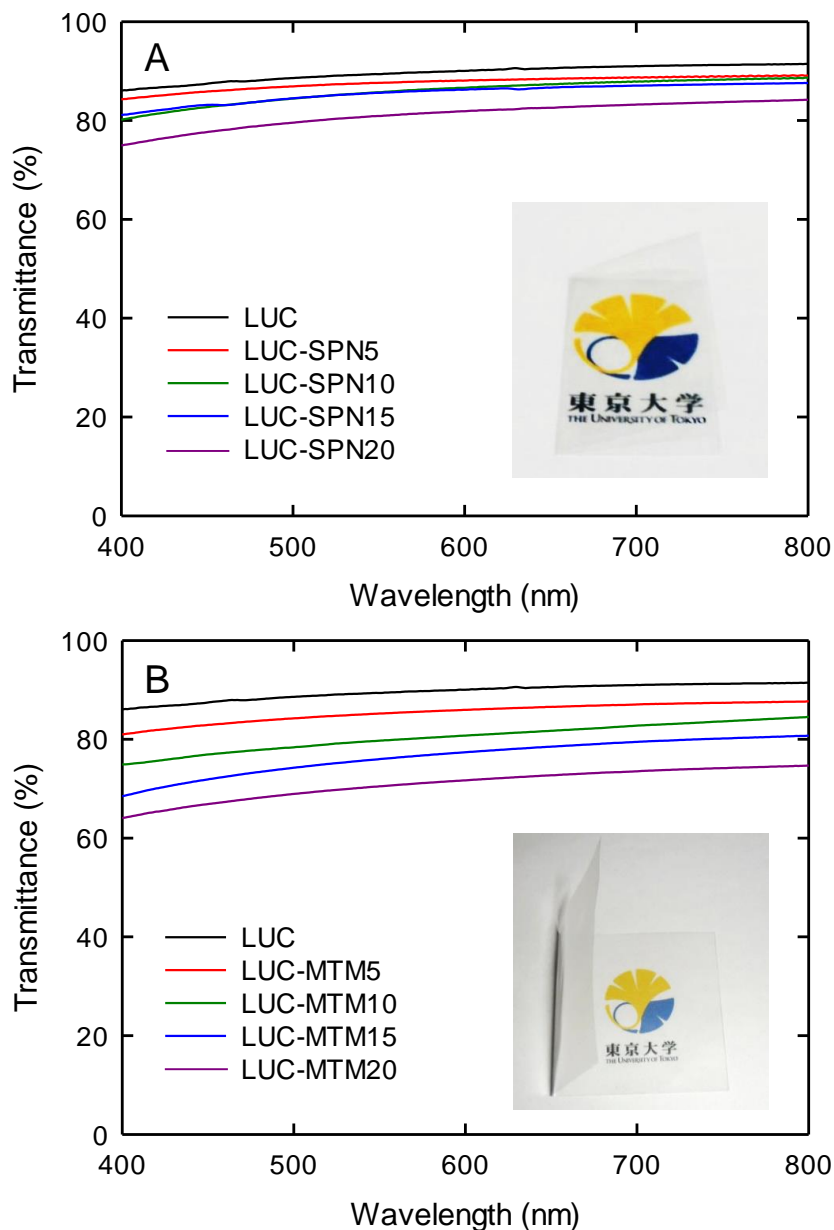


Figure 4.7. Visible light transmittance of (A) LUC and LUC–SPN, and (B) LUC and LUC–MTM nanocomposite films. Insets in (A) and (B) show photographs of LUC–SPN15 and LUC–MTM15 films, respectively, with a thickness of 30 μm . Reproduction from ref. 40 with permission from Elsevier (© Elsevier 2012) and ref. 41 with permission from John Wiley and Sons (© John Wiley and Sons 2013).

4.3.2 Optical and mechanical properties of cellulose–clay nanocomposites

In general, optical transparency is a useful criterion for the compatibility of composite elements.⁴⁴ Figure 4.7 shows the optical transmittance of the LUC, LUC–SPN and LUC–MTM nanocomposite films, as well as photographs of LUC–SPN15 and LUC–MTM15 films. The photographs show the high optical transparency and flexibility of the nanocomposite films. The optical transmittance of the LUC film at 600 nm was 90%, and this value decreased slightly to 86–88% for SPN contents of 5–15 wt %. The optical transmittance of the LUC–SPN20 film was 78%, which is lower than those of the other nanocomposites, indicating some aggregation of SPN platelets in the composite film was caused by a high loading of SPN. The optical transmittance of the LUC–MTM nanocomposite films decreased as the content of MTM was increased, and it was lower than that of the equivalent LUC–SPN film with the same clay content, probably because of the larger size and less uniform morphology of the MTM platelets compared with SPN ones. It is likely many interfaces are present in the LUC–MTM nanocomposite films, which cause optical scattering and refraction when the content of clay is high.

Table 4.2. Mechanical properties of LUC, LUC–SPN and LUC–MTM nanocomposite films.

Sample	Clay content (wt %)	Tensile strength (MPa)	Young's modulus (GPa)	Elongation at break (%)	Work of fracture (MJ/m ³)
LUC	0	116±21	3.4±0.4	37±9	35.0±2.5
LUC–SPN5	5	132±9	3.6±0.3	32±6	33.5±1.6
LUC–SPN10	10	147±17	4.2±0.5	27±9	31.6±2.8
LUC–SPN15	15	161±9	5.2±0.3	18±6	22.6±1.2
LUC–SPN20	20	157±13	5.5±0.6	12±2	14.4±0.8
LUC–MTM5	5	160±18	4.7±0.7	29±8	36.9±2.6
LUC–MTM10	10	169±14	5.4±0.9	20±7	26.7±1.5
LUC–MTM15	15	187±11	6.1±0.8	17±6	25.7±2.4
LUC–MTM20	20	161±10	5.1±0.4	14±3	16.9±1.1
LUC–SPN15D	15	241±10	7.7±0.5	17±3	31.1±0.9
LUC–MTM15D	15	287±12	9.3±0.6	16±5	34.9±1.8

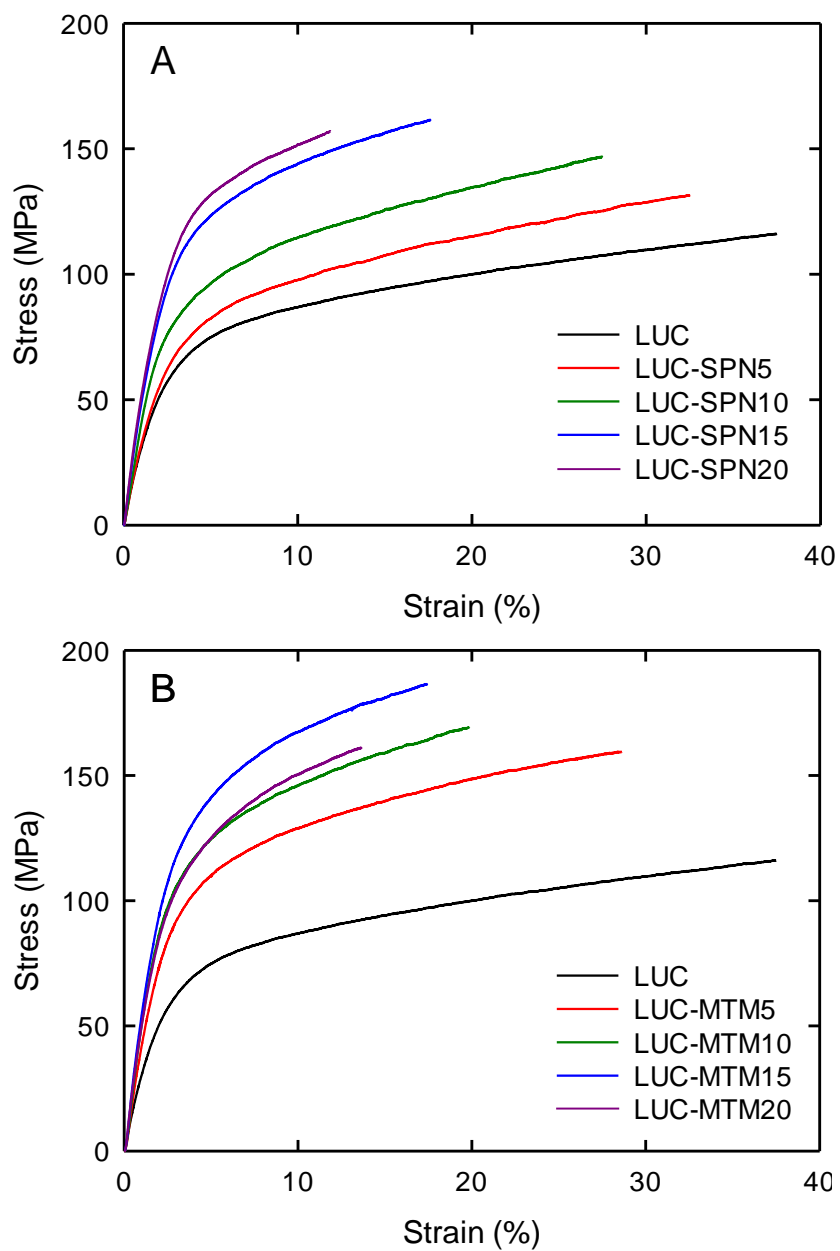


Figure 4.8. Stress–strain curves of (A) LUC and LUC–SPN, and (B) LUC and LUC–MTM nanocomposite films. Reproduction from ref. 40 with permission from Elsevier (© Elsevier 2012) and ref. 41 with permission from John Wiley and Sons (© John Wiley and Sons 2013).

The stress–strain curves of the LUC, LUC–SPN, LUC–MTM, and LUC–SPN15D, LUC–MTM15D nanocomposite films are shown in Figures 4.8 and 4.9. The SPN and MTM films were too brittle to undergo tensile testing. The mechanical properties of the nanocomposite films are listed in Table 4.2. The Young’s modulus of the LUC–SPN nanocomposite films increased from 3.4 to 5.5 GPa as the content of SPN was increased from 0 to 20 wt %. The tensile strength of the LUC film was improved from 116 to 161 MPa when it contained 15 wt % SPN. However, when the SPN content was 20 wt %, the tensile strength decreased to 157 MPa, which may be caused by aggregation of SPN platelets in the composite. The Young’s modulus of the LUC–MTM films increased from 3.4 to 6.1 GPa and the tensile strength increased from 116 MPa to 187 MPa as the MTM content was increased from 0 to 15 wt %. The LUC–MTM nanocomposite films possessed higher tensile strength and Young’s modulus than those of the LUC–SPN nanocomposite films, probably because the MTM platelets had a higher aspect ratio than the SPN ones. The work of fracture of the LUC, LUC–SPN and LUC–MTM films ($17\text{--}37\text{ MJ m}^{-3}$) is higher than those of wood (dry yew), steel (spring), bone, rubber (natural), and nanofibrillated cellulose (NFC) paper, which are 0.5, 1, 3, 10 and 15.1 MJ m^{-3} , respectively.⁴⁵ The elongation at break of the LUC-based films was large (12–37% depending on clay content), so the LUC–SPN and LUC–MTM nanocomposite films are both highly tough and ductile because of the LUC component. In particular, the LUC–MTM5 film possesses a work of fracture of 36.9 MJ m^{-3} and an elongation at break of 29%. The improvement of these mechanical properties indicates that the MTM platelets are sufficiently dispersed state in the cellulose matrix.^{6,16,46,47}

Moreover, the tensile strength and Young’s modulus of the LUC-SPN15D and LUC–MTM15D composite film reached 241 MPa and 7.7 GPa, 287 MPa and 9.3 GPa, respectively, when a simple drawing treatment was applied, probably due to the increase in the orientation of the cellulose II crystallites and SPN platelets in the film (Figure 4.5 and Table 4.1).

4.3.3 Thermal properties of cellulose–clay nanocomposites

The thermal expansion of the films was measured under a nitrogen atmosphere after heating the films at 120 °C for 10 min to remove any residual moisture (Figure 4.10). The coefficient of thermal expansion (CTE) of the LUC–SPN nanocomposite films decreased

from 18.4 to 13.2 ppm K⁻¹ as the SPN content was increased from 0 to 15 wt %. The CTE of the LUC–MTM nanocomposite films decreased to 11.1 ppm K⁻¹ when the content of MTM was 15 wt %. Moreover, the CTE of the LUC–MTM nanocomposite film was lower than that of the LUC–SPN nanocomposite film with the same clay content, probably because of the larger aspect ratio of the MTM platelets.

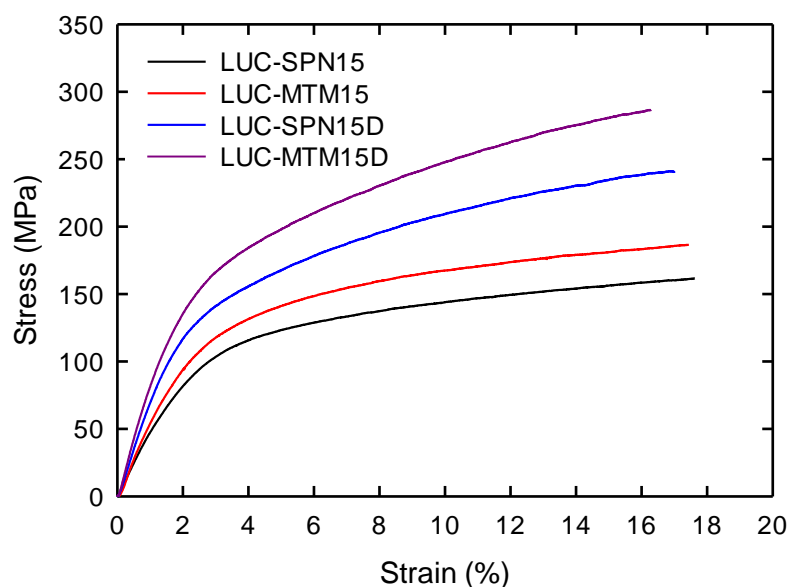


Figure 4.9. Stress–strain curves of LUC–SPN15, LUC–SPN15D, LUC–MTM15, and LUC–MTM15D nanocomposite films.

4.3.4 Gas barrier properties of cellulose–clay nanocomposites

Gas barrier properties of polymer films can be improved by forming composites with inorganic platelets with sufficient aspect ratios, which alter the diffusion path of penetrant gas molecules.⁴ The oxygen transmission rates of the LUC–SPN and LUC–MTM nanocomposite films at 0% RH were less than 0.0005 mL m⁻² day⁻¹ kPa⁻¹, which was the limit of detection of the instrument. This value is much lower than those of practical oxygen barrier films such as ethylene–vinyl alcohol copolymer, poly(vinylidene chloride), and poly(vinyl alcohol).⁴⁸ The

nanolayered structures of the clay platelets in the composites should increase the diffusion length for oxygen according to the tortuous-path model.^{49,6} The original LUC film contains inherently numerous hydrogen bonds formed directly between cellulose molecules under dry conditions, resulting in an extremely low oxygen permeability.³⁶

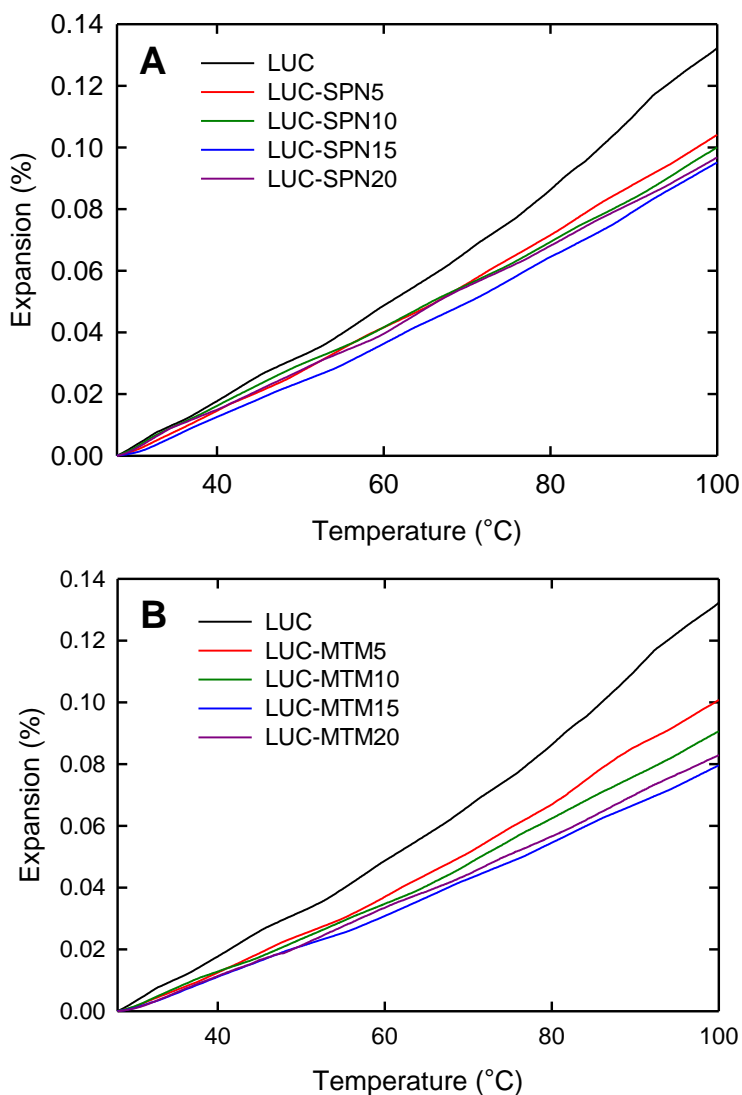


Figure 4.10. Thermal expansion behavior of (A) LUC and LUC–SPN, and (B) LUC and LUC–MTM nanocomposite films. Reproduction from ref. 40 with permission from Elsevier (© Elsevier 2012) and ref. 41 with permission from John Wiley and Sons (© John Wiley and Sons 2013).

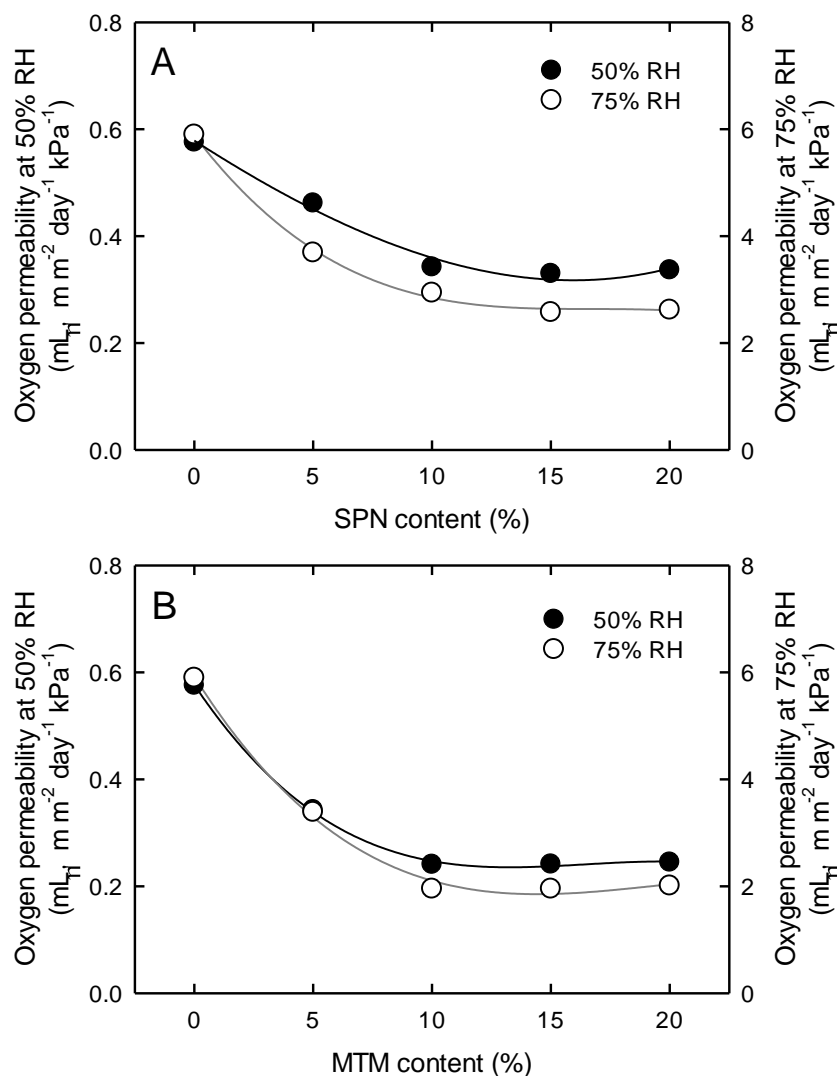


Figure 4.11. Oxygen permeabilities of (A) LUC–SPN and (B) LUC–MTM nanocomposite films at 50% and 75% RH. Reproduction from ref. 40 with permission from Elsevier (© Elsevier 2012) and ref. 41 with permission from John Wiley and Sons (© John Wiley and Sons 2013).

Figure 4.11 shows the oxygen permeabilities of the LUC, LUC–SPN and LUC–MTM nanocomposite films at 50 and 75% RH. The oxygen permeability of the LUC film was 0.58

and $5.9 \text{ mL } \mu\text{m m}^{-2} \text{ day}^{-1} \text{ kPa}^{-1}$ at 50 and 75% RH, respectively. The hydrophilic nature of cellulose molecules results in a high moisture content of $>10\%$ at 50% RH (Figure 4.13), which promotes dissolution and diffusion of oxygen molecules in water molecules absorbed on the LUC film, leading to a significant increase in oxygen permeability.³⁶ On the other hand, the oxygen permeability of the LUC film decreased even at 50 and 75% RH upon forming a composite with SPN or MTM. The LUC–MTM nanocomposite films exhibited higher oxygen barrier properties than the LUC–SPN films, again probably because the MTM platelets had a higher aspect ratio than the SPN ones.

The oxygen permeabilities of the LUC–SPN and LUC–MTM nanocomposite films under high RH are comparable to those of practical oxygen barrier films such as poly(vinylidene chloride) ($0.4\text{--}5.1 \text{ mL } \mu\text{m m}^{-2} \text{ day}^{-1} \text{ kPa}^{-1}$ at 50% RH), and are much lower than that of high density poly(ethylene) ($427 \text{ mL } \mu\text{m m}^{-2} \text{ day}^{-1} \text{ kPa}^{-1}$ at 50% RH) or poly(ethylene terephthalate) ($15.6 \text{ mL } \mu\text{m m}^{-2} \text{ day}^{-1} \text{ kPa}^{-1}$ at 50% RH).⁵⁰ The water vapor permeabilities of the LUC film increased with RH, and decreased slightly when composites with SPN or MTM were formed (Figure 4.12).

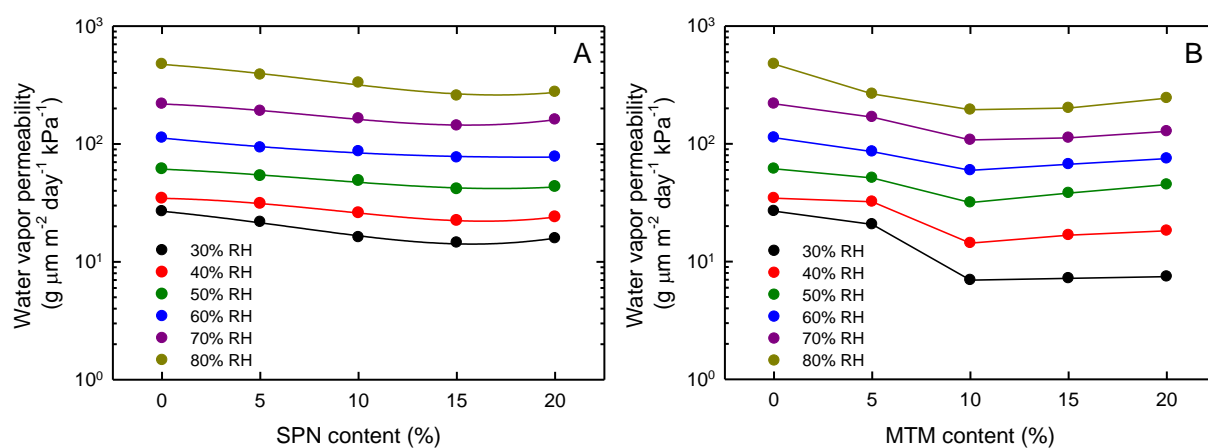


Figure 4.12. Water vapor permeabilities of LUC, LUC-SPN and LUC-MTM nanocomposite films with various clay contents measured at different RH. Reproduction from ref. 40 with permission from Elsevier (© Elsevier 2012) and ref. 41 with permission from John Wiley and Sons (© John Wiley and Sons 2013).

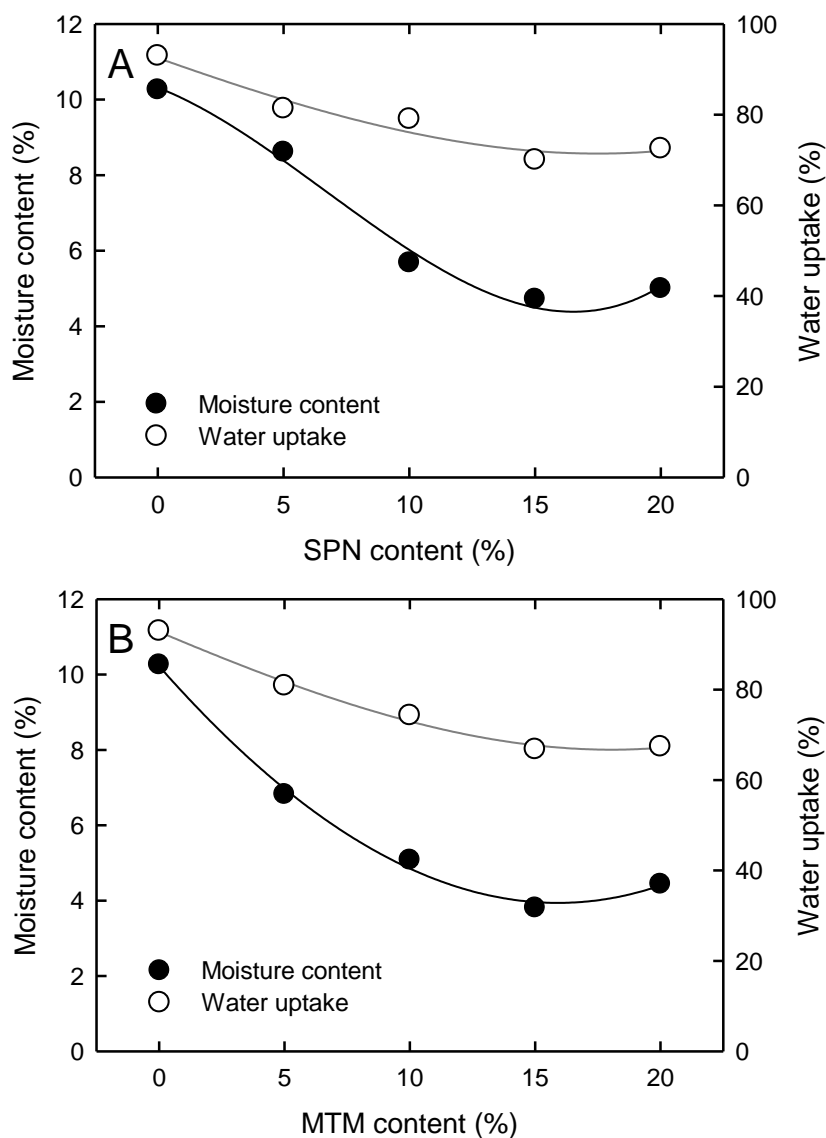


Figure 4.13. Effect of clay content on the moisture content and water uptake of LUC-based films. Moisture content was measured after conditioning the films at 23 °C and 50% RH for 2 days. Water uptake was measured after immersing the films in water for 6 days and then calculating the weights of absorbed water and cellulose in the nanocomposites. Reproduction from ref. 40 with permission from Elsevier (© Elsevier 2012) and ref. 41 with permission from John Wiley and Sons (© John Wiley and Sons 2013).

4.3.5 Hydrophilicity of cellulose–clay nanocomposites

The films were conditioned at 23 °C and 50% RH for 2 days and the moisture contents of the films under these conditions are shown in Figure 4.13. The moisture content of the LUC film decreased from 10.3 to 4.7 and 3.8% when composites containing 15 wt % SPN and MTM, respectively, were formed. In the next experiment, LUC, SPN, MTM, and LUC–SPN and LUC–MTM nanocomposite films were immersed in water for 6 days to measure water uptake under equilibrium conditions (also shown in Figure 4.13). The water uptake of the LUC film decreased from 93 to 70 and 67% when the content of SPN and MTM, respectively, increased from 0 to 15 wt %.

These decreases in moisture content and water uptake for the nanocomposite films cannot be explained simply by the increased clay content or decrease in the content of hydrophilic cellulose. Thus, the LUC film changed from hydrophilic to hydrophobic when SPN or MTM was included. Meanwhile, no weight loss of the LUC, LUC–SPN or LUC–MTM films was observed after immersion in water for an extended period, showing that the SPN and MTM nanoparticles were tightly immobilized in the cellulose matrix, probably by hydrogen bonds. On the other hand, SPN and MTM films turned to powder and dispersed during immersion.

Changes in water contact angles on the LUC, SPN, MTM, LUC–SPN and LUC–MTM nanocomposite films over time are shown in Figure 4.14. Photographs of a water droplet 0.1 s after contact are shown in Figure 4.15. The water contact angles of the LUC, SPN and MTM films were 45, 39 and 28°, respectively, and remained almost unchanged over time, showing these films are intrinsically hydrophilic. In contrast, the LUC–SPN15 and LUC–SPN20 films had higher water contact angles of ~60°, while those of the LUC–MTM10 and LUC–MTM15 films were ~73°. Thus, the results in Figure 4.13 and 4.14 show that the LUC film changed from hydrophilic to hydrophobic by addition of 15–20 wt % of either SPN or MTM. Because each cellulose chain has both hydrophilic OH and hydrophobic CH groups,⁵¹ it is likely that predominantly hydrophobic CH groups are present on the surfaces of the LUC–SPN and LUC–MTM nanocomposite films.⁵² Numerous hydrogen bonds formed between cellulose molecules and either SPN or MTM platelets in the nanocomposites are probably the driving force inducing anisotropic orientation of cellulose chains on the film surfaces.

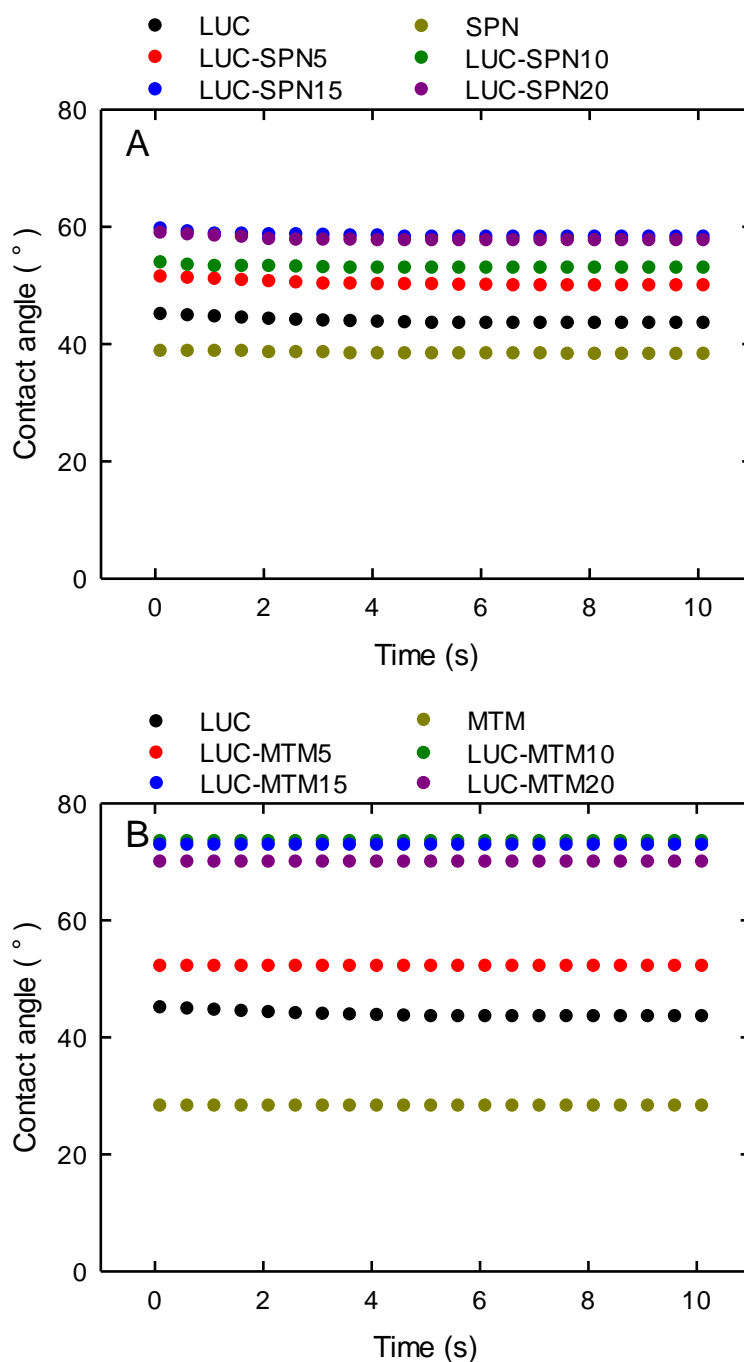


Figure 4.14. Changes in the water contact angle on (A) LUC, SPN, and LUC–SPN, and (B) LUC, MTM and LUC–MTM films over time. Reproduction from ref. 40 with permission from Elsevier (© Elsevier 2012) and ref. 41 with permission from John Wiley and Sons (© John Wiley and Sons 2013).

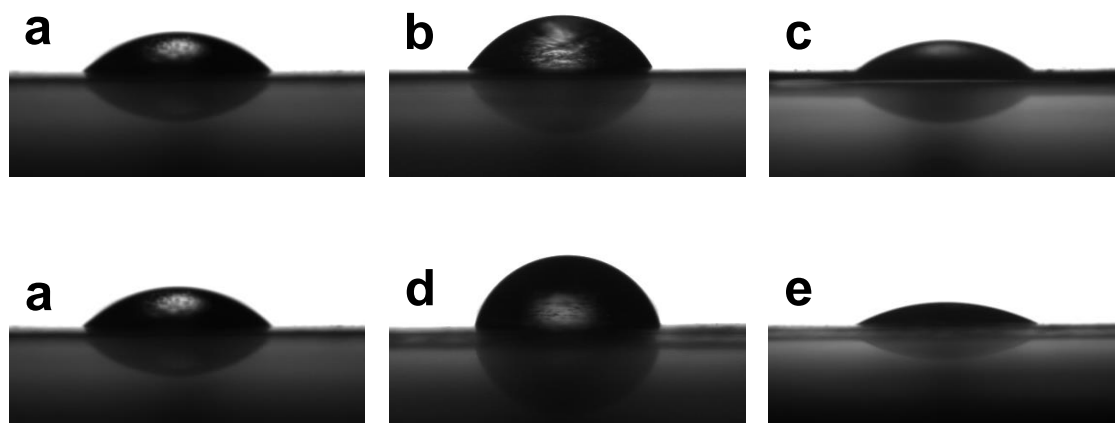


Figure 4.15. Photos of water droplets on (a) LUC, (b) LUC–SPN15, (c) SPN, (d) LUC–MTM15, and (e) MTM films taken 0.1 s after landing. Reproduction from ref. 40 with permission from Elsevier (© Elsevier 2012) and ref. 41 with permission from John Wiley and Sons (© John Wiley and Sons 2013).

4.4 Conclusions

LUC–SPN and LUC–MTM nanocomposites films fabricated from cellulose/LiOH/urea solutions display high mechanical strength and Young’s modulus, and low CTE and oxygen permeability compared with the original LUC film. Formation of regular intercalated nanolayered structures of SPN or MTM platelets in the cellulose matrix is likely to have induced such improvements in film properties. In particular, the LUC–MTM15 nanocomposite film had a tensile strength and Young’s modulus 161 and 180% greater than those of the LUC film, respectively, and its CTE and oxygen permeability at 50–75% RH were 60 and 42–33% lower, respectively, than those of the LUC film. These effects were attributed to the high aspect ratio of the MTM platelets and their nanolayered structure in the composites. Because the LUC–SPN and LUC–MTM nanocomposite films have sufficiently

large work of fracture and elongation at break, they have high toughness and good ductility. Moreover, the LUC film turns from hydrophilic to somewhat hydrophobic when combined with SPN or MTM platelets, probably because the orientation of cellulose chains on the film surface changes in the composites compared with LUC alone.

4.5 References

- (1) Wang, J.; Cheng, Q.; Tang, Z. *Chem. Soc. Rev.* **2012**, *41*, 1111–1129.
- (2) Bonderer, L. J.; Studart, A. R.; Gauckler, L. J. *Science* **2008**, *319*, 1069–1073.
- (3) Podsiadlo, P.; Kaushik, A. K.; Arruda, E. M.; Waas, A. M.; Shim, B. S.; Xu, J.; Nandivada, H.; Pumplun, B. G.; Lahann, J.; Ramamoorthy, A. *Science* **2007**, *318*, 80–83.
- (4) Paul, D. R.; Robeson, L. M. *Polymer* **2008**, *49*, 3187–3204.
- (5) Konduri, S.; Nair, S. J. *Phys. Chem. C*, **2007**, *111*, 2017–2024.
- (6) Liu, A.; Walther, A.; Ikkala, O.; Belova, L.; Berglund, L. A. *Biomacromolecules* **2011**, *12*, 633–641.
- (7) Clarizia, G.; Algieri, C.; Drioli, E. *Polymer* **2004**, *45*, 5671–5681.
- (8) Yang, Y. N.; Wang, P. *Polymer* **2006**, *47*, 2683–2688.
- (9) Liu, S.; Zhang, L.; Zhou, J.; Wu, R. *J. Phys. Chem. C* **2008**, *112*, 4538–4544.
- (10) Braganca, F.; Valadares, L.; Leite, C.; Galembeck, F. *Chem. Mater.* **2007**, *19*, 3334–3342.
- (11) White, L. A. *J. Appl. Polym. Sci.* **2004**, *92*, 2125–2131.
- (12) Tang, T.; Chen, X.; Chen, H.; Meng, X.; Jiang, Z.; Bi, W. *Chem. Mater.* **2005**, *17*, 2799–2802.
- (13) Zhu, J.; Morgan, A. B.; Lamelas, F. J.; Wilkie, C. A. *Chem. Mater.* **2001**, *13*, 3774–3780.
- (14) Lu, Z. H.; Liu, G. J.; Duncan, S. *J. Membr. Sci.* **2003**, *221*, 113–122.
- (15) Taniguchi, A.; Cakmak, M. *Polymer* **2004**, *45*, 6647–6654.
- (16) Walther, A.; Bjurhager, I.; Malho, J. M.; Pere, J.; Ruokolainen, J.; Berglund, L.A.; Ikkala, O. *Nano Lett.* **2010**, *10*, 2742–2748.

- (17) Ren, H.; Zhu, M.; Haraguchi, K. *Macromolecules* **2011**, *44*, 8516–8526.
- (18) Tang, C.; Xiang, L.; Su, J.; Wang, K.; Yang, C.; Zhang, Q.; Fu, Q. *J. Phys. Chem. B* **2008**, *112*, 3876–3881.
- (19) Zhang, C.; Tjiu, W. W. ; Liu, T.; Lui, W. Y.; Phang, I. Y.; Zhang, W.-D. *J. Phys. Chem. B* **2011**, *115*, 3392–3399.
- (20) Herrera-Alonso, J. M.; Marand, E.; Little, J. C.; Cox, S. S. *J. Membr. Sci.* **2009**, *337*, 208–214.
- (21) Priolo, M.; Gamboa, D.; Holder, K. M.; Grunlan, J. C. *Nano Lett.* **2010**, *10*, 4970–4974.
- (22) Thompson, D. W.; Butterworth, J. T. *J. Colloid Interface Sci.* **1992**, *151*, 236–243.
- (23) Ploehn, H. J.; Liu, C. Y. *Ind. Eng. Chem. Res.* **2006**, *45*, 7025–7034.
- (24) Vali, H.; Hesse, R.; Kodama, H. *Clays Clay Miner.* **1992**, *40*, 240–245.
- (25) Sun D.; Chu, C. C.; Sue, H. J. *Chem. Mater.* **2010**, *22*, 3773–3778.
- (26) Haraguchi, K.; Ebato, M.; Takehisa, T. *Adv. Mater.* **2006**, *18*, 2250–2254.
- (27) Ebina, T.; Mizukami, F. *Adv. Mater.* **2007**, *19*, 2450–2453.
- (28) Triantafyllidis, K. S.; LeBaron, P. C.; Park, I.; Pinnavaia, T. J. *Chem. Mater.* **2006**, *18*, 4393–4398.
- (29) Kumar, S. A.; He, Y. L.; Ding, Y. M.; Le, Y.; Kumaran, M. G.; Thomas, S. *Ind. Eng. Chem. Res.* **2008**, *47*, 4898–4904.
- (30) Osman, M. A.; Mittal, V.; Morbidelli, M.; Suter, U. W. *Macromolecules* **2004**, *37*, 7250–7257.
- (31) Ragauskas, A. J.; Williams, C. K.; Davison, B. H.; Britovsek, G.; Cairney, J.; Eckert, C. A.; Rederick, W. J.; Hallett, J. P.; Leak, D. J.; Liotta, C. L.; Mielenz, J. R.; Murphy, R.; Templer, R.; Tschaplinski, T. *Science* **2006**, *311*, 484–489.
- (32) Ohlrogge, J.; Allen, D.; Berguson, B.; DellaPenna, D.; Shachar-Hill, Y.; Stymne, S. *Science* **2009**, *324*, 1019–1020.
- (33) Klemm, D.; Heublein, B.; Fink, H. P.; Bohn, A. *Angew. Chem. Int. Ed.* **2005**, *44*, 3358–3393.
- (34) Mahmoudian, S.; Wahit, M. U.; Ismail, A. F.; Yussuf, A. A. *Carbohydr. Polym.* **2012**, *88*, 1251–1257.
- (35) Cerruti, P.; Ambrogi, V.; Postiglione, A.; Rychlý, J.; Matisová-Rychlá, L.; Carfagna, C.

- Biomacromolecules* **2008**, *9*, 3004–3013.
- (36) Yang, Q.; Fukuzumi, H.; Saito, T.; Isogai, A.; Zhang, L. *Biomacromolecules* **2011**, *12*, 2766–2771.
- (37) Yang, Q.; Fujisawa, S.; Saito, T.; Isogai, A. *Cellulose* **2012**, *19*, 695–703.
- (38) Yang, Q.; Qin, X.; Zhang, L. *Cellulose* **2011**, *18*, 681–688.
- (39) Yang, Q.; Lue, A.; Qi, H.; Sun, Y.; Zhang, X.; Zhang, L. *Macromol. Biosci.* **2009**, *9*, 849–856.
- (40) Yang, Q.; Wu, C.; Saito, T.; Isogai, A. *Carbohydr. Polym.* in press, DOI: 10.1016/j.carbpol.2012.10.044, available online October 26 th, **2012**.
- (41) Yang, Q.; Saito, T.; Isogai, A. in press, *J. Appl. Polym. Sci.* DOI: 10.1002/APP.39564, available online June 13th, **2013**.
- (42) Sehaqui, H.; Mushi, N.; Morimune, S.; Salajkova, M.; Nishino, T.; Berglund, L. A. *ACS Appl. Mater. Inter.* **2012**, *4*, 1043–1049.
- (43) Watanabe, T.; Sato, T. *Clay Sci.* **1988**, *7*, 129–138.
- (44) Krause S. J. *Macromol. Sci. Macromol. Chem.* **1972**, *2*, 251–314.
- (45) Sehaqui, H.; Zhou, Q.; Berglund, L.A. *Soft Matter* **2011**, *7*, 7342–7350.
- (46) Chen, P.; Zhang, L. *Biomacromolecules* **2006**, *7*, 1700–1706.
- (47) Darder, M.; Colilla, M.; Ruiz-Hitzky, E. *Chem. Mater.* **2003**, *15*, 3774–3780.
- (48) Lange, J.; Wyser, Y. *Packag. Technol. Sci.* **2003**, *16*, 149–158.
- (49) Nielsen, L. E. *J. Macromol. Sci.* **1967**, *A1*, 929–942.
- (50) Miller, K.; Krochta, J. *Trends Food Sci. Tech.* **1997**, *8*, 228–237.
- (51) Yamane, C.; Aoyagi, T.; Ago, M.; Sato, K.; Okajima, K.; Takahashi, T. *Polym. J.* **2006**, *38*, 819–826.
- (52) Hirota, M.; Tamura, N.; Saito, T.; Isogai, A. *Cellulose* **2009**, *16*, 841–851.

Chapter 5

Hydrophobization of Cellulose Films by Surface Modification with Alkyl Ketene Dimer (AKD)

5.1 Introduction

Various cellulose and polysaccharide¹⁻³ have been studied as bio-based oxygen barrier films, some of them having quite low oxygen permeabilities under dry conditions⁴⁻⁹ due to abundant hydrogen bond formation between polysaccharide molecules in the films and hence small free volumes¹⁰⁻¹¹. In the previous chapters, regenerated cellulose films prepared from aqueous alkali/urea solutions (AUC) were found to exhibit very high oxygen barrier properties under dry conditions⁴. Moreover, these AUC films possessed good optical transparency, thermal stability, biocompatibility, and biodegradability.¹²⁻¹⁶

However, the presence of abundant hydroxyl groups in cellulose molecules also causes the hydrophilic nature of cellulose materials, resulting in adsorption of moisture, low resistance to water, and significant increase in oxygen permeability under high humidity conditions, thus restricting their potential applications.⁴ Therefore, improvement of water repellency and oxygen barrier properties under high humidity conditions is important for practical application of AUC films. Studies have been carried out to obtain water repellent and high gas barrier films, such as compositing with hydrophobic polymers¹⁷ or inorganic fillers¹⁸, plasma treating¹⁹ or metalizing²⁰ film surfaces, and chemical modification²¹. However, compositing with inorganic fillers, plasma treatment, and metalizing always leads to decreased film transparency,²² and compositing with hydrophobic polymers or chemical modification may decrease film oxygen barrier properties.²³

Alkylketene dimer (AKD) is a typical hydrophobizing chemical used in the papermaking industry.²⁴ Typical addition lies between 0.05 and 0.2 wt % of dry paper pulp weight to provide suitable sizing degrees for printing and writing grades. When AKD dispersions are added to pulp slurries, cationic AKD particles efficiently adsorb on anionic pulp fiber surfaces through electrostatic interactions. Anionic charges in paper pulp fibers result from dissociated

carboxyl groups originally present in the pulps at contents of 0.02–0.08 mmol g⁻¹.²⁵ Three different primary chemical structures are possible for AKD components in cellulose sheets: the original AKDs, hydrolyzed AKDs, or ketones and β -ketoesters with hydroxyl groups from cellulose and/or starch present in AKD dispersions as stabilizers. The mechanisms of efficient paper sizing by AKD have been under debate,^{24–26} but there have been few reports on surface modification of regenerated cellulose films by AKD.²⁷

In the present chapter²⁸, regenerated cellulose films prepared from a LiOH/urea solvent system (AUC) were surface-modified using a simple soaking method in a cationic AKD dispersion. The obtained films exhibited high water repellency and gas barrier properties while maintaining their original light transparency. Relationships between AKD content of the AKD-treated AUC films and the above properties are studied in detail.

5.2 Experimental Section

5.2.1 Materials

A highly purified cotton linters pulp used for filter paper production (filter pulp; Advantec Co. Ltd., Japan) with a viscosity-average molecular weight of 8.6×10^4 g mol⁻¹ was used as the cellulose source.⁴ A cationic papermaking-grade AKD dispersion (AS-202, Seiko PMC Co., Japan) was used after dilution with distilled water to the desired AKD concentration. All reagents and solvents were of laboratory grade and used as received from Wako Pure Chemicals, Tokyo, Japan.

5.2.2 Preparation of AKD-treated AUC films

A LiOH/urea/H₂O solution with a weight ratio of 4.6:15:80.4 was precooled to -12 °C. A desired amount of cellulose was dispersed in this precooled solvent and the mixture was then immediately stirred at 1300 rpm for 2 min to obtain a transparent solution with a cellulose content of 6 wt %. The cellulose solution thus obtained was degassed by centrifugation at 10,000g for 10 min, spread on a glass plate, and then immersed in acetone at room temperature for 30 min to allow regeneration. The resulting sheet-like hydrogels were

thoroughly washed by soaking in fresh water several times, fixed on a poly(methyl methacrylate) plate with adhesive tape to prevent shrinkage, and air-dried at ambient temperature to obtain alkali/urea regenerated cellulose (AUC) films.⁴ The once-dried AUC films were then soaked in AKD dispersion for 10 s followed by rinsing thoroughly with water. The wet films were dried in the same way as the original AUC films and then heated at 100 °C for 10 min. The AKD concentrations of the dispersions were controlled to 0, 0.05, 0.1, and 0.2 wt % by dilution with water, and the corresponding AKD-treated AUC films obtained were denoted AUC, AUC–AKD0.05, AUC–AKD0.1, and AUC–AKD0.2, respectively. The corresponding films produced without heating were denoted AUC–AKD0.05–N, AUC–AKD0.1–N, and AUC–AKD0.2–N, respectively. All AKD-treated AUC films were conditioned at 23 °C and 50 % relative humidity (RH) for more than one day before analyses.

5.2.3 Analyses

AKD contents of the AKD-treated AUC films were determined by pyrolysis-gas chromatography (Py-GC), the operating conditions of which are described elsewhere.²⁵ Fourier transform infrared (FT-IR) spectra of the films were recorded using a Jasco FT/IR-6100 spectrometer in attenuated total reflectance (ATR) mode from 400 to 4000 cm^{-1} with a 1 cm^{-1} resolution. The surfaces and cross-sections (fracture surfaces) of the films were observed with a Hitachi S4800 field emission-type scanning electron microscope (SEM) at 2 kV. The films were frozen in liquid nitrogen, immediately snapped, vacuum-dried, and then coated with osmium using a Meiwafoysis Neo osmium coater at 10 mA for 10 s prior to SEM measurements.

Optical transmittance of the films was measured from 400 to 800 nm using a JASCO V-670 UV-Vis spectrophotometer. Tensile tests were performed using a Shimadzu EZ-TEST instrument equipped with a 500 N load cell. Rectangular strips 2×30 mm in size were cut from the films and tested with a span length of 10 mm at a rate of 1.0 mm min^{-1} . At least 10 measurements were carried out for each sample.

Contact angles on the films for water droplets with a volume of 2 μL were measured at 23 °C and 50 % RH using a FAMAS DM500 instrument (Kyowa Interface Science Co. Ltd., Japan). The film was immersed in deionized water at room temperature for 6 days to reach

swelling equilibrium and the water uptake ($W_{(\text{water uptake})}$) was subsequently calculated from the weights before and after drying the wet film according to the following equation:

$$W_{(\text{water uptake})} = (W_{(\text{wet})} - W_{(\text{dry})}) / W_{(\text{dry})} \times 100\% \quad (1)$$

where $W_{(\text{wet})}$ is the weight of the water-swollen film, $W_{(\text{dry})}$ is that of the same film after heating at 105 °C for 3 h. Transmission rates of oxygen and water vapor for the films were determined at 23 and 37.8 °C, respectively, using a Mocon Ox-Tran Model 2/21MH and Mocon Permatran-W Model 1/50G (Modern Controls Inc., US) under standard conditions (ASTM 3985). Each measurement was continued until the rate of O₂ or water vapor transmission reached a stable value. Gas permeability was calculated from the gas transmission rate and film thickness, and the standard deviations for each film were within ±5 %.

5.3 Results and Discussion

5.3.1 Treatment of AUC film with AKD

Figure 5.1 shows SEM images of the surfaces of AUC, AUC–AKD0.05–N, AUC–AKD0.1–N, and AUC–AKD0.1 films; the AUC–AKD0.1 film was obtained by heating at 100 °C for 10 min after drying at ambient temperature, but the others shown were dried only at ambient temperature. The AUC film displayed a smooth and flat surface. After soaking in the AKD dispersions for 10 s, rinsing thoroughly with water, and drying at ambient temperature, AKD particles with average diameters of ~500 nm were found attached on the surface of the resulting AUC films (Figures 5.1b and 5.1c). Because the melting point of AKD is approximately 50 °C,²⁶ the AKD particles present on the AUC–AKD0.1–N film surface disappeared through melting and spreading (Figure 5.1d) after heating the film at 100 °C for 10 min, resulting in a smooth and flat surface similar to that of the AUC film. SEM images of cross sections of the AUC, AUC–AKD0.1–N, and AUC–AKD0.1 films are shown in Figure 5.2. No AKD dispersion particles were present in the cross sections of the AUC–AKD0.1–N and AUC–AKD0.1 films and their SEM images were similar to that of the AUC film, showing that AKD particles did not penetrate into the film. However, it is of

course possible that AKD molecules present on the film surface partially penetrated the films as the particles melted by the heat treatment.

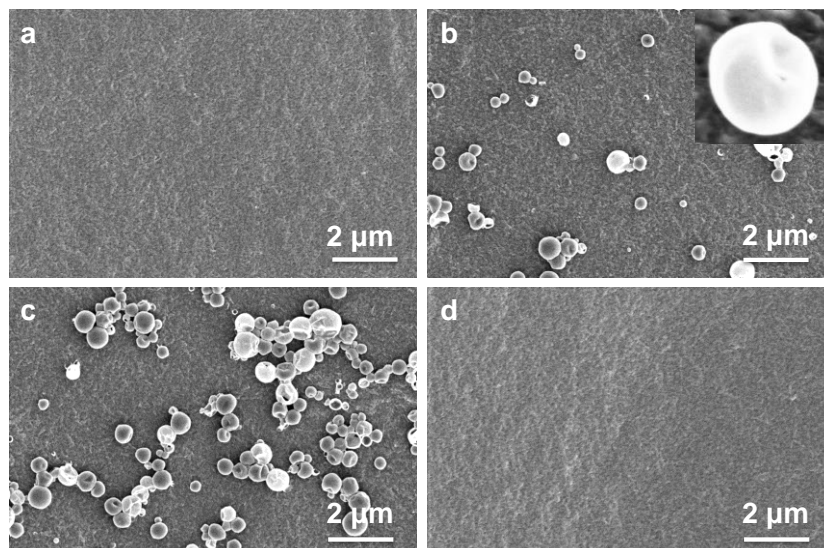


Figure 5.1. SEM images of surfaces of (a) AUC, (b) AUC-AKD0.05-N, (c) AUC-AKD0.1-N, and (d) AUC-AKD0.1 films. The inset in (b) shows an AKD dispersion particle ~500 nm in diameter at high magnification. Reproduction from ref. 28 with permission from Springer (© Springer 2012).

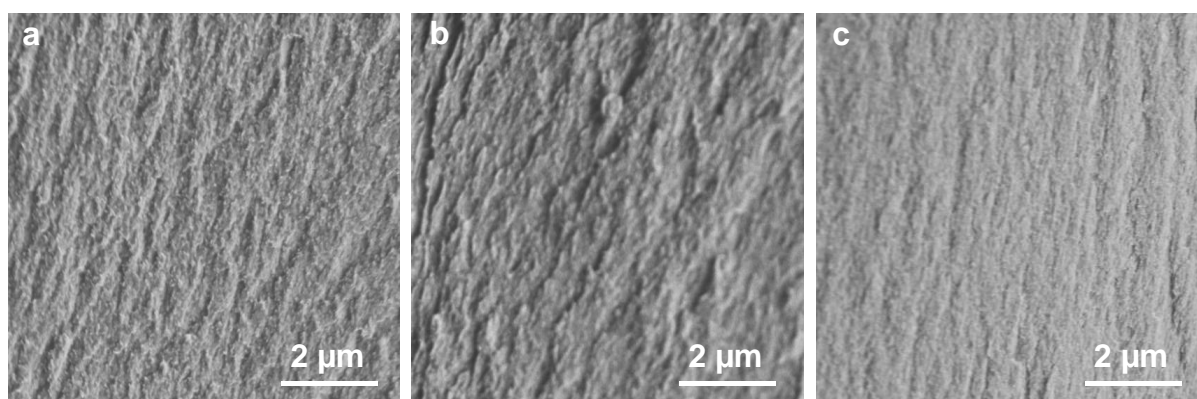


Figure 5.2. SEM images of cross-sections of (a) AUC, (b) AUC-AKD0.1-N, and (c) AUC-AKD0.1 films. Reproduction from ref. 28 with permission from Springer (© Springer 2012).

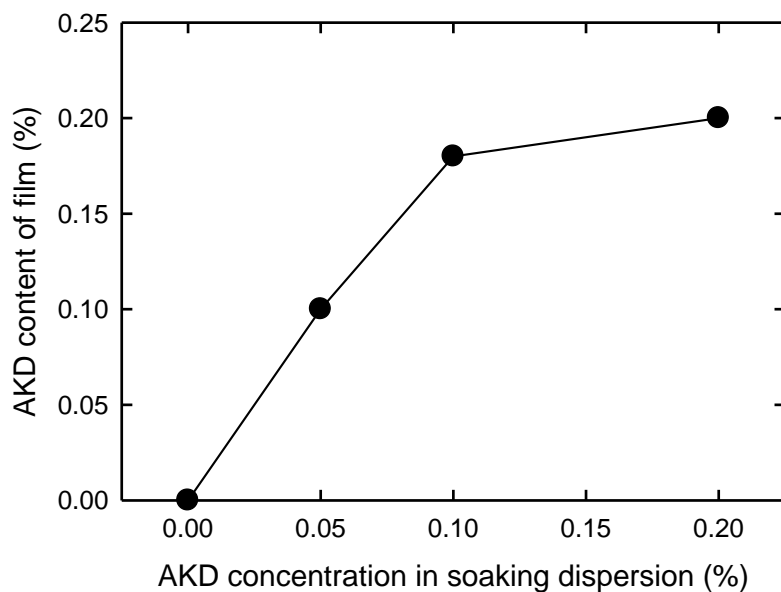


Figure 5.3. Effects of soaking dispersion AKD concentration on AKD content of AKD-treated AUC films. Reproduction from ref. 28 with permission from Springer (© Springer 2012).

Effects of soaking dispersion AKD concentration on the AKD content of the AKD-treated AUC films are shown in Figure 5.3. The AKD content of the films increased with AKD concentration, and reached 0.2 wt % when the AKD concentration in the soaking dispersion was 0.2 %. Electrostatic interactions or formation of ionic bonds between cationic particles in the AKD dispersion and anionically-charged dissociated cellulose carboxyl groups may be the driving force for AKD particles to efficiently adsorb onto AUC film surfaces.²⁵ The cotton linters cellulose used for preparation of the AUC films in this study may have had quite a low amount of carboxyl groups and had an anionic surface charge of approximately -25 mV;²⁹ titration using a methyl red indicator³⁰ gave the carboxyl content of the cotton linters cellulose to be lower than 0.000 mmol g^{-1} .

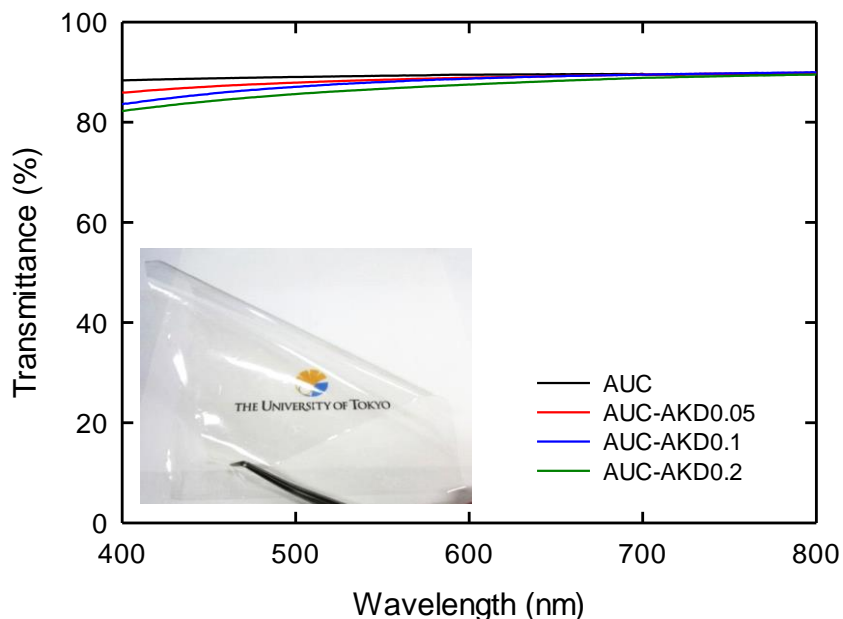


Fig 5.4. Visible light transmittance of AUC and AKD-treated AUC films with 30 μm thickness. The inset shows a photograph of AUC–AKD0.1 film. Reproduction from ref. 28 with permission from Springer (© Springer 2012).

5.3.2 Optical and mechanical properties of AKD-treated AUC films

The high optical transparency of the AUC film was maintained in the AKD-treated AUC films (Figure 5.4), the light transmittances of which were all higher than 87 % at a wavelength of 600 nm. Hence, surface AKD treatment of the AUC films and successive heating treatment had little influence on film transparency.

Stress-strain curves of the AUC and AKD-treated AUC films are shown in Figure 5.5. The tensile strength, Young's modulus, and work of fracture of the AKD-treated AUC films were slightly higher than those of the AUC film. The high elongations at break (29 %) and works of fracture (35–38 MJ m^{-3}) indicated good ductility and toughness of the films. Especially, the works of fracture of the AKD-treated AUC films were much higher than those of wood (dry yew), steel (spring), bone, and rubber (natural), which are 0.5, 1, 3, and 10 MJ

m^{-3} , respectively.³¹ It is not plausible that hydrophobic AKD and its related compounds (hydrolyzed AKDs and others) present on the AUC film surfaces contributed to this observed improvement of mechanical properties. A cationic starch present in the commercial AKD dispersion as one of the dispersion stabilizers³² probably had some contribution to the slight increases in mechanical properties.

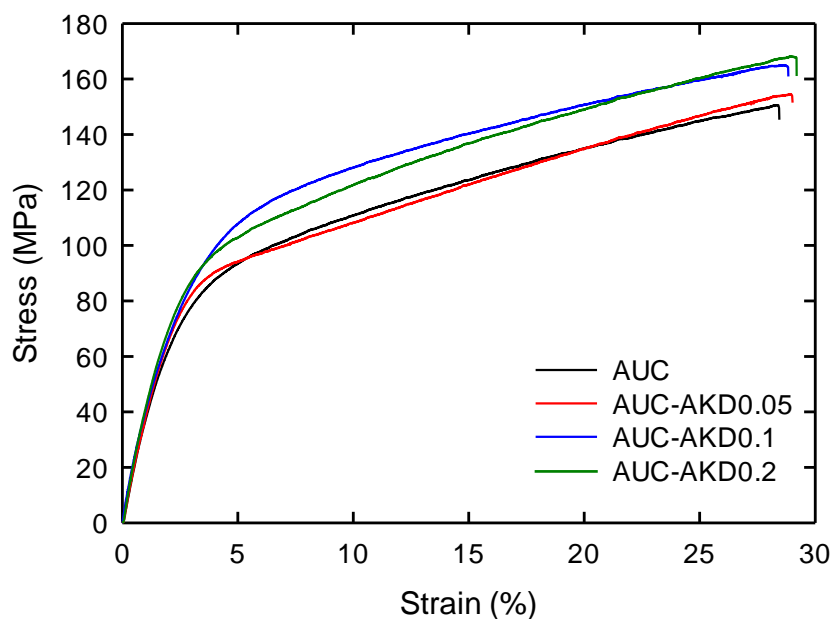


Figure 5.5. Stress-strain curves of AUC and AKD-treated AUC films. Reproduction from ref. 28 with permission from Springer (© Springer 2012).

5.3.3 Hydrophobicity of AKD-treated AUC films

Changes in water contact angles on AUC and AKD-treated AUC films over time after contact are shown in Figure 5.6, and photographs of a water droplet 0.1 s after contact with each film are shown inset. The AUC film was hydrophilic and had an initial water contact angle of 50° . This value gradually decreased with time by partial spreading or absorption of the water droplet on or into the film. In contrast, the AKD-treated AUC films had high water

contact angles (103° , 110° , and 110° for AUC–AKD0.05, AUC–AKD0.1, and AUC–AKD0.2, respectively) which were unchanged for more than 10 s, showing that the films had a sufficiently hydrophobic nature. This was because the hydrophilic AUC molecules were fully or partly covered with hydrophobic AKD (and related) components. Thus, the hydrophilic nature of AUC films was efficiently converted to hydrophobic by the present simple AKD treatment.

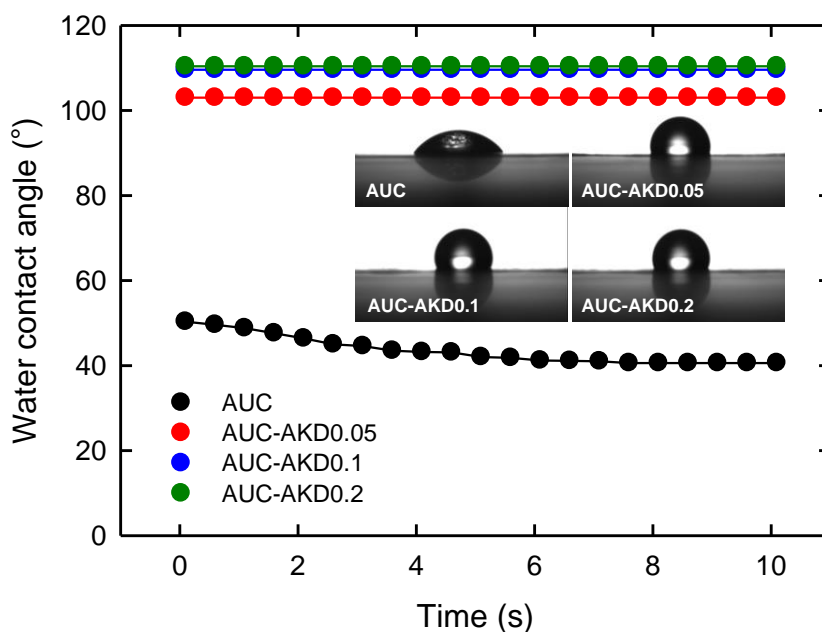


Figure 5.6. Changes in water contact angle on AUC and AKD-treated AUC films over time, and photographs of water droplets on (a) AUC, (b) AUC–AKD0.05, (c) AUC–AKD0.1, and (d) AUC–AKD0.2 films, taken 0.1 s after landing. Reproduction from ref. 28 with permission from Springer (© Springer 2012).

The AKD-treated AUC films were immersed in water for 6 days to measure water uptake under equilibrium conditions (Figure 5.7). The water uptake of the AUC film decreased remarkably from 92 to 25–20 % when the AKD content of the film increased from 0 to 0.1–

0.2 %. Thus, the AKD treatment of the AUC films effectively decreased water uptake through surface hydrophobization. Because the observed moisture contents of the air-dried AUC films were approximately 10 %, ⁴ water had partially penetrated inside the AUC film, indicating that AKD or its related compounds did not fully cover the AUC film surface.

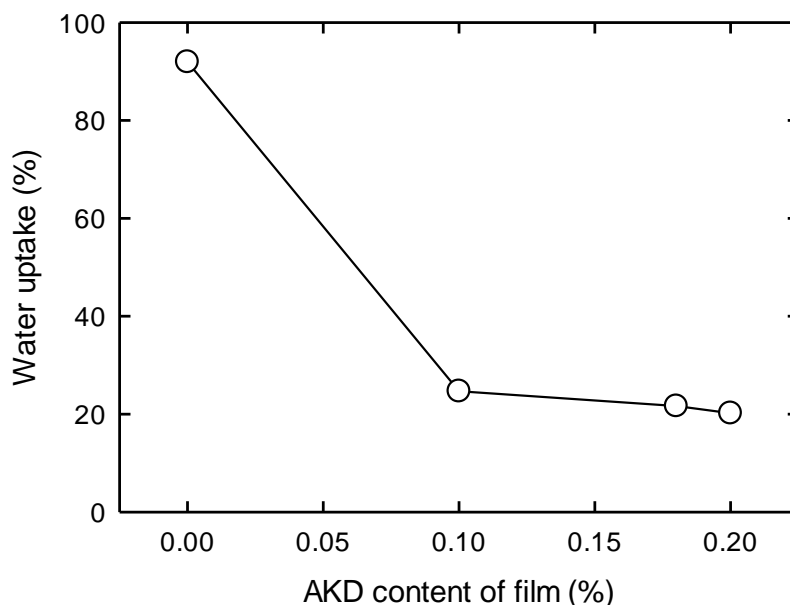


Figure 5.7. Effect of AKD content of AKD-treated AUC films on water uptake. Reproduction from ref. 28 with permission from Springer (© Springer 2012).

5.3.4 Gas barrier properties of AKD-treated AUC films

Oxygen transmission rates of AKD-treated AUC films at 0% RH were less than $0.0005 \text{ mL m}^{-2} \text{ day}^{-1} \text{ kPa}^{-1}$, which was the lowest detection limit of the instrument, showing the high oxygen barrier properties under dry conditions. Figure 5.8 shows oxygen permeabilities of AUC and AKD-treated AUC films at 0, 50 and 75 % RH. The oxygen permeabilities of the AUC film were 0.56 and $5.8 \text{ mL } \mu\text{m m}^{-2} \text{ day}^{-1} \text{ kPa}^{-1}$ at 50 and 75 % RH, respectively. The hydrophilic nature of AUC films results in a significant increase in oxygen permeability under

high humidity conditions.⁴ However, the oxygen permeability of the AUC film clearly decreased to 0.13 and 2.1 mL $\mu\text{m m}^{-2} \text{day}^{-1} \text{kPa}^{-1}$ (lower than approximately one third of the original values) at 50 and 75 % RH, respectively, when the AKD content of the film was increased from 0 to 0.2 %.

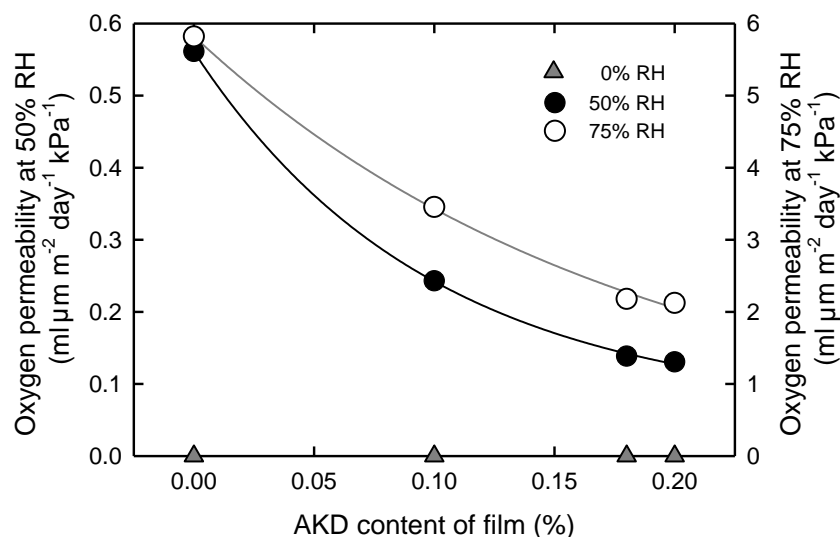


Figure 5.8. Relationships between AKD content of AKD-treated AUC film and oxygen permeability at 0, 50 or 75% RH. Reproduction from ref. 28 with permission from Springer (© Springer 2012).

Thus, the observed surface hydrophobization of the AUC films by AKD treatment was effective in improving their oxygen barrier properties even under high RH conditions. The oxygen permeabilities of the AKD-treated AUC films under high RH conditions, shown in Figure 5.8, were comparable to those of practical oxygen barrier films such as poly(vinylidene chloride) (0.4–5.1 mL $\mu\text{m m}^{-2} \text{day}^{-1} \text{kPa}^{-1}$ at 50 % RH), and were much lower than those of high density poly(ethylene) (427 mL $\mu\text{m m}^{-2} \text{day}^{-1} \text{kPa}^{-1}$ at 50 % RH) or poly(ethylene terephthalate) (15.6 mL $\mu\text{m m}^{-2} \text{day}^{-1} \text{kPa}^{-1}$ at 50 % RH).³³ However, because

the oxygen permeabilities of the AKD-treated AUC films at 50 and 75 % RH were much higher than those at 0 % RH, it was further indicated that the film surfaces were not fully covered with hydrophobic AKD or related compounds. Water vapor was able to penetrate the films at surface spots not covered with AKD or its related compounds, resulting in remarkable increases in oxygen permeability compared with that at 0 % RH.

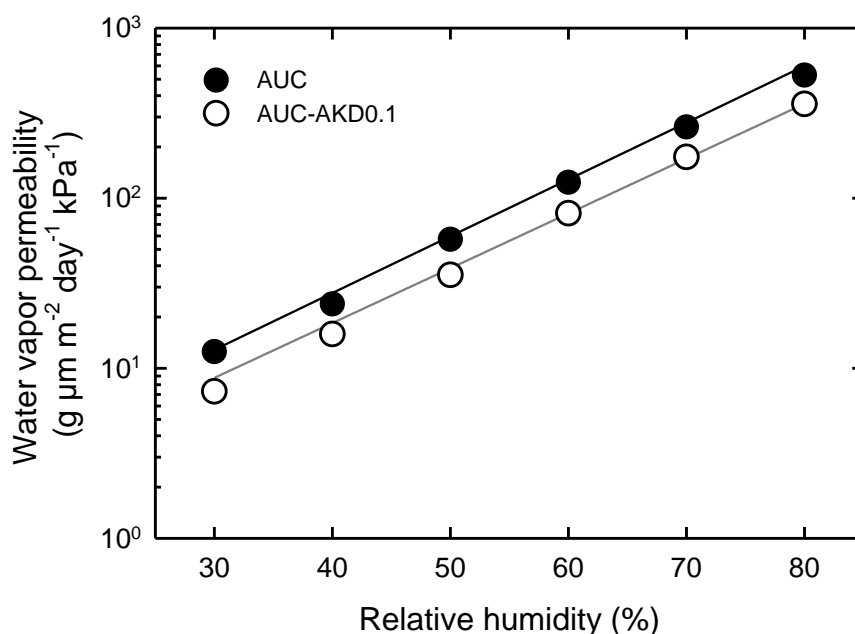


Figure 5.9. Effect of relative humidity on water vapor permeability of AUC and AUC–AKD0.1 films. Reproduction from ref. 28 with permission from Springer (© Springer 2012).

The above hypothesis was proved by water vapor permeability testing of the AKD-treated AUC films. Water vapor permeability of the AUC film increased with RH, whereas that of the AKD-treated AUC films was clearly lower at the same RH (Figure 5.9). However, the water vapor permeability of the AKD-treated AUC films did clearly increase with RH.

These results confirmed that water vapor penetrated into the AKD-treated AUC films at surface spots not covered with AKD or related compounds.

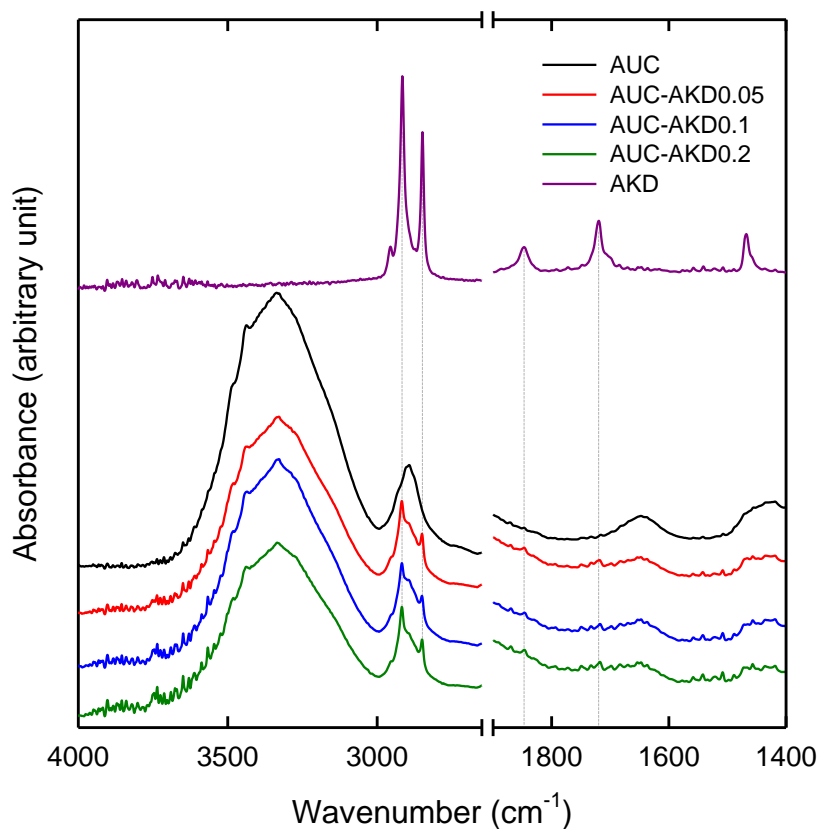


Figure 5.10. FT-IR spectra of AUC and AKD-treated AUC films. Reproduction from ref. 28 with permission from Springer (© Springer 2012).

5.3.5 Chemical structures of AKD components on the AKD-treated AUC film surface

There are three primary chemical structures possible for AKD components present on the AKD-treated and heated AUC films: the original AKDs, hydrolyzed AKDs, or ketones and β -ketoesters with hydroxyl groups from cellulose and/or cationic starch originally present in the commercial AKD dispersion used in this study. FT-IR spectra of the AUC and AKD-treated AUC films are shown in Figure 5.10 with that of the AKD wax. Two sharp absorption peaks

at 2918 and 2850 cm^{-1} for the AKD-treated AUC films were assigned to C–H stretching vibrations of methyl and/or methylene groups of alkyl chains of AKD or its related compounds. The C–H stretching vibration band due to cellulose at 2893 cm^{-1} disappeared after AKD treatment, indicating that the cellulose molecules on the film surface were covered with AKD or related compounds. The relative absorbance of the cellulose hydroxyl band around 3400 cm^{-1} decreased with increasing AKD content, further confirming that the cellulose film surfaces were covered with AKD or its related compounds.

AKDs have typical C=O and C=C stretching vibration bands at 1847 and 1719 cm^{-1} , respectively (Figure 5.10). Ketones have one C=O stretching vibration band at 1701 cm^{-1} , and AKD/cellulose β -ketoesters have two C=O bands at 1710 and 1740 cm^{-1} .³⁴ Even though the AKD-treated AUC film spectra did not show good signal/noise ratios in the C=O absorption range, peaks due to AKD were slightly visible for all AKD-treated AUC films, whereas no C=O absorption band due to ketones or β -ketoesters was detected. The FT-IR spectra in Figure 5.10 were recorded approximately 2 months after storing the AKD-treated AUC films at 23 °C and 50 % RH. Thus, AKD molecules were present at least on the surfaces of the AKD-treated AUC films without hydrolysis and brought about the hydrophobic nature of the AUC films shown in Figures 5.5–5.8; these molecules were stable at least for 2 months without hydrolysis even though they were exposed to conditions at 23 °C and 50 % RH. The chemical structures of AKD-related components at the AKD/cellulose interface will be reported in detail in the following work.

5.4 Conclusions

AUC films prepared from an aqueous LiOH/urea system were surface-treated with AKD by the simple method of soaking dried AUC films in AKD dispersions before drying and heating. The AKD content of the films increased with the increase in AKD concentration in the soaking dispersion to a maximum AKD content of 0.2 wt %. AKD-treated and heated AUC films exhibited highly water repellent and high gas barrier properties even under high humidity conditions because the normally hydrophilic AUC film surfaces were covered with

hydrophobic AKD components. The AUC–AKD0.2 film, having 0.2 wt % AKD content, possessed an optical transmittance of 88 % at 600 nm, tensile strength of 168 MPa, elongation at break of 29 %, work of fracture of 37 MJ m^{-3} , water contact angle of 110° , water uptake of 20 %, and oxygen permeability of 0.13 and $2.1 \text{ mL } \mu\text{m m}^{-2} \text{ day}^{-1} \text{ kPa}^{-1}$ at 50 and 75 % RH, respectively. Moreover, the oxygen transmission rates of AKD-treated AUC films at 0 % RH were less than $0.0005 \text{ mL m}^{-2} \text{ day}^{-1} \text{ kPa}^{-1}$, which was the lowest detection limit of the instrument. FT-IR analysis of the films showed that AKD molecules were still primarily present on the AKD-treated AUC films without hydrolysis even 2 months after conditioning the films at 23°C and 50 % RH. Thus, AKD molecules present on the AUC film surfaces were stable and contributed to the hydrophobic nature of the AKD-treated AUC films.

5.5 References

- (1) Gross, R. A.; Kalra, B. *Science* **2002**, *297*, 803–806.
- (2) Yu, L.; Dean, K.; Li, L. *Prog. Polym. Sci.* **2006**, *31*, 576–602.
- (3) Klemm, D.; Heublein, B.; Fink, H. P.; Bohn, A. *Angew. Chem. Int. Ed.* **2005**, *44*, 3358–3393.
- (4) Yang, Q.; Fukuzumi, H.; Saito, T.; Isogai, A.; Zhang, L. *Biomacromolecules* **2011**, *12*, 2766–2771.
- (5) Fukuzumi, H.; Saito, T.; Iwata, T.; Kumamoto, Y.; Isogai, A. *Biomacromolecules* **2009**, *10*, 162–165.
- (6) Zhu Ryberg, Y. Z.; Edlund, U.; Albertsson, A. C. *Biomacromolecules* **2011**, *12*, 1355–1362.
- (7) Edlund, U.; Zhu Ryberg, Y. Z.; Albertsson, A. C. *Biomacromolecules* **2010**, *11*, 2532–2538.
- (8) Hartman, J.; Albertsson, A. C.; Sjöberg, J. *Biomacromolecules* **2006**, *7*, 1983–1989.
- (9) Siró, I.; Plackett, D. *Cellulose* **2010**, *17*, 459–494.
- (10) Miller, K. S.; Krochta, J. M. *Trends Food Sci. Technol.* **1997**, *8*, 228–237.
- (11) Fukuzumi, H.; Saito, T.; Iwamoto, S.; Kumamoto, Y.; Ohdaira, T.; Suzuki, R.; Isogai, A.

- Biomacromolecules* **2011**, *12*, 4057–4062.
- (12) Yang, Q.; Fujisawa, S.; Saito, T.; Isogai, A. *Cellulose* **2012**, *19*, 695–703.
- (13) Yang, Q.; Lue, A.; Qi, H.; Sun, Y.; Zhang, X.; Zhang, L. *Macromol. Biosci.* **2009**, *9*, 849–856.
- (14) Yang, Q.; Lue, A.; Zhang, L. *Compos. Sci. Technol.* **2010**, *70*, 2319–2324.
- (15) Yang, Q.; Qin, X.; Zhang, L. *Cellulose* **2011**, *18*, 681–688.
- (16) Yang, Q.; Qi, H.; Lue, A.; Hu, K.; Cheng, G.; Zhang, L. *Carbohydr. Polym.* **2011**, *83*, 1185–1191.
- (17) Zhang, L.; Zhou, Q. *Ind. Eng. Chem. Res.* **1997**, *36*, 2651–2656.
- (18) Liu, A.; Walther, A.; Ikkala, O.; Belova, L.; Berglund, L. A. *Biomacromolecules* **2011**, *12*, 633–641.
- (19) Balu, B.; Breedveld V.; Hess, D. W. *Langmuir* **2008**, *24*, 4785–4790.
- (20) Revell, K. M. US Patent 5021298, 1991.
- (21) Bras, J.; Vaca-Garcia, C.; Borredon, M. E.; Glasser, W. *Cellulose* **2007**, *14*, 367–374.
- (22) Sehaqui, H.; Liu, A.; Zhou, Q.; Berglund, L. A. *Biomacromolecules* **2010**, *11*, 2195–2198.
- (23) Fujisawa, S.; Saito, T.; Isogai, A. *Cellulose* **2012**, *19*, 459–466.
- (24) Roberts, J. C. *Paper Chemistry, Second Edition*, 1996, Chapman & Hall, London.
- (25) Isogai, A.; Kitaoka, C.; Onabe, F. J. *Pulp Paper Sci.* **1997**, *23*, J215–J219.
- (26) Isogai, A. *J. Pulp Paper Sci.* **1999**, *25*, 251–255.
- (27) Kannangara, D.; Shen, W. *Colloids Surfaces A.* **2008**, *330*, 151–160.
- (28) Yang, Q.; Fujisawa, S.; Saito, T.; Isogai, A. *Cellulose* **2012**, *19*, 1913–1921.
- (29) Isogai, A.; Onabe, F.; Usuda, M. *Sen'i Gakkaishi* **1992**, *48*, 649–654.
- (30) Obokata, T.; Isogai, A. *Colloids Surfaces A.* **2007**, *302*, 525–531.
- (31) Sehaqui, H.; Zhou, Q.; Berglund, L. A. *Soft Matter* **2011**, *7*, 7342–7350.
- (32) Isogai, A.; Taniguchi, R.; Onabe, F.; Usuda, M. *Nord. Pulp Paper Res. J.* **1992**, *6*, 205–211.
- (33) Miller, K.; Krochta, J. *Trends Food Sci. Tech.* **1997**, *8*, 228–237.
- (34) Yoshida, Y.; Yanagisawa, M.; Isogai, A.; Suguri, N.; Sumikawa, N. *Polymer* **2005**, *46*, 2548–2557.

Chapter 6

Chemical Structures of Alkylketene Dimer (AKD) at the AKD/Cellulose Interfaces

6.1 Introduction

Alkylketene dimer (AKD) is a typical sizing agent for papermaking industry, and generally only a little addition levels give good sizing to paper.^{1,2} AKD components in cellulose sheets are possible to form three different chemical structures: the original AKDs, hydrolyzed AKDs (namely ketones), and β -ketoesters with hydroxyl groups of cellulose and/or starch present in AKD dispersions as one of the stabilizers. The mechanism of alkylketene dimer (AKD) sizing has been extensively studied since the 1970s, whereas it is still under debate.^{1,3}

The first mechanism for the efficient sizing of paper by AKD is explained that AKD and hydroxyl groups of cellulose formed β -ketoesters on pulp surfaces, resulting in orientation of hydrophobic alkyl chains of AKD on surface.⁴⁻⁸ The primary reasons to support this hypothesis are as follows: 1) Some of AKD in paper sheets could not be extracted completely and the sizing degrees are maintained on AKD-sized papers even after chloroform-extractions in sheet form which were regarded as “bonded AKD”.^{5,9-13} 2) β -ketoesters were isolated from reaction products of cellobiose and AKD under non-aqueous conditions in the presence of an organic base.¹² 3) Ester peaks were observed using solid-state ¹³C-NMR analysis after extraction of sized paper with tetrahydrofuran (THF).¹⁴ On the other hand, some researchers^{12,15-20} disputed the reactivity of AKD, and suggested that AKD may not form β -ketoesters with hydroxyl groups of cellulose under the conditions of papermaking. The primary reasons to support this hypothesis are as follows: 1) The reaction of AKD in papermaking took place with water molecules, and was reported to be faster than the reaction with cellulose.^{21,22} Moreover, all model experiments using amorphous cellulose samples showed that no β -ketoesters were formed between AKD and hydroxyl groups of

polysaccharides during curing and conditioning treatments, as long as water was present in the system.¹² 2) Amounts of AKD and ketones extracted under neutral conditions were almost equal to those extracted under alkaline conditions for AKD-sized sheets, when the extractions were associated with fiberization of the sheets.¹² 3) Most AKD components in AKD-sized handsheets were removed by organic solvents after fiberization of AKD-sized sheets and swelling of pulp fibers.¹² 4) Solid-state ¹³C-NMR spectra of handsheets prepared with ¹³C-labeled AKD suggested that AKD, ketones and ¹³CO₃²⁻ were present as the size components in the handsheets; nearly no covalent bonds were formed between AKD and hydroxyl groups of cellulose in paper even after heat treatments.²³

In the previous chapter, regenerated cellulose films prepared from aqueous alkali/urea solvent system (AUC)²⁴⁻³¹ were hydrophobized by surface-modification using a simple soaking method in cationic AKD dispersion.³² Furthermore, cellulose gels prepared from aqueous alkali/urea solvent were reported to have different surface polarity depending on the coagulant species.³³ The cellulose gels from aqueous coagulants tend to form hydrophilic hydroxyl-rich surfaces, whereas those from organic coagulants tend to have hydrophobic C–H group-rich surfaces. Therefore, the AUC films with different surface polarity are good models to study the hydrophobization mechanism of the AKD modified cellulose materials. On the other hand, TEMPO (2,2,6,6-tetramethylpiperidine-1-oxyl radical)-oxidized cellulose nanofibril films (TOCNs) developed in our group have almost no C6-OH groups but sodium C6-carboxylate groups on the microfibril surfaces.³⁴⁻³⁷ They can form strong electrostatic interaction with cationic AKD dispersion but are probably impossible to form β-ketoesters with AKD because of lack of C6-OH groups. Therefore, TOCNs are also good models to compare with AUC films to study the chemical structures of AKD-related components at the AKD/cellulose interface.

In this chapter, the AKD-modified AUC films and AKD-modified TOCN films were treated by a sequential extraction of original AKDs, hydrolyzed AKDs or ketones and β-ketoesters formed with hydroxyl groups of starch, using chloroform, hot water, and dioxane/water mixture. Then the AKD contents and water contact angles of the extraction-treated films were measured to study the chemical structures of AKD-related components at the AKD/cellulose interfaces.

6.2 Experimental Section

6.2.1 Materials

A highly purified cotton linter pulp used for filter paper production (filter paper pulp; Advantec Co. Ltd., Japan) with a viscosity-average molecular weight of $8.6 \times 10^4 \text{ g mol}^{-1}$ was used as the cotton cellulose source. A never-dried softwood bleached kraft pulp (Nippon Paper, Japan), which contained 90% cellulose and 10% hemicelluloses, was used as the original wood cellulose sample. Cationic papermaking-grade AKD dispersion (AS-202, Seiko PMC Co., Japan) was used after dilution with distilled water to the desired AKD concentration. All reagents and solvents were of laboratory grade and used as received from Wako Pure Chemicals, Tokyo, Japan.

6.2.2 Preparation of cellulose-AKD films

The cellulose films were prepared according to a previously reported methods.^{26,32} Briefly, a LiOH/urea/H₂O solution with a weight ratio of 4.6:15:80.4 was precooled to $-12 \text{ }^\circ\text{C}$. A desired amount of cotton linter cellulose was dispersed in this precooled solvent and the mixture was then immediately stirred at 1300 rpm for 2 min to obtain a transparent solution with a cellulose content of 6 wt %. The cellulose solution thus obtained was degassed by centrifugation at 10,000g for 10 min, spread on a glass plate, and then immersed in acetone for 30 min or in 5 wt % H₂SO₄ for 5 min at ambient temperature to allow regeneration. The resulting sheet-like hydrogels were thoroughly washed by soaking in fresh water several times, fixed on a poly(methyl methacrylate) plate with adhesive tape to prevent shrinkage, and air-dried at ambient temperature to obtain alkali/urea regenerated cellulose films. The alkali/urea regenerated cellulose films prepared by regeneration in acetone were denoted to AUC and in 5 wt % H₂SO₄ were denoted to AUCH, respectively.

A TEMPO oxidized cellulose was prepared from the wood cellulose by the TEMPO/NaBr/NaClO system in water at pH 10, according to a previously reported method.³⁴⁻³⁶ The TEMPO-oxidized cellulose thus obtained was further treated with 1% w/v NaClO₂ at pH 4.8 for 2 days to oxidize the C6-aldehyde groups remaining in the cellulose to C6-carboxyls.³⁴ The two-step-oxidized cellulose had a carboxylate content of 1.21 mmol

g^{-1} .³⁴ The TEMPO-oxidized cellulose/water slurry at a 0.11% w/v consistency was mechanically treated with a double-cylinder type homogenizer for 1 min and subsequently with an ultrasonic homogenizer for 6 min. The unfibrillated fraction was removed by centrifugation at 12 000g for 20 min. The supernatant was used as the nanofibril dispersion, the concentration of which was adjusted to 0.1% w/v using a rotary evaporator under reduced pressure. The nanofibril dispersion was poured in a polystyrene Petri dish and oven-dried at 40 °C for 3 days to prepare the TEMPO-oxidized cellulose nanofibril films, denoted to TOCN.

The AUC, AUCH, and TOCN films were then soaked in cationic 0.05 wt % AKD dispersion for 10 s followed by rinsing thoroughly with water. The wet films were air-dried at ambient temperature and denoted to AUC–AKD–N, AUCH–AKD–N, and TOCN–AKD–N, respectively. These films were further heated at 100 °C for 10 min, and the resulting films were denoted to CA, CAH, and TA, respectively.

6.2.3 Extractions of AKD from the cellulose-AKD films

The CA, CAH, and TA films were first immersed in chloroform for 24 h in a Soxhlet extractor and the resulting films were denoted to CA1, CAH1, and TA1, respectively. Then the CA1, CAH1, and TA1 films were further immersed in hot water at 80 °C for 2 h, then air dried at ambient temperature, and the resulting films were denoted to CA2, CAH2, and TA2, respectively. Finally the CA2, CAH2, and TA2 films were immersed in a dioxane/water (1:1 by weight) mixture solution at 90 °C for 2 h, then air dried at ambient temperature, and the resulting films were denoted to CA3, CAH3, and TA3, respectively. All the cellulose-AKD films were conditioned at 23 °C and 50 % relative humidity (RH) for more than one day before analyses.

6.2.4 Analyses

AKD contents of the films were determined by pyrolysis-gas chromatography (Py-GC), the operating conditions of which were described elsewhere.³⁸ Fourier transform infrared (FT-IR) spectra of the films were recorded using a Jasco FT/IR-6100 spectrometer in attenuated total reflectance (ATR) mode from 400 to 4000 cm^{-1} with a 1 cm^{-1} resolution. The $^{12}\text{C}^-$ and $^{16}\text{O}^-$ ion intensities of the films were measured by the NanoSIMS 50L using cesium as a

primary ion source which were carried out on a $10\ \mu\text{m} \times 10\ \mu\text{m}$ area of the film. Then the $^{12}\text{C}^-$ / $^{16}\text{O}^-$ ratios of the films were calculated from the intensities of $^{12}\text{C}^-$ and $^{16}\text{O}^-$ ions. Surface observation of the films was carried out by atomic force microscopy (AFM), using a Nanoscope IIIa, Veeco Instruments Inc. The instrument was operated in tapping mode and images were obtained with silicon nitride cantilever tips. Film roughness and particle height were analyzed from these images. The surface of the film was observed with a Hitachi S4800 field emission-type scanning electron microscope (SEM) at 2 kV. The film was coated with osmium using a Meiwafoysis Neo osmium coater at 10 mA for 10 s prior to SEM measurements. To examine dye adsorption, the films were cut down to triangles with side lengths of 2 cm and then soaked in 0.01% congo red or toluidine blue solution for 5 min at room temperature, followed by washing with distilled water and then drying at room temperature. The photographs of the stained films were obtained by scanning using a Brother MFC-9970CDW Printer (Brother Industries, Ltd., Japan). Light absorbance of the stained films was investigated with a JASCO V-670 UV-Vis spectrophotometer to evaluate the adsorption of dyes. Contact angles on the films for water droplets with a volume of $2\ \mu\text{L}$ were measured at $23\ ^\circ\text{C}$ and 50 % RH using a FAMAS DM500 instrument (Kyowa Interface Science Co. Ltd., Japan).

6.3 Results and Discussion

6.3.1 Extractions of AKD from CA film

Figure 6.1 show AKD contents of the CA, CA1, CA2, and CA3 films. AKD contents were determined by pyrolysis-gas chromatography, which included all the AKD contents of AKD-related components. The AKD content of CA decreased much from 0.1 to 0.02 wt % (decrease of 80%) after extraction of AKD with chloroform, probably owing to the extraction of original AKD and ketone. The AKD content of CA1 further decreased from 0.02 to 0.01 wt % (decrease of 10%) after extraction of AKD with hot water, probably owing to the extraction of β -ketoesters of AKD with hydroxyl groups of starch present in AKD dispersions as one of the stabilizers which could dissolve in hot water. Finally, the AKD content

decreased to almost 0 after the following extraction with dioxane/water mixture, probably owing to the extraction the AKD and ketone which formed very strong physical interaction with cellulose molecules and could only be removed after swelling of cellulose. From the result, almost all the AKD components of CA films were removed after the three extraction treatments. It indicated that the original AKD was the main component of AKD of the CA films and about 10 wt % AKD formed β -ketoesters with hydroxyl groups of starch which was present in AKD dispersions.

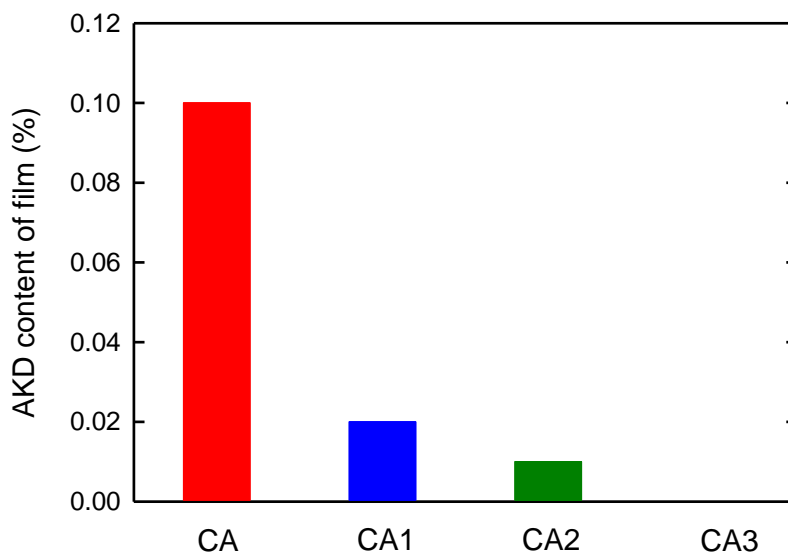


Figure 6.1. AKD contents of CA, CA1, CA2, and CA3 films.

ATR-FTIR spectra of the AUC, CA, and CA3 films are shown in Figure 6.2. The CA film show clear sharp absorption peaks at 2918 and 2850 cm^{-1} assigned to C–H stretching vibrations of methyl and/or methylene groups of alkyl chains of AKD or its related compounds, and slight C=O and C=C stretching vibration bands at 1847 and 1719 cm^{-1} .³² However, these peaks disappeared and the C–H stretching vibration band due to cellulose at

2893 cm^{-1} appeared in CA3 after extractions of AKD. Meanwhile, the relative absorbance of the cellulose hydroxyl band around 3400 cm^{-1} increased after the extractions of AKD, further confirming that the AKDs on the surface of the cellulose film were removed by the extraction treatments.

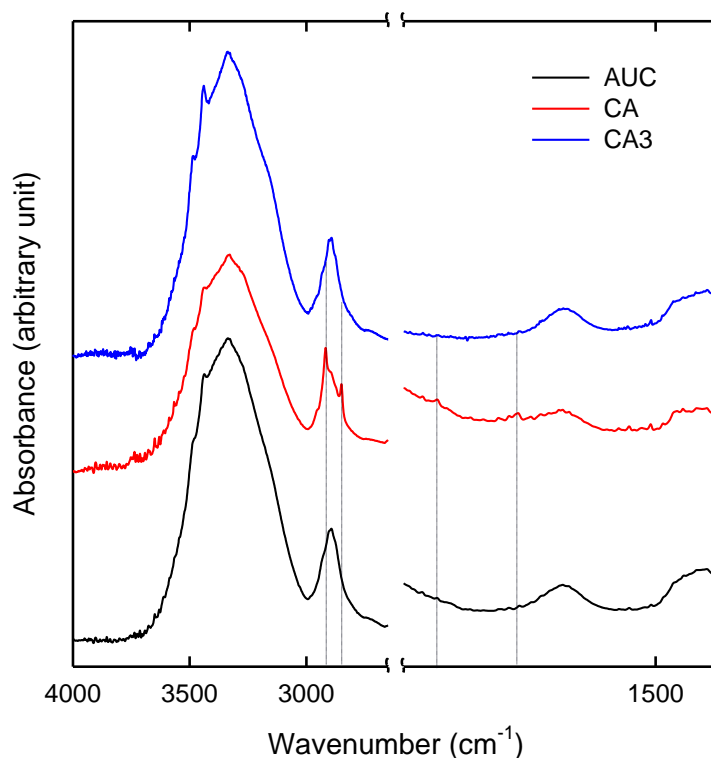


Figure 6.2. ATR-FTIR spectra of AUC, CA, and CA3 films.

The effect of ion sputtering time of NanoSIMS on $^{12}\text{C}^-/^{16}\text{O}^-$ ratios of the AUC, CA, and CA3 films is shown in Figure 6.3. The ion sputtering time of NanoSIMS is related to the depth of films, although estimation of the exact depth is difficult. $^{12}\text{C}^-/^{16}\text{O}^-$ ratio of AUC film reached 0.67 and the peak appeared in a region closed to the film surface and then decrease to 0.37 after 1200 s. On the other hand, maximum $^{12}\text{C}^-/^{16}\text{O}^-$ ratio of the CA film was 1.40,

which was much higher than that of the AUC film, indicating the presence of AKD on the CA film. Moreover, the $^{12}\text{C}^-/^{16}\text{O}^-$ ratio of the CA film further decreased to 0.59 after 1200 s, which was similar to that of AUC. It seemed that AKDs were mainly present on the surface of the AUC film. After the extraction treatments, the $^{12}\text{C}^-/^{16}\text{O}^-$ ratios of the CA3 film decreased much compared with the CA film, and they were similar to those of the AUC film. The results of NanoSIMS further indicated that the AKD components were presented on the surface of the AUC films and almost all of them were removed after the three extraction treatments.

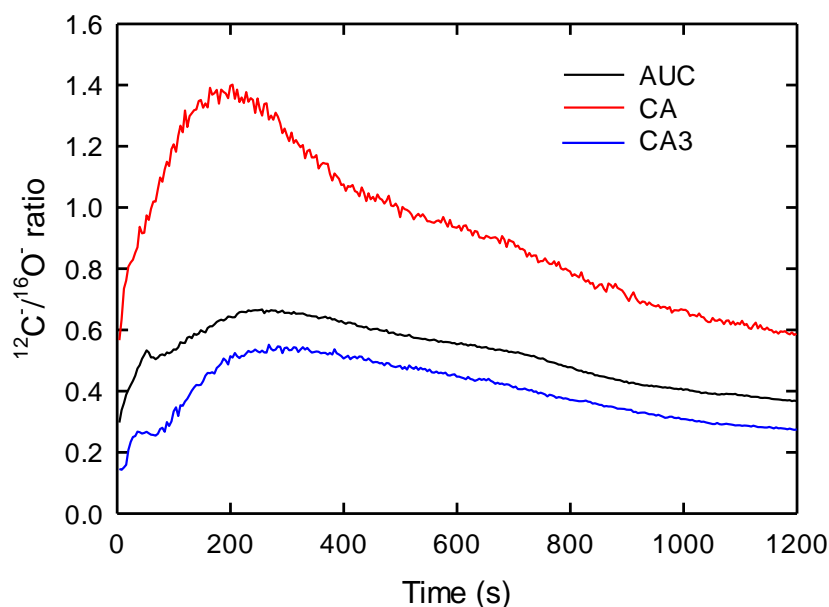


Figure 6.3. Effect of ion sputtering time of NanoSIMS on $^{12}\text{C}^-/^{16}\text{O}^-$ ratios of AUC, CA, and CA3 films.

AFM height and phase images of surfaces of the AUC, CA, and CA3 films are shown in Figure 6.4. The average roughness values of AUC, CA, and CA3 calculated from the entire images ($2 \times 2 \mu\text{m}^2$) were 3 nm, 22 nm, and 24 nm, respectively. The roughness of CA was similar to CA3, and higher than AUC. Some very small AKD particles were present on the

surface of the CA film (Figure 6.4b and e) and their average height was calculated to be about 37 nm (Figure 6.5). The average distance between the two AKD particles was calculated to be about 400 nm. It's possible for AKD particles to melt after heating and solidify again to become much more smaller particles after cooling³⁹ with the diameters decrease from ca. 500 nm (see Figure 5.1b)³² to ca. 37 nm, forming sea/island-like structures. Moreover, such sea/island-like structures were probably easy to trap air and were responsible for the high water repellency of the CA film with (Figure 6.7), which have good correlation with the Cassie's law (Figure 6.6).⁴⁰ However, these AKD particles disappeared from the surface of the CA3 film after the three extraction treatments (Figure 6.4c and f).

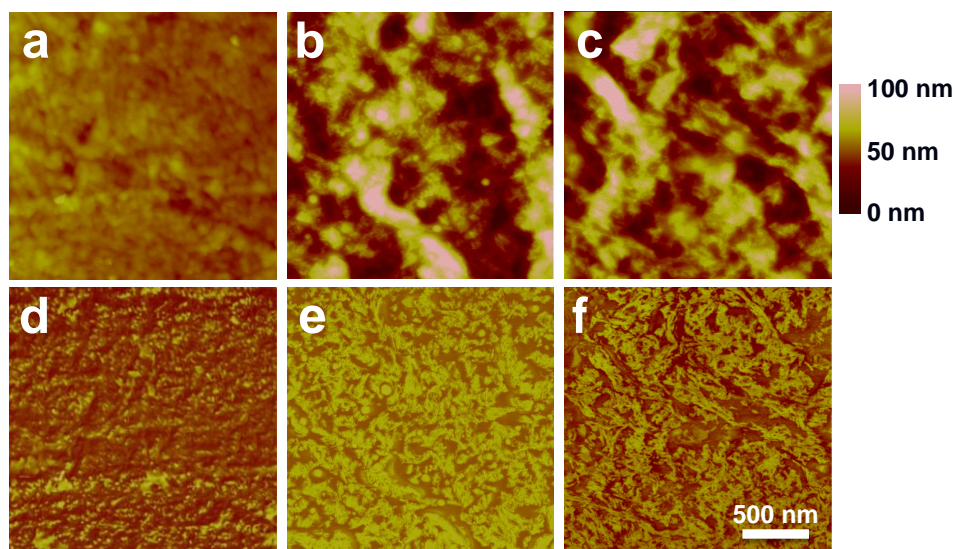


Fig 6.4. AFM height (a, b, c) and phase (d, e, f) images of surfaces of AUC (a, d), CA (b, e), and CA3 (c, f) films.

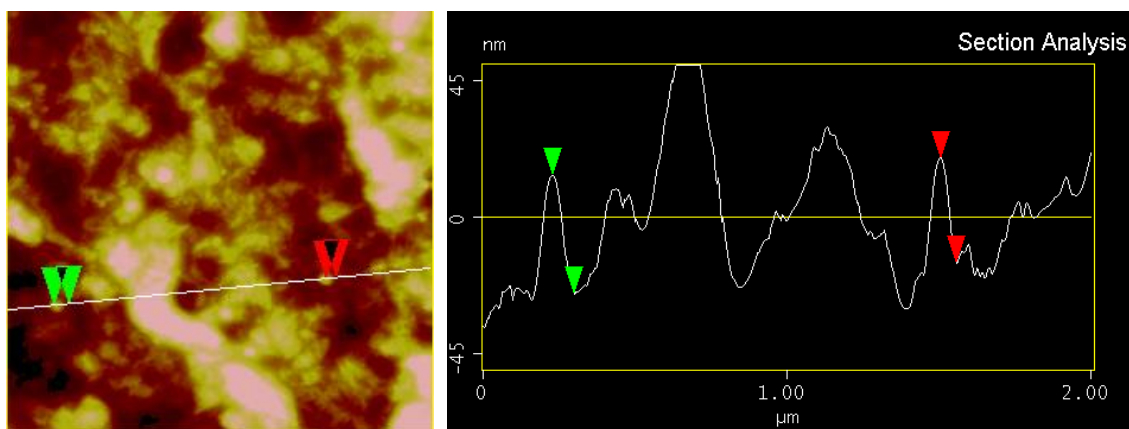


Figure 6.5. An AFM height image of the CA film (left) and two height plots at the white line are depicted right showing the relative height.

In order to further clarify whether AKD or its related compounds fully covered the film surface, dye adsorptions of AUC, CA, and CA3 films were studied. Photographs of AUC, CA, and CA3 films stained by either toluidine blue or congo red and their relevant light absorbance spectra are shown in Figure 6.7. Toluidine blue is a cationic dye, which is possible to form electrostatic interactions or ionic bonds with the AUC film owing to the small amount of anionically-charged dissociated cellulose carboxyl groups present in AUC film.³² On the other hand, congo red is a direct dye, well-known for its strong affinity toward cellulose, due to hydrophobic interaction with the pyranose rings of cellulose molecules. However, both of toluidine blue and congo red could not be adsorbed on cationic AKD components. The results show that after dye adsorption the AUC films exhibited clear blue (Figure 6.7a) or red color (Figure 6.7d) and the relevant absorbance peaks of toluidine blue at 641 nm for toluidine blue stained AUC film and congo red of 514 nm for congo red stained AUC film were clearly detected in light absorbance spectra, indicating good adsorption of toluidine blue and congo red on the AUC film.⁴² The dye stained CA films also show blue or red color and relevant absorbance peaks, although their colors and adsorption peaks were weaker than those of the AUC film. It indicated that some cellulose molecules were present on the surface of the CA

film, leading to adsorption of dyes. And cationic AKD components were partially covered the cellulose film surface in the CA film, leading to the decrease in dye colors and absorbance peaks. This result is in good agreement with the results of AFM images and increase of gas permeabilities of CA films at high humid conditions (see Figure 5.8). On the other hand, dye stained CA3 film shows similar color and absorbance peaks with AUC film, indicating almost complete extractions of AKDs from CA film after the treatments. Therefore, all the results of AKD content, ATR-FTIR, NanoSIMS, AFM, and dye adsorption showed that almost all the AKD components were removed after the three extraction treatments, indicating that almost all the AKD components formed physical interaction with cellulose.¹²

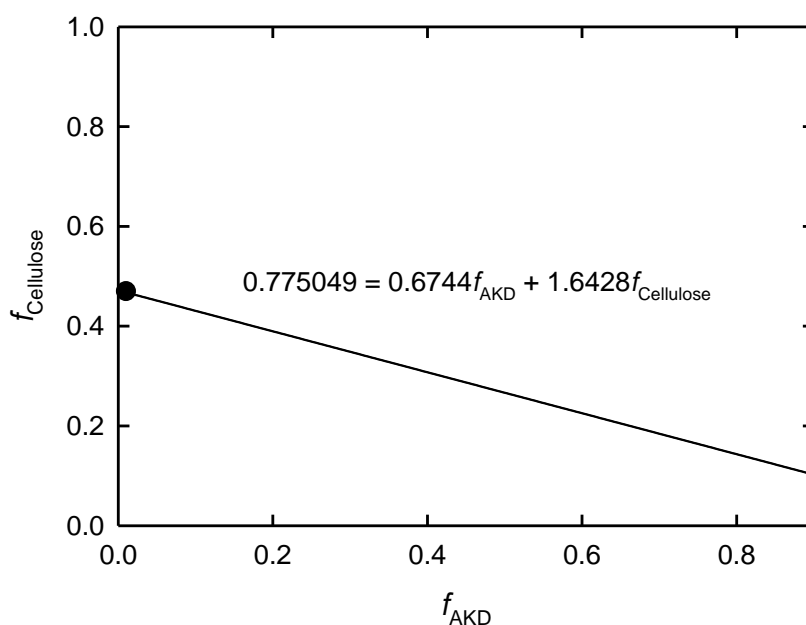


Figure 6.6. Calculated relation between areal fraction of AKD (f_{AKD}) and areal fraction of cellulose ($f_{Cellulose}$) following Cassie's law $\cos\theta_c = f_{AKD} \cos\theta_{AKD} + f_{Cellulose} \cos\theta_{AKD} + f_{Air} \cos\theta_{Air}$, where θ_c is water contact angle of the CA film (103°), θ_{AKD} is water contact angle of the AKD film (109°),⁴¹ $\theta_{Cellulose}$ is water contact angle of the AUC film (50°), θ_{Air} is water contact angle of the air (180°), $f_{AKD} + f_{Cellulose} + f_{Air} = 1$, $f_{Air} + f_{Cellulose} \leq 1$. The f_{AKD} calculated from the AFM image (Figure 6.4) was about 0.01 (equal or less), and the relevant $f_{Cellulose}$ was calculated to be about 0.47, shown as a black dot in this figure.

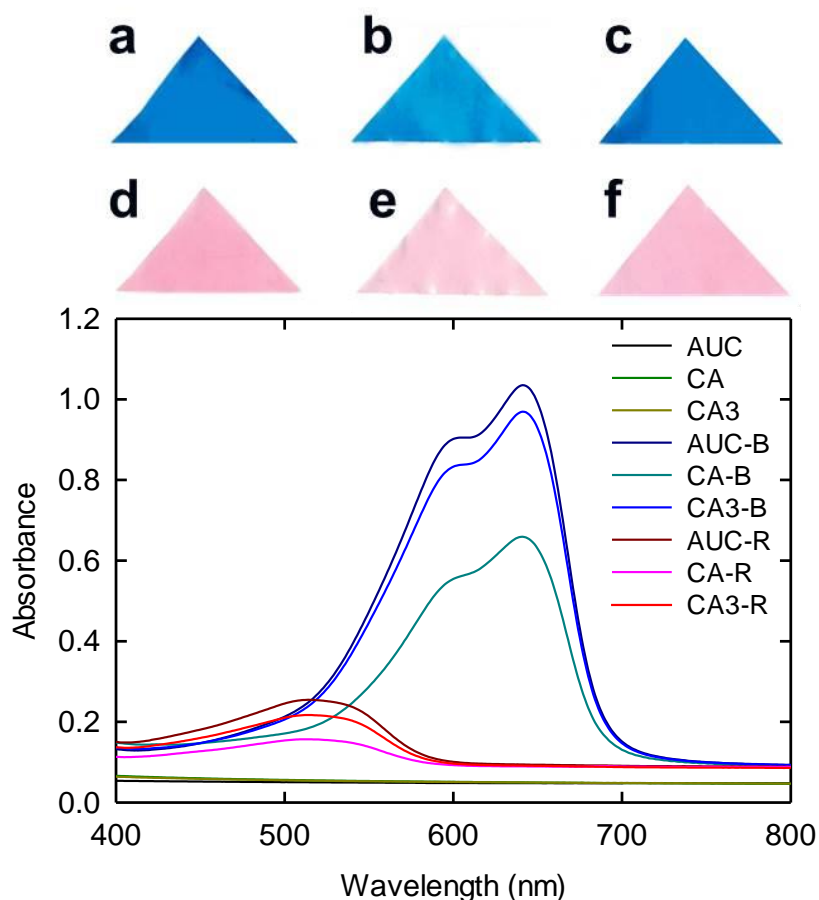


Figure 6.7. Photographs (top) of AUC (a, d), CA (b, e), and CA3 (c, f) films stained by either toluidine blue (a, b, c) or congo red (d, e, f) and light absorbance spectra (bottom) of AUC, CA, CA3 and the relevant stained films by either toluidine blue (AUC-B, CA-B, CA3-B) or congo red (AUC-R, CA-R, CA3-R). All the films have a thickness of 30 μm .

Changes in water contact angles on AUC, CA and extraction treated CA films over time after contact are shown in Figure 6.8, and photographs of a water droplet 0.1 s after contact with each film are shown inset. The contact angles of CA film were 103° and remained unchanged for more than 20 s. After the extraction treatments of AKD, however, the contact

angles of CA1, CA2, and CA3 almost did not change. It was likely that a very small amount of β -ketoesters formed at the AKD/AUC interfaces, which could not be removed by extraction treatments, thus leading to the remaining hydrophobicity of the films. In order to support this viewpoint, two other experiments were done to compare with AUC.

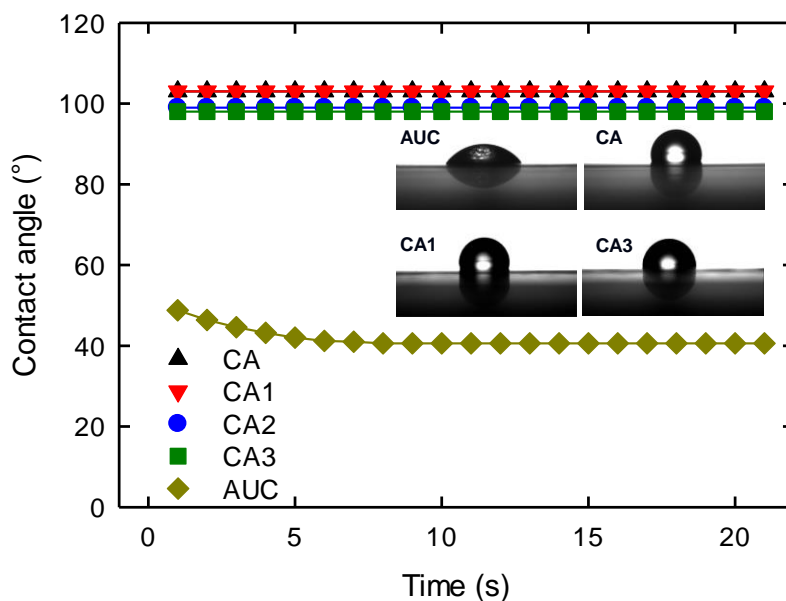


Figure 6.8. Changes in water contact angles on AUC, CA and extraction treated CA films over time after contact and photographs of a water droplet 0.1 s after contact with each film.

6.3.2 Extractions of AKD from CAH films

The cellulose films prepared from aqueous alkali/urea solvent by regeneration with aqueous coagulants tend to form hydrophilic hydroxyl-rich surfaces, and those regeneration with organic coagulants tend to have hydrophobic C–H group-rich surfaces.³³ The previous AUC films were prepared from acetone as the coagulant, which should have hydrophobic C–H group-rich surfaces. Therefore, the AUCH films were prepared from aqueous coagulant (5

wt % H_2SO_4), which should have hydrophilic hydroxyl-rich surfaces. The AUCH films were difficult to form strong hydrophobic interaction with AKD because of their hydrophilic hydroxyl-rich surfaces. Figure 6.9 shows AKD contents of the CAH, CAH1, CAH2, and CAH3 films. The AKD content of the CAH film was 0.09 wt %, a little lower than that of the CA film which was 0.1 wt %. The AKD content of the CA film decreased after the extraction treatments and the CAH3 film had an AKD content of 0, which was similar to the extraction treated CA films.

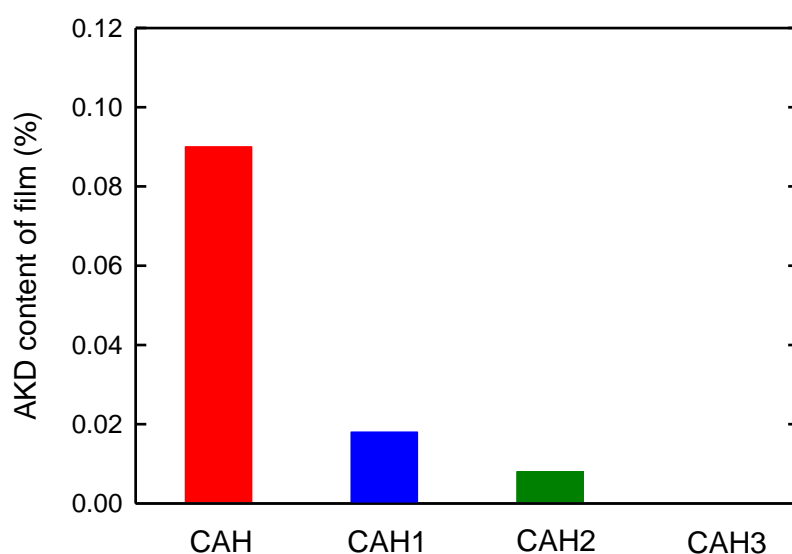


Figure 6.9. AKD contents of CAH, CAH1, CAH2, and CAH3 films.

Changes in water contact angles on AUCH, CAH and extraction treated CAH films over time after contact are shown in Figure 6.10, and photographs of a water droplet 0.1 s after contact with each film are shown inset. The contact angle of CAH was 102° and was unchanged for more than 20 s, similar to that of CA. No obvious decrease in contact angles were found in CAH1, CAH2, and CAH3 films. Therefore, the CAH films showed the similar change in AKD contents and water contact angles compared with the CA films after

extractions of AKD. These results indicated the remained hydrophobicity of the CA3 and CAH3 films after AKD extraction treatments shouldn't be owing to the hydrophobic interaction between AKD and cellulose.

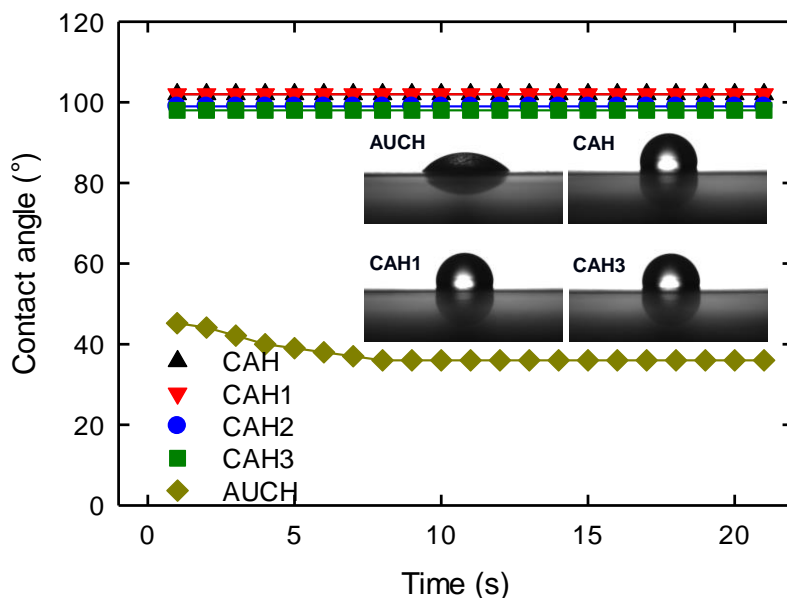


Figure 6.10. Changes in water contact angles on AUCH, CAH and extraction treated CAH films over time after contact and photographs of a water droplet 0.1 s after with each film.

6.3.3 Extractions of AKD from TA films

TEMPO-oxidized cellulose nanofibril films (TOCN) have almost no C6-OH groups but sodium C6-carboxylate groups on the microfibril surfaces. They are probably impossible to form β -ketoesters with AKD and only can form electrostatic interaction with cationic AKD dispersion. Therefore, they were also prepared to compare with AUC to clarify the interaction between AKD and cellulose. Figure 6.11 shows AKD contents of the TA, TA1, TA2, and TA3 films. The AKD content of the TA film was 0.5 wt %, which was much higher than that

of the CA film, probably owing to the strong electrostatic interaction between the anionic TOCN surface and the cationic AKD dispersion particels. The AKD contents of the TA film decreased to 0.02 wt % after the extraction of AKD with chloroform (TA1), and further decreased to 0 after extraction with hot water (TA2 and TA3).

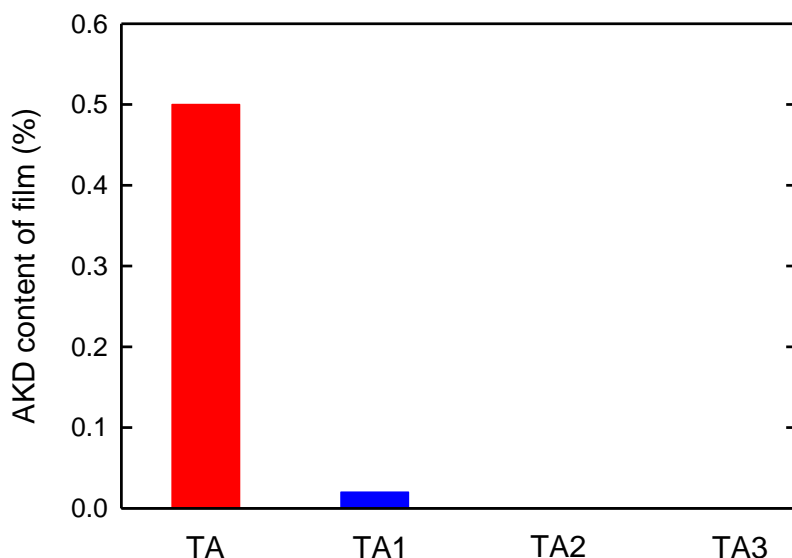


Figure 6.11. AKD contents of TA, TA1, TA2, and TA3 films.

Changes in water contact angles on TOCN, TA and extraction treated TA films over time after contact are shown in Figure 6.12, and photographs of a water droplet 0.1 s after contact with each film are shown inset. The contact angle of TA was 110° and was unchanged for more than 20 s. On the other hand, the contact angles of the TA film decreased to 64° after the extraction of AKD with chloroform (TA1), and further decreased to 48° after extraction with hot water and dioxane/water mixture (TA3), which was similar to that of the TOCN film (43°). These results further indicated that β -ketoesters are likely to form at the AKD/cellulose interfaces, which could not be removed by extraction treatments, whereas no β -ketoester

formed at the AKD/TOCN interfaces and the AKD could be removed by extraction treatments.

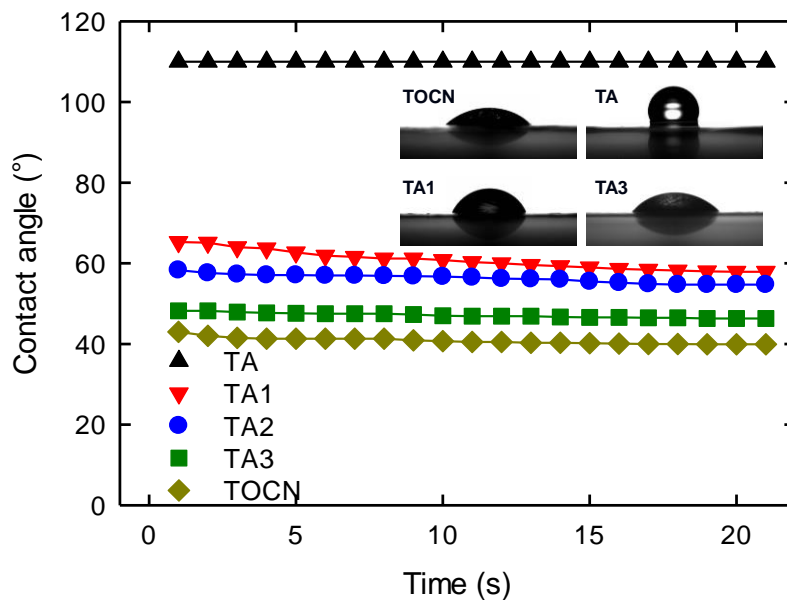


Figure 6.12. Changes in water contact angles on TOCN, TA and extraction treated TA films over time after contact, and photographs of a water droplet 0.1 s after contact with each film.

Based on these results and interpretation, possible hydrophobization mechanisms of cellulose films by AKD can be illustrated as in Figure 6.13. AKD components were present on the surface of the AUC film, which melted and became much smaller particles after heating. Original AKD was the main AKD component of the composites. However, a small amount of β -ketoesters are likely to form at the AKD/AUC interfaces, which could not be removed by extraction treatments. On the other hand, no β -ketoesters formed at the AKD/TOCN interfaces and the AKD components could be completely removed from the TOCN surfaces by extraction treatments.

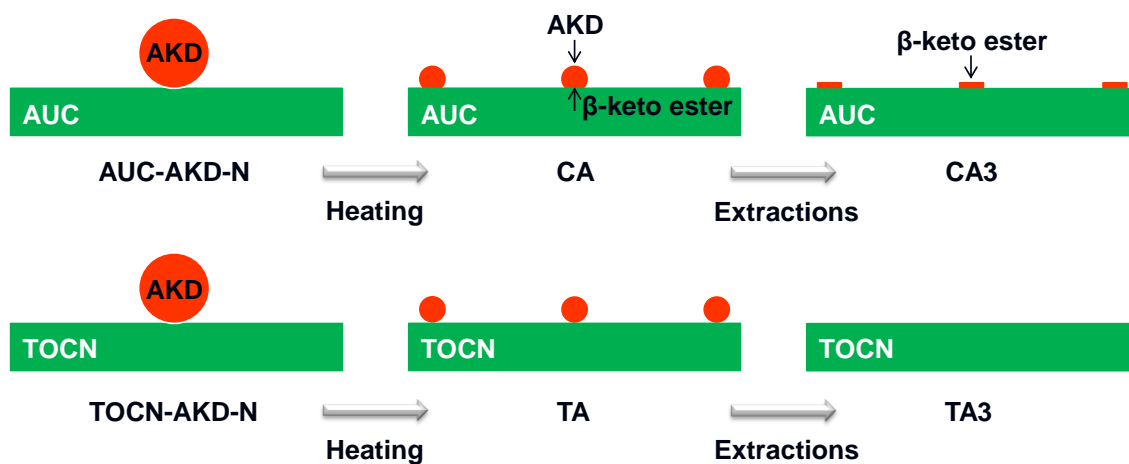


Figure 6.13. Schematic models of hydrophobization of AUC and TOCN with AKD and extractions of AKD.

6.4 Conclusions

The hydrophobization mechanism of regenerated cellulose films modified by AKD and the chemical structures of AKD-related components present at the AKD/cellulose interfaces were studied after a sequential extraction of the AKD components non-reacted with cellulose by chloroform, hot water, and dioxane/water mixture. The AKD content of the films decreased to nearly 0 by the extractions. However, water-contact angles of the film surfaces almost didn't change. Moreover, both of the regenerated cellulose films regenerated with aqueous coagulant (5 wt % H_2SO_4) and organic coagulant (acetone) showed the same trend in AKD contents and water contact angles after the sequential extraction. However, after the sequential extraction, water-contact angles of AKD/TOCN films decreased much, with the decrease in AKD content. These results indicated that original AKD was the main AKD component of the AKD/regenerated cellulose films. However, a small amount of β -ketoesters are likely to form at the AKD/regenerated cellulose interfaces, which couldn't be removed by

extraction treatments. On the other hand, AKD form physical interaction with TOCN at the AKD/TOCN interfaces and the AKD components could be completely removed from the TOCN surfaces by extraction treatments. The hydrophobization mechanism of regenerated cellulose films modified by AKD should also be useful for understanding the mechanism of paper sizing by AKD in papermaking industry.

6.5 References

- (1) Roberts, J. C. In Paper Chemistry; 2nd ed. Roberts, J. C. Ed.; Chapman and Hall, London, 1996.
- (2) Lindström, T.; Larsson P. T. *Nordic Pulp Paper Res. J.* **2008**, *23*, 202–209.
- (3) Hubbe, M. A. *Bioresources* **2006**, *2*, 106–145.
- (4) Davis, J. W.; Robertson, W. H.; Weisgerber, C. A. *Tappi* **1956**, *39*, 21–23.
- (5) Roberts, J. C.; Garner, D. N. *Tappi J.* **1985**, *68*, 118–121.
- (6) Lindström, T.; Söderberg, G. *Nordic Pulp Paper Res. J.* **1986**, *1*, 26–33.
- (7) Nahm, S. H. *J. Wood Chem. Tech.* **1986**, *6*, 89–95.
- (8) Ödberg, L.; Lindström, T.; Liedberg, B.; Gustavsson, J. *Tappi J.* **1987**, *70*, 135–139.
- (9) Lindström, T.; O'Brian, H. *Nordic Pulp Paper Res. J.* **1986**, *6*, 34–42.
- (10) Dumas, D. H.; Evans, D. B. *Tappi Papermakers Conf.* **1986**, p. 31–35.
- (11) Marton, J. *Tappi J.* **1990**, *73*, 139–143.
- (12) Isogai, A.; Taniguchi, R.; Onabe, F.; Usuda, M. *Nordic Pulp Paper Res. J.* **1992**, *7*, 193–199.
- (13) Chen, M.; Biemmann, C. J. *Tappi J.* **1995**, *78*, 120–126.
- (14) Bottorff, K. J. *Proc.TAPPI 1993 Papermakers Conf.* **1993**, TAPPI Press, Atlanta, 441–450.
- (15) Pisa, L.; Murckova, E. *Papir Celluloza* **1981**, *36*, V15–V21.
- (16) Roberts, J. C.; Garner, D. N. *Cellulose Chem. Technol.* **1984**, *18*, 275–280.
- (17) Gess, J. M.; Lund, R. C. *Tappi J.* **1991**, *74*, 111–118.
- (18) Rohringer, P.; Bernheim, M.; Weatherman, D. P. *Tappi J.* **1985**, *68*, 83–86.

- (19) Taniguchi, R.; Isogai, A.; Onabe, F.; Usuda, M. *Nordic Pulp Paper Res. J.* **1993**, *8*, 352–361.
- (20) Seo, W. S.; Cho, N. S.; Ohga, S. *J. Fac. Agr., Kyushu Univ.* **2008**, *53*, 405–410.
- (21) Bottroff, K. J.; Sullivan, M. J. *Nordic Pulp Paper Res. J.* **1993**, *8*, 86–95.
- (22) Seo, W. S.; Cho, N. S. *Appita J.* **2005**, *58*, 122–126.
- (23) Isogai, A. *J. Pulp Paper Sci.* **1999**, *25*, 251–255.
- (24) Cai, J.; Zhang, L. *Macromol. Biosci.* **2005**, *5*, 539–548.
- (25) Qi, H.; Chang, C.; Zhang, L. *Green Chemistry* **2009**, *11*, 177–184.
- (26) Yang, Q.; Fukuzumi, H.; Saito, T.; Isogai, A.; Zhang, L. *Biomacromolecules* **2011**, *12*, 2766–2771.
- (27) Yang, Q.; Fujisawa, S.; Saito, T.; Isogai, A. *Cellulose* **2012**, *19*, 695–703.
- (28) Yang, Q.; Lue, A.; Qi, H.; Sun, Y.; Zhang, X.; Zhang, L. *Macromol. Biosci.* **2009**, *9*, 849–856.
- (29) Yang, Q.; Lue, A.; Zhang, L. *Compos. Sci. Technol.* **2010**, *70*, 2319–2324.
- (30) Shi, X.; Lu, A.; Cai, J.; Zhang, L.; Zhang, H.; Li, J.; Wang, X. *Biomacromolecules* **2012**, *13*, 2370–2378.
- (31) Shi, X.; Zhang, L.; Cai, J.; Cheng, G.; Zhang, H.; Li, J.; Wang, X. *Macromolecules* **2011**, *44*, 4565–4568.
- (32) Yang, Q.; Saito, T.; Isogai, A. *Cellulose* **2012**, *19*, 1913–1921.
- (33) Isobe, N.; Kim, U.-J.; Kimura, S.; Wada, M.; Kuga, S. *J. Colloid Interface Sci.* **2011**, *359*, 194–201.
- (34) Shinoda, R.; Saito, T.; Okita, Y.; Isogai, A. *Biomacromolecules* **2012**, *13*, 842–849.
- (35) Isogai, A.; Saito, T.; Fukuzumi, H. *Nanoscale* **2011**, *3*, 71–85.
- (36) Saito, T.; Kimura, S.; Nishiyama, Y.; Isogai, A. *Biomacromolecules* **2007**, *8*, 2485–2491.
- (37) Fukuzumi, H.; Saito, T.; Iwata, T.; Kumamoto, Y.; Isogai, A. *Biomacromolecules* **2009**, *10*, 162–165.
- (38) Isogai, A.; Kitaoka, C.; Onabe, F. *J. Pulp Paper Sci.* **1997**, *23*, J215–J219.
- (39) Shibuichi, S.; Onda, T.; Satoh, N.; Tsujii, K. *J. Phys. Chem.* **1996**, *100*, 19512–19517.
- (40) Gao, X.; Jiang, L. *Nature* **2004**, *432*, 36–36.

- (41) Onda, T.; Shibuichi, S.; Satoh, N.; Tsujii, K. *Langmuir* **1996**, *12*, 2125–2127.
- (42) Qi, Z.; Saito, T.; Fan, Y.; Isogai, A. *Biomacromolecules* **2012**, *13*, 553–558.

Chapter 7

Summary

7.1 High gas barrier cellulose films

Transparent and bendable regenerated cellulose films prepared from aqueous alkali/urea solutions exhibited high oxygen barrier properties at 0% RH, which are superior to those of conventional cellophane, poly(vinylidene chloride), and poly(vinyl alcohol). The oxygen permeabilities of these cellulose films varied widely depending on the conditions used to prepare them. The oxygen permeabilities of the cellulose films were negatively correlated with their densities, and cellulose films prepared from solutions with high cellulose concentrations by regeneration in a solvent at low temperatures generally had low oxygen permeabilities. Moreover, mechanical, thermal and oxygen barrier properties of regenerated cellulose films prepared from aqueous cellulose/alkali/urea solutions can be markedly improved by controlling the drying conditions of the films. By pre-pressing followed by vacuum drying under compression, the tensile strength, Young's modulus, coefficient of thermal expansion and oxygen permeability of the dried film reached 263 MPa, 7.3 GPa, 10.3 ppm K⁻¹ and 0.0007 mL μm m⁻² day⁻¹ kPa⁻¹, respectively. It should be noted that the oxygen transmission rate of this cellulose film was lower than the lowest detection limit of the instrument. Thus, films produced in this way show the highest performance of regenerated cellulose films with no orientation of cellulose chains reported to date. These improved properties are accompanied by a clear increase in cellulose II crystallinity from 50 to 62% during pre-pressing/press-vacuum drying process. At the same time, the film density increased from 1.45 to 1.57 g cm⁻³.

7.2 High-performance cellulose biocomposite materials

The hydrophilicity of cellulose materials results in greater amounts of moisture sorption and a significant increase in the oxygen permeability under higher humid conditions, thus

restricting their potential applications. Hence, the cellulose films were composited with nanoclay or surface modified by alkyl ketene dimers (AKDs) which are both from natural resources to improve their oxygen barrier properties at high humid conditions.

7.2.1 Cellulose based nanocomposites reinforced with nanoclay. Transparent flexible regenerated cellulose–nanoclay (saponite or montmorillonite) nanocomposite films were prepared from cellulose/LiOH/urea solutions. The composites possessed intercalated nanolayered structures of clay platelets. They exhibited high mechanical strength, Young's modulus, and gas barrier properties, and lower coefficients of thermal expansion than those of the original LiOH/urea regenerated cellulose film. In particular, the composite film containing 85% cellulose and 15 wt % natural montmorillonite clay exhibited tensile strength and Young's modulus that were 161 and 180% greater than those of the cellulose film, respectively, and its coefficient of thermal expansion and oxygen permeability at 50–75% RH were 60 and 42–33% lower than those of the cellulose film, respectively. Moreover, the initial hydrophilic nature of the cellulose film changes to somewhat hydrophobic through incorporation of hydrophilic clay platelets.

7.2.2 Hydrophobization of cellulose films by surface modification with AKD. Transparent and water repellent gas barrier cellulose films were fabricated by surface modification of LiOH/urea regenerated cellulose films by soaking in cationic AKD dispersion, drying, and heating. AKD-treated cellulose films still exhibited very low oxygen transmission rates which were lower than the lowest detection limit of the instrument at 0% RH. Water contact angles on the cellulose film increased from 50 to 110° after AKD treatment, and water uptake (immersion in water for 6 days) decreased from 92 to 20 %. Moreover, oxygen permeability decreased from 0.56 and 5.8 to 0.13 and 2.1 mL $\mu\text{m m}^{-2} \text{day}^{-1} \text{kPa}^{-1}$ at 50 and 75 % RH, respectively, when the AKD content of the film was increased from 0 to 0.2 wt %. The present AKD-treated cellulose film also had high light transparency and mechanical properties. AKD components were stable on the AKD-treated film surfaces without hydrolysis at 2 months. The results of extraction treatments of AKD from AKD-treated cellulose films indicated original AKD was the main AKD component of the AKD/regenerated cellulose films. However, a small amount of β -ketoesters are likely to form at the AKD/regenerated cellulose interfaces.

Research Achievement

Journal Articles

Documents submitted from The University of Tokyo, Japan

1. Quanling Yang, Hayaka Fukuzumi, Tsuguyuki Saito, Akira Isogai, and Lina Zhang, Transparent cellulose films with high gas barrier properties fabricated from aqueous alkali/urea solutions, *Biomacromolecules*, Vol. 12, No 6, pp. 2766-2771, **2011**.
2. Quanling Yang, Shuji Fujisawa, Tsuguyuki Saito, and Akira Isogai, Improvement of mechanical and oxygen barrier properties of cellulose films by controlling drying conditions of regenerated cellulose hydrogels, *Cellulose*, Vol. 19, No 3, pp. 695-703, **2012**.
3. Quanling Yang, Tsuguyuki Saito, and Akira Isogai, Facile fabrication of transparent cellulose films with high water repellency and gas barrier properties, *Cellulose*, Vol. 19, No 6, pp. 1913-1921, **2012**.
4. Quanling Yang, Tsuguyuki Saito, and Akira Isogai, Transparent, flexible, and high-strength regenerated cellulose/saponite nanocomposite films with high gas barrier properties, *Journal of Applied Polymer Science*, Vol. 130, No 5, pp. 3168–3174, **2013**.
5. Quanling Yang, Chun-Nan Wu, Tsuguyuki Saito, and Akira Isogai, Cellulose-clay layered nanocomposite films fabricated from aqueous cellulose/LiOH/urea solution, *Carbohydrate Polymers*, Vol. 100, pp. 179–184, **2014**.
6. Quanling Yang, Miyuki Takeuchi, Tsuguyuki Saito, and Akira Isogai, Formation of nano-sized islands of dialkyl β -ketoester bonds for efficient hydrophobization of cellulose film surface, to be submitted.
7. Buapan Puangsina, Quanling Yang, Tsuguyuki Saito, and Akira Isogai, Comparative characterization of TEMPO-oxidized cellulose nanofibril films prepared from non-wood

resources, *International Journal of Biological Macromolecules*, Vol. 59, pp. 208-213, **2013**.

Documents submitted from Wuhan University, China

8. Quanling Yang, Ang Lue, Haisong Qi, Yunxia Sun, Xianzheng Zhang, and Lina Zhang, Properties and bioapplications of blended cellulose and corn protein films, *Macromolecular Bioscience*, Vol. 9, No 9, pp. 849-856, **2009**.
9. Quanling Yang, Ang Lue, and Lina Zhang, Reinforcement of ramie fibers on regenerated cellulose films, *Composites Science and Technology*, Vol. 70, No 16, pp. 2319-2324, **2010**.
10. Quanling Yang, Haisong Qi, Ang Lue, Kai Hu, Gongzhen Cheng, and Lina Zhang, Role of sodium zincate on cellulose dissolution in NaOH/urea aqueous solution at low temperature, *Carbohydrate Polymers*, Vol. 83, No 3, pp. 1185-1191, **2011**.
11. Quanling Yang, Xingzhen Qin, and Lina Zhang, Properties of cellulose films prepared from NaOH/urea/zincate aqueous solution at low temperature, *Cellulose*, Vol. 18, No 3, pp. 681-688, **2011**.
12. Ruping Zhang, Quanling Yang, Haisong Qi, Jinping Zhou, and Lina Zhang, Preparation and properties of cellulose/poly (vinyl alcohol) blend films based on dissolution in a non-toxic solvent system, *Journal of Biobased Materials and Bioenergy*, Vol. 3, No 2, pp. 199-204, **2009**.
13. Haisong Qi, Quanling Yang, Lina Zhang, Tim Liebert, and Thomas Heinze, The dissolution of cellulose in NaOH-based aqueous system by two-step process, *Cellulose*, Vol. 18, No 2, pp. 237-245, **2011**.

Conference

International conferences

1. Quanling Yang, Shuji Fujisawa, Tsuguyuki Saito, Akira Isogai, and Lina Zhang, High gas barrier and strong cellulose films fabricated by controlling preparation and drying conditions of regenerated cellulose hydrogels, *The 243th American Chemical Society National Meeting*, San Diego, CA, USA, Mar. **2012**. [Oral]
2. Quanling Yang, Chun-Nan Wu, Tsuguyuki Saito, and Akira Isogai, Properties of regenerated cellulose/clay nanocomposite films, *3rd International Cellulose Conference*, Sapporo, Japan, Oct. **2012**. [Poster]
3. Quanling Yang, Chun-Nan Wu, Tsuguyuki Saito, and Akira Isogai, Cellulose–clay nanocomposite films with high gas barrier properties, *4th International Conference on Pulping, Papermaking and Biotechnology*, Nanjing, China, Nov. **2012**. [Oral]
4. Quanling Yang, Tsuguyuki Saito, and Akira Isogai, Hydrophobization of cellulose films by surface modification with alkyl ketene dimer (AKD), *The 245th American Chemical Society National Meeting*, CELL, New Orleans, LA, USA, Apr. **2013**. [Oral]
5. Lina Zhang, Quanling Yang, Haisong Qi, Ang Lue, Role of zincate on improvement of cellulose dissolution in NaOH/urea aqueous solution, *The 239th American Chemical Society National Meeting*, San Francisco, CA, USA, Mar. **2010**. [Oral]
6. Chun-Nan Wu, Quanling Yang, Miyuki Takeuchi, Zi-Dong Qi, Tsuguyuki Saito, and Akira Isogai, Highly tough and transparent layered composites of nanocellulose and clay nanoplatelets, *3rd International Cellulose Conference*, Sapporo, Japan, Oct. **2012**. [Poster]
7. Buapan Puangsin, Quanling Yang, Shuji Fujisawa, Tsuguyuki Saito, and Akira Isogai, Preparation and characterization of cellulose nanofiber films prepared from non-wood celluloses through the TEMPO-mediated oxidation, *3rd International Cellulose Conference*, Sapporo, Japan, Oct. **2012**. [Poster]

Conferences in Japan

1. Quanling Yang, Hayaka Fukuzumi, Tsuguyuki Saito, Akira Isogai, and Lina Zhang, High gas barrier transparent and flexible cellulose films fabricated from aqueous alkali/urea solutions, *Annual Meeting of Japanese Society of Fiber Science and Technology*, Tokyo, Japan, Jun. **2011**. [Oral]
2. Quanling Yang, Hayaka Fukuzumi, Tsuguyuki Saito, Akira Isogai, and Lina Zhang, High gas-barrier cellulose films fabricated from aqueous alkali/urea solutions, *The 20th Annual Meeting of The Society of Packaging Science & Technology, Japan*, Kyoto, Japan, Jul. **2011**. [Poster]
3. Quanling Yang, Hayaka Fukuzumi, Tsuguyuki Saito, Akira Isogai, and Lina Zhang, Transparent cellulose films with high gas barrier properties prepared from aqueous alkali/urea solutions, *The 18th Annual Meeting of The Cellulose Society of Japan*, Nagano, Japan, Jul. **2011**. [Poster]
4. Quanling Yang, Chun-Nan Wu, Tsuguyuki Saito, and Akira Isogai, Cellulose-based nanocomposites reinforced with saponite using cellulose/alkali/urea solvent, *Annual Meeting of Japanese Society of Fiber Science and Technology*, Tokyo, Japan, Jun. **2012**. [Poster]
5. Quanling Yang, Chun-Nan Wu, Tsuguyuki Saito, and Akira Isogai, Cellulose–clay layered nanocomposites fabricated from aqueous cellulose/alkali/urea solutions, *The 19th Annual Meeting of The Cellulose Society of Japan*, Nagoya, Japan, Jul. **2012**. [Poster]
6. Quanling Yang, Miyuki Takeuchi, Tsuguyuki Saito, and Akira Isogai, Hydrophobization mechanism of cellulose films by alkyl ketene dimer, *The 80th Pulp and Paper Research Conference of Japan*, Tokyo, Japan, Jun. **2013**. [Oral]
7. Quanling Yang, Miyuki Takeuchi, Tsuguyuki Saito, and Akira Isogai, Structure and properties of cellulose/alkyl ketene dimer (AKD) composite films, *The 20th Annual*

Meeting of The Cellulose Society of Japan, Kyoto, Japan, Jul. 2013. [Poster]

8. Chun-Nan Wu, Tsuguyuki Saito, Quanling Yang, and Akira Isogai, Ultrastrong and transparent TOCN/nanoclay composites, *The 19th Annual Meeting of Cellulose Society of Japan, Nagoya, Japan, Jul. 2012.* [Poster]
9. Chun-Nan Wu, Quanling Yang, Miyuki Takeuchi, Zi-Dong Qi, Tsuguyuki Saito, and Akira Isogai, Strong transparent and water repellent TOCN/nanoclay composites, *The 63rd Annual Meeting of the Japan Wood Research Society, Morioka, Japan, Mar. 2013.* [Oral]
10. Buapan Puangsin, Quanling Yang, Tsuguyuki Saito, and Akira Isogai, Preparation and characterization of cellulose nanofiber films prepared from non-wood cellulose through the TEMPO-mediated oxidation, *The 20th Annual Meeting of The Cellulose Society of Japan, Kyoto, Japan, Jul. 2013.* [Poster]

Patents (Granted)

Documents submitted from Wuhan University, China

1. Lina Zhang, Haisong, Qi, and Quanling Yang, A method of dissolving cellulose, *China Patent, ZL200710052533.4, Sep. 2009.*
2. Lina Zhang, Haisong, Qi, and Quanling Yang, Preparation and applications of blended cellulose and corn protein solution, *China Patent, ZL200710168520.3, Sep. 2010.*
3. Lina Zhang, Haisong, Qi, Chunyu Chang, and Quanling Yang, A method of preparing the fluorescent cellulose films, *China Patent, ZL200810236785.7, Apr. 2011.*
4. Lina Zhang, Haisong, Qi, Chunyu Chang, and Quanling Yang, A method of preparing the luminescent cellulose films, *China Patent, ZL200810236783.8, Nov. 2011.*

Honors and Awards

1. Research Fellowship for Young Scientists, Japan Society for the Promotion of Science (JSPS DC2), Apr. **2012**.
2. The Poster Award, the 20th Annual Meeting of The Society of Packaging Science & Technology, Japan, Jul. **2011**.
3. Chinese Government Scholarship for Doctoral Course Students Abroad (CSC Scholarship), Sep. **2010**.

Acknowledgement

This thesis is a compilation of studies carried out from October 2010 to September 2013 under the supervision of Professor Akira Isogai in the University of Tokyo. I am grateful to Professor Isogai for giving me such a good chance to study in the world famous The University of Tokyo. Professor Isogai taught me much during these three years, not only how to do research, but also how to be an upright person and upright researcher. I would like to express my deepest respect and gratitude to Professor Isogai for his considerate guidance, supports and continuous warm encouragement throughout this study, and also for his kindness, toleration and careful consideration to me, a foreign student.

I am greatly indebted to Associate Professor Tsuguyuki Saito. Associate Professor Saito gave me precious instructions and suggestions for this study. Thanks to the extensive discussions with Associate Professor Saito and his warm encouragements, I could begin this study in a short time. And I am also thankful for his great and patient helps of writing scientific papers and a lot of experiment techniques. His careful attention to detail left a deep impression on me. I am grateful to Professor Minoru Kimura for his concern, continuous encouragements and advices. I am thankful to Professor Assistant Miyuki Takeuchi for the help of NanoSIMS and suggestions for this study. I am also grateful to Professor Toshiharu Enomae of University of Tsukuba for his kindness, warm encouragement and suggestions.

I would like to express many thanks to Dr. Hayaka Fukuzumi of Tokyo Institute of Technology for all her kind help. Dr. Fukuzumi gave me much useful suggestions on gas barrier properties and taught me much on gas permeability tests. Special thanks to Mr. Zidong Qi for the numerous help with translations and instructions during my life and study, since I came to Japan. Without Mr. Qi's kindly help, I couldn't study and live so conveniently here. I am also grateful to Mr. Chun-Nan Wu for a lot of help in my study and life, such as tensile tests, TG analysis, discussion of this study, and share of experience of life. I would like to thank Mr. Shuji Fujisawa for the helps of TMA analysis and many other helps in study and life, Dr. Laurent Heux of Centre de Recherches sur les Macromolécules Végétales, CNRS/ICMG/UJF, France for the helps of the Solid NMR analysis and the relevant

calculation of crystallinity, Professor Assistant Hirotaka Koga of Osaka University for the helps of FTIR analysis, Ms. Kayoko Kobayashi and Mr. Yu Ogawa for the helps of XRD, Ms. Buapan Puangsin for the helps of microscope and viscometer analysis, Dr. Takehiko Uematsu of Kao Corporation for the helps of elementary analysis, Ms. Yuko Ono for the helps of all kinds of documents, Dr. Naoyuki Tamura of Nippon Paper Industries Co., Ltd. for the helps of computer, and the other former and present members of the Cellulose, Pulp & Paper Science laboratory for their kind cooperation, advices, and cares of my study and life.

I am grateful to Professor Yimin Fan of Nanjing Forestry University, China, Associate Professor Shilin Liu of Jiangnan University, China, Dr. Xiaobo Su of Asahi Kasei Corporation, Dr. Yu Huang of The National Institute of Advanced Industrial Science and Technology (AIST), for all the helps before and after I came to The University of Tokyo.

I am thankful to Professor Lina Zhang of Wuhan University, China for her help and advice to this study.

I would like to thank Professor Yuji Matsumoto, Professor Tadahisa Iwata, Professor Akira Isogai, Associate Professor Masahisa Wada, and Associate Professor Tsuguyuki Saito for their devotion to judgment of this thesis.

Thanks for my wife, Zhuqun Shi, for her accompany, endless encouragement and help, and sharing every happiness and sadness with me. I sincerely thank my family for their devoted support and encouragement.

I would like to express my gratitude again to all the above-mentioned people. Their selfless helps and kindly cares make me have a good time during the three year doctoral course period! I wish them healthy, prosperous, successful, and everything goes well!

Finally, I am grateful to the Japan Society for the Promotion of Science (JSPS) for financial support of this study and I am also grateful to China Scholarship Council (CSC) for support of my study abroad.

楊 全嶺
YANG Quanling
August, 2013